
UNIVERSITÀ DEGLI
STUDI DI SALERNO

*Ministero dell'Istruzione, dell'Università e della Ricerca*

**Facoltà di Ingegneria**

Dipartimento di Ingegneria dell'Informazione ed Elettrica e Matematica Applicata

Dottorato di Ricerca in Ingegneria dell'Informazione
XIII Ciclo – Nuova Serie

TESI DI DOTTORATO

# Diffraction by dielectric wedges: high frequency and time domain solutions

CANDIDATO: **MARCELLO FRONGILLO**

COORDINATORE: **PROF. MAURIZIO LONGO**

TUTOR: **PROF. GIOVANNI RICCIO**

Anno Accademico 2014 – 2015

*A tutti i professori che ho incontrato nella mia vita. Una parte di ognuno di loro è presente in questo lavoro.*

*Soprattutto, ai migliori professori che ho avuto: mio padre e mia madre.*

# Contents

# Chapter 1

# Introduction

The knowledge of the propagation characteristics of the electromagnetic fields is fundamental in the analysis and planning of antennas and optical systems. The propagation prediction models based on ray-tracing are the most employed techniques in modern radio communication systems. The ray-based models allow one to calculate magnitude and phase of the received electromagnetic field and also the delay of each ray due to the propagation mechanisms. These last are often complex and can be generally attributed to the phenomena of reflection, transmission, diffraction and scattering. As well known, when the dimensions of the systems are large in terms of the electromagnetic wavelength, diffraction contributions due to material discontinuities can't be negligible and must be accurately calculated. By using the numerical discretization methods such as the Finite-Difference Time-Domain (FDTD) method, the Finite Element Method (FEM), and the Method of Moments is possible to obtain reliable solutions for the scattering problems. Unfortunately, such techniques have the drawback of the increasing with frequency of the number of unknowns and so the computations become inefficient or intractable at the high frequencies. Furthermore, the physical understanding of the propagation mechanisms is difficult with this kind of approach.

The asymptotic methods result to be an efficient alternative for solving high frequency scattering problems. The Geometrical Theory of Diffraction (GTD) [1] has received great attention in the last decades because of its simplicity and strength. It is based on the ray-oriented theory of the Geometrical Optics (GO) and describes the diffraction at the edge of a structure like a local phenomenon at the high frequencies basing on a generalization of the Fermat principle. The major GTD disadvantage is the presence of field singularities at the GO shadow boundaries. Therefore, a uniform version of GTD was

elaborated, the Uniform Theory of Diffraction (UTD) [2]. It uses the same GTD rays but furnishes uniform asymptotic solutions for the diffracted field that are valid also in the transition regions. As consequence of the local properties of high frequency electromagnetic fields, the diffraction phenomenon depends only on the geometric and electromagnetic features of the obstacle in proximity of the diffraction point. Accordingly, for many canonical structures (half-plane, wedge, etc.) the corresponding diffraction coefficients, associating the diffracted field to the incident field, are available in literature. It's important to highlight that the rigorous, closed form diffraction coefficients have been derived only for particular canonical configurations and material. In [1], [2] the authors produced the exact diffractions coefficients for structures with perfectly conducting surfaces. In the next research activities the material discontinuities have been modelled by impedance or transmissive boundary conditions, and the solutions are generally expressed in terms of the Maliuzhinets' function ([6], [14], [19]-[21]). This last is almost complicated and can be easily evaluated only for particular geometric configurations. Therefore, their application to the new practical engineering problems is limited.

This work has the purpose to produce approximate but reliable, closed form Uniform Asymptotic Physical Optics (UAPO) solutions for several canonical problems of diffraction concerning wedges made of dielectric materials. UAPO diffraction coefficients are quite accurate and easy to handle since expressed in terms of the GO response of the structure and the transition function of the UTD. Furthermore, their knowledge allows one to evaluate the corresponding diffraction coefficients in the time domain (TD) for the same geometries. The thesis is structured as follows.

In Chapter 2 are presented some of the most common high frequency techniques for analysing wave propagation in presence of obstacles. In particular GO, GTD, Physical Optics (PO) methods are discussed and the UAPO technique is introduced.

In Chapter 3 the state of research about diffraction by dielectric wedges is examined and a high-frequency solution for the problem of plane wave diffraction by an arbitrary-angled dielectric wedge is shown. Although such a problem has been already tackled in literature [26]-[32], the solution proposed here is fully formulated in the UTD

framework and then, it is a user-friendly worthwhile alternative for the considered diffraction problem. It is obtained by a decomposition of the considered scattering problem into two sub-problems, respectively external and internal to the wedge region. For each of them, is considered a PO approximation of the electric and magnetic equivalent surface currents in the radiation integral and a uniform asymptotic evaluation of this last is performed. The found UAPO solution has been implemented in a computer code, and the simulations show that it compensates the GO field discontinuities at the shadow boundaries. Moreover, its accuracy is weighed by the good agreement achieved with numerical results obtained via the commercial tool *Comsol Multiphysics*® based on FEM and via a FDTD computer code.

Chapter 4 is devoted to the study of the diffraction of plane waves by an arbitrary-angled dielectric wedge in the TD framework. Differently from the Frequency Domain (FD) framework, in the TD one no closed form solutions are available in literature for this kind of problem, except those concerning right- and obtuse-angled lossless wedges [58], [59]. The inverse Laplace transform is applied to the FD-UAPO solutions for the diffraction coefficients found in Chapter 3 by taking advantage of their UTD-like nature. Then, the transient diffracted field is evaluated via a convolution integral. The results provided by simulations for these solutions have verified their goodness. The TD-UAPO formulation has the same advantages and limitations of the FD-UAPO ones, arising from the use of a PO approximation. Anyway, at the writing time of this thesis the TD-UAPO formulation is the only one analytical solutions to TD scattering problems involving penetrable wedges.

Although unavoidably approximate, the FD-UAPO solutions are simple, efficient and quite accurate for solving several diffraction problems involving penetrable obstacles. Furthermore, the corresponding TD-UAPO solutions are reliable and the only available in closed form for solving the same problems in the TD framework. Accordingly, they can be surely useful from an engineering viewpoint when no rigorous and efficient solutions for the diffracted field are available.

# Chapter 2

# High frequency techniques

The intent of this chapter is to discuss some of the most common high frequency techniques for analysing the propagation of electromagnetic waves in presence of obstacles. As well-known, when an object is inserted in the path of a propagating electromagnetic wave it modifies the field distribution in the surrounding space. Then, the total field at a given observation point is given by the superposition of the incident field and the scattered field. The evaluation of the scattered field can be performed via different analytical techniques. In particular, *Geometrical Optics* (GO), *Geometrical Theory of Diffraction* (GTD) and *Physical Optics* (PO) are illustrated in the following, because they constitute the bases for the UAPO method shown at last.

## 2.1 Geometrical Theory of Diffraction

When the dimensions of a radiating element or a scattering object are large in terms of wavelength, is possible to use the high frequency asymptotic techniques to solve in a quite simple way many problems that would otherwise be mathematically intractable. In the past years GTD, defined by Keller [1] and later developed by Kouyoumjian and Pathak [2], has received great attention. It is an extension of GO which is an approximate and well-known high frequency technique based on the theory of propagation of electromagnetic waves along rays. According to GO, only direct, reflected and refracted rays exist; as a consequence the field exhibits sharp transitions in correspondence of the shadow boundaries and it is null in the space regions not directly illuminated by the incident field. In the framework of GTD, a new type of rays, namely the *diffracted rays*, is introduced to overcome the GO inaccuracies.

The GTD is based on the *principle of locality* and on a generalization of the *Fermat's principle*. The first one states that, at the high frequencies, reflection, refraction and diffraction are local phenomena depending only on the geometric and electromagnetic properties of an object in proximity of the reflection, refraction and diffraction point, respectively. Therefore, many diffraction coefficients relating the diffracted field to the incident field have been determined for several canonical problems. For example, the simplest configurations are the wedges of infinite dimension, made of perfectly conducting material and illuminated by uniform plane waves. Its diffraction coefficients have been determined by rigorous solutions of Maxwell's equations. As consequence, the basic method of GTD to tackle and solve a scattering problem is to decompose the original geometry in simpler geometric configurations, whose diffraction coefficients are known. In fact, is possible to obtain the final solution as the superposition of the contributions relevant to each canonical problem.

The generalization of the Fermat's principle allows one the ray tracing and the determination of the diffraction points. As well-known, it states that in a homogeneous medium a ray moves along the shortest path from the source to the observation point. Such a principle can be also generalized to diffracted rays.

The application of GTD to solve scattering problems is simple in principle but some problems may arise. At first, the number of rays to consider grows rapidly with the geometrical complexity of the problem. Moreover, even diffraction coefficients related to simple structures are still unknown. Finally, it is difficult to determinate the lower frequency limit beyond which the results obtained by GTD can be considered accurate.

According to GTD, when an electromagnetic wave at high frequency is incident on a truncated surface, it generates a reflected wave, an edge diffracted wave and a surface wave propagating along the structure. This last, can also be excited in the shadow region of a curved surface. Such a phenomenon is represented in Fig. 2.1, where a plane perpendicular to the edge at the diffraction point $D$ is shown. A ray impinging on the edge at the point $D$ produces edge diffracted rays (*ed*) and surface rays (*sr*). With reference to convex geometries, the surface ray produce rays diffracted from the surface at any point $Q$

along its path. As a result, *ES* is the borderline between the rays diffracted from the edge and the rays diffracted from the surface and it is tangent to the surface in *D*. Moreover, *SB* bounds the zone illuminated by incident field and *RB* that illuminated by reflected rays. The structure in Fig. 2.1 is non penetrable otherwise also refracted rays and diffracted rays in the inner region must be considered. When both the surfaces are illuminated by the incident field, there are no shadow boundaries but two reflection boundaries arise. Since the behaviour of the optic rays is different in the two regions delimited by a boundary (*ES*, *SB*, *RB*), a transition region wherein the field exhibits an abrupt variation is found near each boundary.

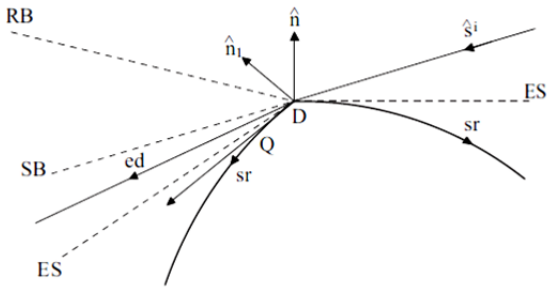


**Figure 2.1** Incident, reflected and diffracted rays. Shadow boundaries.

It is assumed in the following that the field sources and the observation point are far enough from both the surface and the boundary *ES* in order to neglect the contributions due to the surface rays. Consequently, the total electric field can be expressed as:

$$\underline{E} = \underline{E}^i + \underline{E}^r + \underline{E}^d \tag{2.1}$$

wherein $\underline{E}^i$ denotes the incident electric field, namely the field free space which is null in the shadow region, $\underline{E}^r$ is the reflected field and $\underline{E}^d$ is the diffracted field.

## 2.2 Geometrical Optics

### 2.2.1 General expression for the field

In line with the GO, rays can be interpreted as flux lines of the power density and the variation of the field intensity along a ray can be determined by applying the principle of conservation of the power flux in a tube of rays. Let's suppose that a point source emanates isotropically waves and denote with $L_0$ and $L_0 + \Delta L$ wavefronts at the time $t$ and $t + \Delta t$, respectively (see Fig. 2.2).

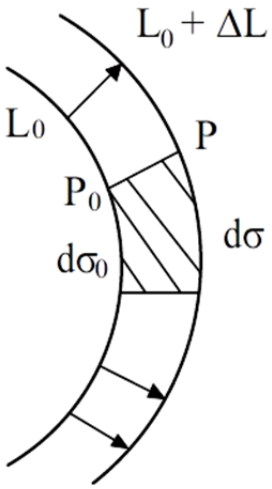


**Figure 2.2** Primary and secondary wavefronts of a radiated wave.

It is possible to consider the tube of rays between the cross-sectional areas $d\sigma_0$ at $P_0$ and $d\sigma$ at $P$ through which the power flux is constant. Therefore, the following identity holds:

$$S_0 d\sigma_0 = S d\sigma \tag{2.2}$$

wherein

$$S = \frac{|\underline{E}|^2}{2\zeta} \tag{2.3}$$

is the power density and $\zeta$ the intrinsic impedance of the medium. Eq. (2.2) can be rewritten as:

$$|\underline{E}_0|^2 \, d\sigma_0 = |\underline{E}|^2 \, d\sigma \tag{2.4}$$

or

$$|\underline{E}| = |\underline{E}_0| \sqrt{\frac{d\sigma_0}{d\sigma}} \tag{2.5}$$

It can be useful to express $d\sigma_0$ and $d\sigma$ in terms of the curvature radii of the wavefronts. To this end, let us consider the general case of an astigmatic tube of rays shown in Fig. 2.3.

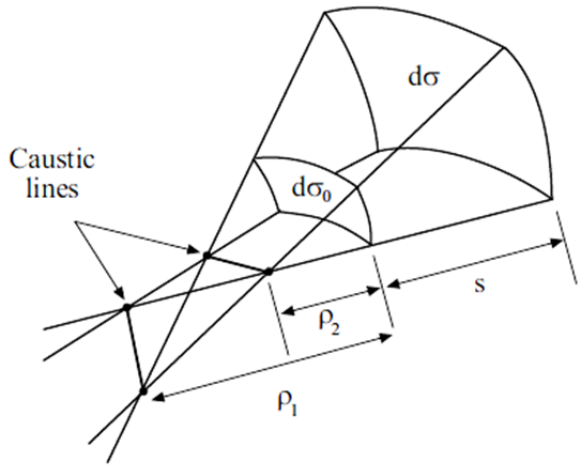


**Figure 2.3** Astigmatic tube of rays.

The surfaces $d\sigma_0$ and $d\sigma$ have principal radii of curvature $\rho_1$, $\rho_2$ and $\rho_1 + s$, $\rho_2 + s$, respectively, where $s$ denotes the distance along

the ray path from $P_0$ to $P$. Since both $d\sigma_0$ and $d\sigma$ subtend the same solid angle, it results:

$$\frac{d\sigma_0}{\rho_1\rho_2} = \frac{d\sigma}{(\rho_1+s)(\rho_2+s)} \tag{2.6}$$

or equivalently

$$|\underline{E}| = |\underline{E}_0|\sqrt{\frac{\rho_1\rho_2}{(\rho_1+s)(\rho_2+s)}} \tag{2.7}$$

It is evident in Fig. 2.3 that rays focus (cross) at different points. As a matter of fact, the tube of rays degenerates into a line and the field intensity approaches infinity when $s=-\rho_1$ or $s=-\rho_2$. The locus of points where this occurs is called *caustic*. It must be stressed that fields have always a finite value and, as a consequence, neither GO or GTD can be used to predict the field strength at caustic points.

As the phase variation along a ray is given by $-ks$, the electric field along a ray can be written as follows:

$$\underline{E} = \underline{E}_0 A(s) e^{-jks} \tag{2.8}$$

wherein $\underline{E}_0$ denotes the electric field at a reference point $P_0$ ($s=0$), $k$ is the propagation constant and $A(s)$ is the spatial attenuation factor, also known as spreading factor. This last reduces to the following expressions in the special case of plane wave ($\rho_1=\infty, \rho_2=\infty$), cylindrical wave ($\rho_1=\infty, \rho_2=\rho$) and spherical wave ($\rho_1=\rho$, $\rho_2=\rho$):

$$A(s) = \begin{cases} 1 & \text{plane-wave} \\ \sqrt{\rho/(\rho+s)} & \text{cylindrical-wave} \\ \rho/(\rho+s) & \text{spherical-wave} \end{cases} \tag{2.9}$$

It is worth to note that when a caustic is crossed, $\rho_i + s$ changes the sign and this corresponds to a phase variation of π/2. Eq. (2.8) allows evaluating the field at a given point $P$ in terms of its value at a reference point $P_0$. It has been derived by using the principle of conservation of energy in a tube of rays. Although it is a valid high frequency approximation for light waves, it could be not accurate for electromagnetic waves of lower frequencies.

### 2.2.2 Reflection from surfaces

GO laws such as Snell's law can be used to determine the field reflected from surfaces. Let us consider a uniform plane wave impinging on a planar surface $S$ assumed perfectly conducting. This case is illustrated in Fig. 2.4, where $\hat{s}^i$ and $\hat{s}^r$ denote the unit vectors in the incidence and reflection directions, respectively. The total field at the reflection point $Q_r$ on $S$ must meet the boundary condition:

$$\hat{n} \times \left( \underline{E}^i + \underline{E}^r \right) = 0 \tag{2.10}$$

$\hat{n}$ being the unit vector normal to $S$.

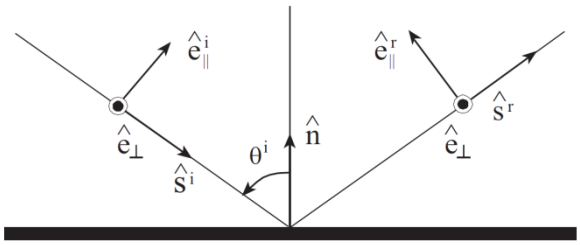


**Figure 2.4** Reflection from a planar surface.

It is opportune to express the incident and reflected fields $\underline{E}^i$ and $\underline{E}^r$ in terms of their components parallel and perpendicular to the incidence plane (that is the plane defined by $\hat{s}^i$ and $\hat{n}$):

$$\underline{E}^i = E^i_{\parallel}\hat{e}^i_{\parallel} + E^i_{\perp}\hat{e}^i_{\perp} \tag{2.11}$$

$$\underline{E}^r = E^r_{\parallel}\hat{e}^r_{\parallel} + E^r_{\perp}\hat{e}^r_{\perp} \tag{2.12}$$

Equation (2.12) can be rewritten in a compact form:

$$\begin{pmatrix} E^r_{\parallel} \\ E^r_{\perp} \end{pmatrix} = \underline{\underline{R}} \begin{pmatrix} E^i_{\parallel} \\ E^i_{\perp} \end{pmatrix} \tag{2.13}$$

where $\underline{\underline{R}} = \begin{pmatrix} 1 & 0 \\ 0 & -1 \end{pmatrix}$ is the dyadic reflection coefficient for a perfectly conducting surface.

With reference to Fig. 2.4, $\hat{e}_{\perp}$ is a unit vector normal to the incidence plane, and $\hat{e}^i_{\parallel}$, $\hat{e}^r_{\parallel}$ are unit vectors parallel to the incidence plane defined by:

$$\hat{e}^i_{\parallel} = \hat{e}^i_{\perp} \times \hat{s}^i \tag{2.14}$$

$$\hat{e}^r_{\parallel} = \hat{e}_{\perp} \times \hat{s}^r \tag{2.15}$$

In agreement with the principle of locality, the field reflected from a surface does not change when this last is no more planar, being always possible to consider the local plane tangent at $Q_r$. Obviously, the spreading factor changes to account for the variation of the reflected wavefront. Therefore, it is possible to express the reflected field as follows:

$$\underline{E}^r(s) = \underline{\underline{R}} \cdot \underline{E}^i(Q_r) A(s) e^{-jks} \tag{2.16}$$

wherein

$$A(s) = \sqrt{\frac{\rho^r_1 \rho^r_2}{\left(\rho^r_1 + s\right)\left(\rho^r_2 + s\right)}} \tag{2.17}$$

and $s$ is the distance between the reflection point $Q_r$ and the observation point $P$. In addition, $\rho_1^r$ and $\rho_2^r$ are the principal curvature radii of the reflected wavefront in $Q_r$. They are related to the principal curvature radii of the incident wavefront $\rho_1^i$. $\rho_2^i$ and to those relevant to the surface $S$ ($a_1$ and $a_2$). It can be shown that $\rho_1^r$ and $\rho_2^r$ are given by [2]:

$$\frac{1}{\rho_1^r} = \frac{1}{2}\left(\frac{1}{\rho_1^i} + \frac{1}{\rho_2^i}\right) + \frac{1}{f_1} \tag{2.18}$$

$$\frac{1}{\rho_2^r} = \frac{1}{2}\left(\frac{1}{\rho_1^i} + \frac{1}{\rho_2^i}\right) + \frac{1}{f_2} \tag{2.19}$$

wherein the parameters $f_1$ and $f_2$ in the particular but more interesting case of spherical wave incidence simplify to:

$$\frac{1}{f_{1,2}} = \frac{1}{\cos\theta^i}\left(\frac{\sin^2\theta_2}{a_1} + \frac{\sin^2\theta_2}{a_2}\right) \pm \pm\sqrt{\frac{1}{\cos\theta^i}\left(\frac{\sin^2\theta_2}{a_1} + \frac{\sin^2\theta_2}{a_2}\right) - \frac{4}{a_1 a_2}} \tag{2.20}$$

In eq. (2.20), $\theta^i$ is the incidence angle, $\theta_1$ and $\theta_2$ are the angles formed by $\hat{s}^i$ and the directions associated to the principal radii of curvature of *S*. In the far field approximation, eq. (2.16) reduces to:

$$\underline{E}^r(s) = \underline{\underline{R}} \cdot \underline{E}^i(Q_r)\sqrt{\rho_1^r \rho_2^r}\,\frac{e^{-jks}}{s} \tag{2.21}$$

It is immediate to verify that in the case of plane wave incidence it results:

$$\sqrt{\rho_1^r \rho_2^r} = \sqrt{a_1 a_2} \tag{2.22}$$

Accordingly, GO fails predicting the reflected field when one or both the curvature radii of $S$ are infinite.

## 2.3 Diffracted Field

In agreement with eq. (2.8), the diffracted field can be expressed as:

$$\underline{E}^d(s) = \underline{E}^d(O') \sqrt{\frac{\rho\rho'}{(\rho+s)(\rho'+s)}} e^{-jks} \tag{2.23}$$

$\underline{E}^d(O')$ being the diffracted field at a reference point $O'$. It is convenient to choose the diffraction point $Q_d$ as reference point.

Let us consider the case of diffraction from an edge which is, obviously, a caustic for the diffracted rays. Accordingly, the limit

$$\lim_{\rho' \to 0} \underline{E}^d(O') \sqrt{\rho'} \tag{2.24}$$

exists and is not zero. Moreover, the diffracted field must be proportional to the incident field in $Q_d$ and thus it is possible to write:

$$\lim_{\rho' \to 0} \underline{E}^d(O') \sqrt{\rho'} = \underline{\underline{D}}\, \underline{E}^i(Q_d) \tag{2.25}$$

wherein $\underline{\underline{D}}$ is usually referred to as dyadic diffraction coefficient. As a consequence, the field diffracted from the point $Q_d$ on the edge is given by:

$$\underline{E}^d(s) = \underline{\underline{D}}\, \underline{E}^i(Q_d) \sqrt{\frac{\rho}{\rho+s}} e^{-jks} \tag{2.26}$$

$\rho$ being the distance between the caustic at the edge and the second caustic for the diffracted rays. In [2] it has been demonstrated that:

$$\frac{1}{\rho} = \frac{1}{\rho_e^i} - \frac{\hat{n}_e \cdot \left(\hat{s}^i - \hat{s}\right)}{a \sin^2 \beta'} \tag{2.27}$$

where $\rho_e^i$ is the curvature radius of the incident wavefront in $Q_d$, taken in the plane containing the incident ray and the unit vector $\hat{e}$ tangent to the edge in $Q_d$ (see Fig. 2.5). Moreover, $a$ is the curvature radius of the edge and $\hat{n}_e$ is the unit vector normal to the edge directed away from the center of curvature. When the distance $\rho$ is positive, the diffracted ray encounters no caustic along its path. Indeed, such a distance is negative only when the second caustic is located on the same side of the observation point. It is opportune to remark that the diffracted field expressed by eq. (2.26) is undefined at the caustic points and crossing such points implies a phase variation of $\pi/2$.

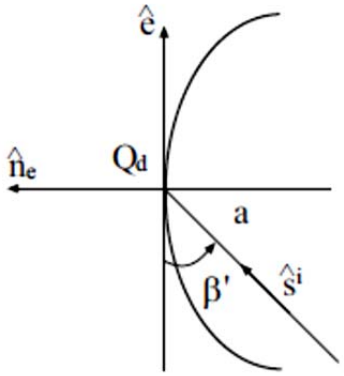


**Figure 2.5** Diffraction from a curved edge.

In the case of vertex diffraction, diffracted rays are originated from a point caustic. Accordingly, it is possible to write:

$$\lim_{\rho' \to 0} \underline{E}^d(O')\rho' = \underline{\underline{D}}\,\underline{E}^i(Q_v) \tag{2.28}$$

and the field diffracted from the vertex can be evaluated as:

$$\underline{E}^d(s) = \underline{\underline{D}}\,\underline{E}^i(Q_v)\frac{e^{-jks}}{s} \tag{2.29}$$

### 2.3.1 Diffraction by perfectly conducting surfaces

The canonical problem of plane wave diffraction by a perfectly conducting edge with planar surfaces has been treated by many authors but the most popular results have been presented by Keller [1]. The related diffraction coefficients are non-uniform, namely not valid at the GO shadow boundaries. This limitation has been overcome thanks to the solution provided by Kouyoumjian [2], [3].

Let us consider a radiating source at a point *S* in presence of a perfectly conducting wedge and observe the field at a point *P*. In accordance with the Fermat's principle, the diffraction points can be determined by minimizing the distance $SQ_dP$. This leads to the law of diffraction:

$$\hat{s}^i \cdot \hat{e} = \hat{s} \cdot \hat{e} \tag{2.30}$$

where $\hat{e}$ is the unit vector directed along the edge, $\hat{s}^i$ and $\hat{s}$ are the unit vectors in the incidence and diffraction directions, respectively. As consequence of eq. (2.30), when a ray impinges on the edge at oblique incidence forming an angle $\beta'$ with respect to $\hat{e}$, the diffracted rays lie on a conical surface whose semi-aperture angle is still $\beta'$. The incident ray direction is usually described by a couple of angles $(\beta', \phi')$ and the position of the diffracted ray on the cone is fixed by the angle $\phi$ (Fig. 2.6).

As suggested by Kouyoumjian and Pathak, it is convenient to define the incidence plane (that containing the incident ray and the unit vector $\hat{e}$) and the diffraction plane (that containing the diffracted ray and the unit vector $\hat{e}$). A reference system in the incidence plane is introduced and fixed by the unit vectors $\hat{\phi}'$, $\hat{\beta}'$, $\hat{s}^i$. In a similar way, a reference system fixed by $\hat{\phi}$, $\hat{\beta}$, $\hat{s}$ is introduced for the

diffracted ray. The unit vectors $\hat{\phi}'$ and $\hat{\phi}$ are perpendicular to the incidence and diffraction planes, respectively. The unit vectors $\hat{\beta}'$ and $\hat{\beta}$ are parallel to the incidence and diffraction planes and defined by:

$$\hat{\beta}' = \hat{s}^i \times \hat{\phi}' \tag{2.31}$$

$$\beta = \hat{s} \times \hat{\phi} \tag{2.32}$$

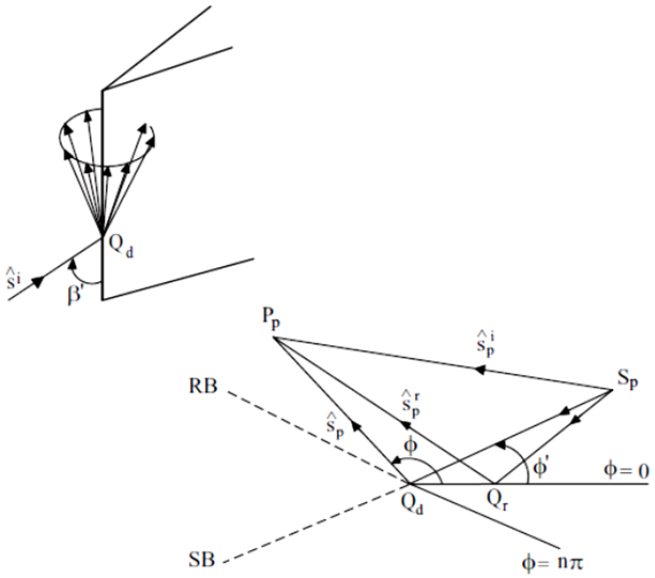


**Figure 2.6** Reflection and diffraction by a wedge.

When adopting these ray-fixed reference systems for describing the incident and diffracted fields, it results:

$$\begin{pmatrix} E_\beta^d \\ E_\phi^d \end{pmatrix} = \begin{pmatrix} -D_s & 0 \\ 0 & -D_h \end{pmatrix} \begin{pmatrix} E_{\beta'}^d \\ E_{\phi'}^d \end{pmatrix} \sqrt{\frac{\rho}{s(\rho+s)}} e^{-jks} \tag{2.33}$$

wherein $D_{s,h}$ are the scalar diffraction coefficients for the *Dirichlet* (soft) and *Neumann* (hard) boundary conditions, respectively.

The uniform diffraction coefficients for a perfectly conducting wedge [2] are reported in the following for reader's convenience:

$$D_{s,h}(\phi,\phi',\beta') = -\frac{e^{-j\pi/4}}{2n\sqrt{2\pi k}\sin\beta'}\cdot$$
$$\cdot\left\{\cot\left(\frac{\pi+(\phi-\phi')}{2n}\right)F\left[kLa^{+}(\phi-\phi')\right]+\right.$$
$$+\cot\left(\frac{\pi-(\phi-\phi')}{2n}\right)F\left[kLa^{-}(\phi-\phi')\right]\mp$$
$$\mp\cot\left(\frac{\pi+(\phi+\phi')}{2n}\right)F\left[kLa^{+}(\phi+\phi')\right]\mp$$
$$\left.\mp\cot\left(\frac{\pi-(\phi+\phi')}{2n}\right)F\left[kLa^{-}(\phi+\phi')\right]\right\} \qquad (2.34)$$

where:

$$F(x) = 2j\sqrt{x}e^{jx}\int_{\sqrt{x}}^{+\infty} e^{-j\tau^2}d\tau \qquad (2.35)$$

is the UTD transition function, $a^{+}$ and $a^{-}$ are defined by:

$$a^{\pm} = 2\cos^2\left(\frac{2n\pi N^{\pm}-x}{2}\right) \qquad (2.36)$$

$N^{\pm}$ being the nearest integers satisfying the following relation:

$$2n\pi N^{\pm} - x = \pm\pi \qquad (2.37)$$

The distance parameter $L$ in (2.34) can be determined by imposing the continuity of the total field at the shadow boundaries [4], thus obtaining:

$$L = \frac{s\left(\rho_e^i + s\right)\rho_1^i \rho_2^i \sin^2 \beta'}{\rho_e^i \left(\rho_1^i + s\right)\left(\rho_2^i + s\right)} \tag{2.38}$$

where $\rho_1^i$, $\rho_2^i$ are the principal radii of curvature of the incident wavefront and $\rho_e^i$ is the curvature radius of the incident wavefront taken in the incidence plane.

Diffraction coefficients for the half-plane can be easily found by setting $n = 2$ in eq. (2.34).

It can be easily verified that in correspondence of a shadow boundary one of the cotangent functions becomes singular whereas its product with the corresponding transition function is finite. Grazing incidence must be considered separately. In this case, $D_s = 0$ and the expression of $D_h$ in eq. (2.34) must be multiplied by the factor 1/2.

When the wedge surfaces are curved (see Fig. 2.1), it is possible to consider in accordance with the principle of locality a wedge with planar surfaces tangent to the faces of the curved wedge. Moreover, the diffraction coefficients (2.34) can be still applied but the parameter $L$ must be properly modified to account for the curvature of the reflected wavefront [2].

## 2.3.2 Slope diffraction

In addition to the edge diffraction contribution (2.33), it is often necessary to consider a higher order term which is proportional to the normal derivative of the incident field at $Q_d$. This contribution may be not negligible when the amplitude of the incident field at $Q_d$ is small. Such type of diffraction is usually referred to as slope diffraction. By similar arguments, it is possible to consider high order slope diffraction terms. When only the first slope diffraction term is considered, the total diffracted field reads as:

$$U_d = \left[ U_i\left(Q_d\right) + \left(\frac{1}{jk}\right)\frac{\partial D_{s,h}}{\partial \phi'}\frac{\partial U_i\left(Q_d\right)}{\partial n} \right] A(s) e^{-jks} \tag{2.39}$$

where $U_d$ denotes a component of the diffracted field, $\partial D_{s,h} / \partial \phi'$ are the slope diffraction coefficients and $\partial U_i / \partial n$ is the normal derivative of the incident field in $Q_d$. Compact expressions for the slope diffraction coefficients relevant to a perfectly conducting wedge can be found in [3].

### 2.3.3 Diffraction by finite conductivity surfaces: UTD heuristic solutions

In the past years, the UTD has been successfully applied to solve a large variety of electromagnetic wave interaction problems with perfectly conducting surfaces, such as the analysis of radiation characteristics of simple and complex antenna systems [5]. However, its extension to finite conductivity structures is in general a non-trivial problem and still subject of continuing research. This interest is justified since in many application fields, such as radio propagation, Radar Cross Section (RCS) prediction, analysis of novel antenna systems, diffraction from not perfectly conducting objects is very frequent and the use of diffraction coefficients (2.34) could lead to inaccurate results. As a consequence, it is essential to have reliable solutions for the field diffracted by not perfectly conducting structures in order to make accurate field predictions. It is opportune to note that rigorous and exact diffraction coefficients have been developed for different surface impedance structures with the Maliuzhinets theory [6]. These are rather cumbersome and, due to their complexity, often not easy to use in routine applications such as propagation prediction tools. Thus, the difficulty arising in using such solutions forces simplifications to be made and to use approximate techniques.

Heuristic solutions have been proposed in the literature with reference to various scattering problems. They are not based on a rigorous solution of Maxwell's equations but on a suitable modification to the diffraction coefficients (2.34) with the aim to compensate the geometrical optics field discontinuities at the shadow boundaries. Moreover, they are easy to handle and computationally simple. The problem of plane wave scattering by a thin lossless dielectric slab has been treated in both the normal and oblique incidence case [7]. The derived diffraction coefficients are an

extension of diffraction coefficients for the perfectly conducting half-plane. Following the same idea in [7], two-dimensional diffraction coefficients have been proposed by Luebbers for the finite conductivity wedge [8] and are currently used in many ray tracing tools. Based on this solution, UTD slope diffraction coefficients have been later developed by the same author [9]. As discussed by Luebbers, the accurate use of these diffraction coefficients is restricted to applications involving wedges with large interior angles, and to the observation in proximity of shadow boundaries. Alternative heuristic UTD diffraction coefficients for not perfectly conducting wedges have been proposed in the recent years to improve the Luebbers' solution accuracy within a wider angular region [10]-[12].

## 2.4 Physical Optics

The field scattered in the far zone by a perfectly conducting object illuminated by an electromagnetic wave is given by:

$$\underline{E}^S = -jk_0\zeta_0 \iint_S \left(\underline{\underline{I}} - \hat{R}\hat{R}\right)\underline{J}_S G\left(\underline{r},\underline{r}'\right) dS \tag{2.40}$$

where $\underline{J}_S$ denotes the current distribution induced on the surface $S$ of the object, $k_0$ and $\zeta_0$ are the wavenumber and the impedance of free space, $G(\underline{r},\underline{r}') = e^{-jk_0|\underline{r}-\underline{r}'|}\Big/\left(4\pi|\underline{r}-\underline{r}'|\right)$ is the Green function and $\underline{r}$, $\underline{r}'$ denote the position vectors at the observation and integration points respectively, $\hat{R}$ is the unit vector from the radiating element at $\underline{r}'$ to the observation point and $\underline{\underline{I}}$ is the (3×3) identity matrix.

Physical Optics approximates the current distribution $\underline{J}_S$ by using geometrical optics and provides accurate results only when the object is far enough from the sources so that the incident field can be described in terms of wavefronts and rays. According to this approximation, the surface current is null in the shadow region. Whereas, at any point $P$ on the object surface in the illuminated region it can be determined by assuming that the incident electric field is

reflected in the same way as it would be from the infinite plane tangent to the surface at $P$ [13].

When the surface $S$ is perfectly conducting, the surface current distribution can be evaluated according to:

$$\underline{J}_S = \hat{n} \times \underline{H} = \hat{n} \times \left( \underline{H}^i + \underline{H}^r \right) = 2\hat{n} \times \underline{H}^i \tag{2.41}$$

where $\hat{n}$ is the unit vector normal to the surface at the incidence point and $\underline{H}^i$ is the incident magnetic field. As a matter of fact, when a plane wave impinges on a perfectly conducting surface, it results for both polarizations (see Figs. 2.7(a) and 2.7(b)):

$$\hat{n} \times \underline{H}^i = \hat{n} \times \underline{H}^r \tag{2.42}$$

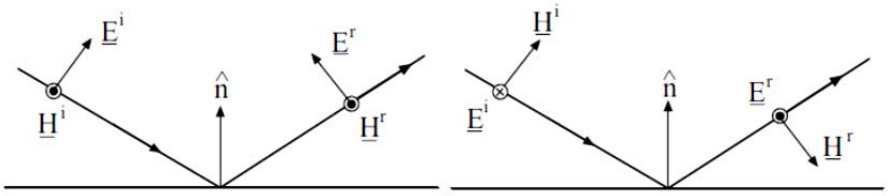


(a) (b)

**Figure 2.7** Reflection from a perfectly conducting surface. Parallel polarization (a). Perpendicular polarization (b).

PO can be also employed to evaluate the field scattered from finite conductivity objects. In such a case, both electric $\underline{J}_s$ and magnetic $\underline{J}_{ms}$ surface currents must be taken into account in the radiation integral and so eq. (2.40) becomes:

$$\underline{E}^s = -jk_0 \iint_S \left[ \left( \underline{\underline{I}} - \hat{R}\hat{R} \right) \left( \zeta_0 \underline{J}_s \right) + \underline{J}_{ms} \times \hat{R} \right] G\left( \underline{r}, \underline{r}' \right) dS \tag{2.43}$$

The accuracy of the results attainable with the PO method depends on the degree of approximation for the surface currents and on the observation direction. As a matter of fact, when the contributions due

to the parts of the object not directly illuminated by the incident field are not negligible, some limitations in the field prediction are expected.

## 2.5 Uniform Asymptotic Physical Optics approach

In the recent years, Uniform Asymptotic Physical Optics solutions have been developed to solve various diffraction problems [14]-[18]. The basic idea to obtain such solutions is the use of a PO approximation of the equivalent surface currents induced by an incident field on a structure. As well-known, the scattered field is expressed by means of the radiation integral (eqns. (2.40) and (2.43)) and it includes both the geometrical optics and the diffraction contributions. The application of the steepest descent method and a uniform asymptotic evaluation of the radiation integral allow deriving the diffraction coefficients in closed form. These last are expressed in terms of the UTD transition function and perfectly compensate the GO field discontinuities. It is opportune to point out that these solutions are inevitably approximate since the surface currents in the radiation integral are not exact but based on a PO approximation. In spite of this they are quite accurate when compared with more rigorous solutions and are simple, easy to handle and to implement. For these reason, they are potentially useful for practical applications when no exact analytical solutions are available or when these last cannot be evaluated in an efficient way. Although heuristic and efficient solutions have been proposed in the literature (see Subsec. 2.3.3) to solve diffraction problems having no exact solutions, they are not based on a rigorous analytical procedure and, therefore, should be used with considerable attention.

The key points showing how to construct a UAPO solution are reviewed in the following with reference to the problem of plane wave diffraction by a penetrable half-plane surrounded by free-space [18].

Let us consider the oblique incidence of an arbitrarily polarized plane wave over a penetrable half-plane surrounded by free-space (see Fig. 2.8). The incidence direction is fixed by the angles $\beta'$ and $\phi'$. In particular, $\beta'$ is a measure of the incidence direction skewness with

respect to the edge ($\beta' = \pi/2$ corresponds to the normal incidence). The observation direction is specified by the angles $\beta$ and $\phi$. It is convenient to introduce the ray-fixed coordinate systems $\left(\hat{s}, \hat{\beta}', \hat{\phi}'\right)$ and $\left(\hat{s}, \hat{\beta}, \hat{\phi}\right)$ for the source and the observation points, respectively (see Fig. 2.8) and to assume the observation point *P* on the Keller's diffraction cone, i.e. $\beta = \beta'$.

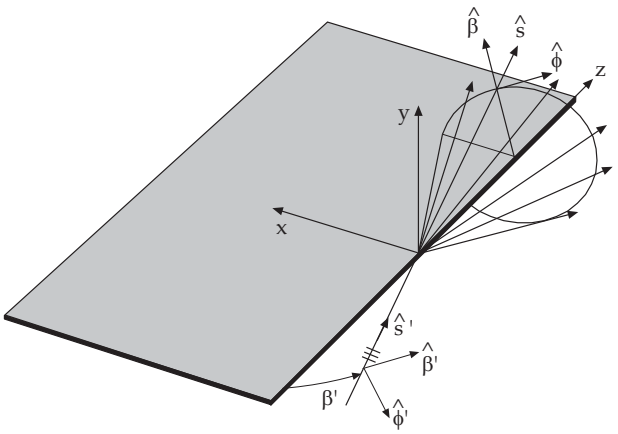


**Figure 2.8** Diffraction by the half-plane edge.

At any observation point *P*, the total electric field $\underline{E}$ is given by the superposition of the incident field $\underline{E}^i$ and the scattered field $\underline{E}^s$. By applying the equivalence theorem, the surface currents induced by an incident plane wave on the surface *S* of the half-plane can be interpreted as sources of $\underline{E}^s$ and therefore, in the far-field approximation, the scattered field can be expressed by means of the following radiation integral

$$\underline{E}^s = -jk_0 \iint_S \left[ (\underline{\underline{I}} - \hat{R}\hat{R})\zeta_0 \underline{J}_s^{PO} + \underline{J}_{ms}^{PO} \times \hat{R} \right] G(\underline{r}, \underline{r}')\, dS \qquad (2.44)$$

in which the observation and source points are denoted by $\underline{r} = x\,\hat{x} + y\,\hat{y} + z\,\hat{z} = \underline{\rho} + z\,\hat{z}$ and $\underline{r}' = x'\,\hat{x} + z'\,\hat{z} = \underline{\rho}' + z'\,\hat{z}$.

By using a PO approximation for the equivalent electric and magnetic surface currents on $S$ and expressing the fields in terms of their parallel and perpendicular components, it results:

$$\zeta_0 \underline{J}_s^{PO} = \zeta_0 \underline{J}_s^{*}\, e^{jk_0(x'\sin\beta'\cos\phi' - z'\cos\beta')} \tag{2.45}$$

$$\underline{J}_{ms}^{PO} = \underline{J}_{ms}^{*} e^{jk_0(x'\sin\beta'\cos\phi' - z'\cos\beta')} \tag{2.46}$$

and the three-dimensional Green function can be written as:

$$G(\underline{r},\underline{r}') = \frac{e^{-jk_0|\underline{r}-\underline{r}'|}}{4\pi|\underline{r}-\underline{r}'|} = \frac{e^{-jk_0\sqrt{|\underline{\rho}-\underline{\rho}'|^2+(z-z')^2}}}{4\pi\sqrt{|\underline{\rho}-\underline{\rho}'|^2+(z-z')^2}} \tag{2.47}$$

To evaluate the edge diffraction confined to the Keller cone for which $\beta = \beta'$, it is possible to approximate $\hat{R}$ by the unit vector $\hat{s}$ in the diffraction direction [19]

$$\hat{R} = \hat{s} = \sin\beta'\cos\phi\;\hat{x} + \sin\beta'\sin\phi\;\hat{y} + \cos\beta'\;\hat{z} \tag{2.48}$$

Accordingly, it results:

$$\underline{E}^s = -\frac{jk_0}{4\pi}\left[(\underline{\underline{I}} - \hat{s}\hat{s})\zeta_0\underline{J}_s^{*} + \underline{J}_{ms}^{*}\times\hat{s}\right]\cdot$$

$$\cdot\int_0^{\infty}\int_{-\infty}^{\infty} e^{jk_0(x'\sin\beta'\cos\phi' - z'\cos\beta')}\frac{e^{-jk_0\sqrt{|\underline{\rho}-\underline{\rho}'|^2+(z-z')^2}}}{\sqrt{|\underline{\rho}-\underline{\rho}'|^2+(z-z')^2}}\,dz'\,dx' =$$

$$= \left[(\underline{\underline{I}} - \hat{s}\hat{s})\zeta_0\underline{J}_s^{*} + \underline{J}_{ms}^{*}\times\hat{s}\right] I_s \tag{2.49}$$

The expressions of the PO surface currents in terms of the incident electric field are here obtained by assuming such currents as

equivalent sources originated by the discontinuities of the tangential GO field components across the layer, i.e.,

$$\underline{J}_s^{PO} = \hat{y}\times\left(\underline{H}^+ - \underline{H}^-\right)\Big|_S = \hat{y}\times\left(\underline{H}^i + \underline{H}^r - \underline{H}^t\right)\Big|_S = \\ = \hat{y}\times\left(\underline{H}_0^i + \underline{H}_0^r - \underline{H}_0^t\right)e^{jk_0\left(x'\sin\beta'\cos\phi' - z'\cos\beta'\right)} \tag{2.50}$$

$$\underline{J}_{ms}^{PO} = \left(\underline{E}^+ - \underline{E}^-\right)\Big|_S \times \hat{y} = \left(\underline{E}^i + \underline{E}^r - \underline{E}^t\right)\Big|_S \times \hat{y} = \\ = \left[\left(\underline{E}_0^i + \underline{E}_0^r - \underline{E}_0^t\right)\times\hat{y}\right]e^{jk_0\left(x'\sin\beta'\cos\phi' - z'\cos\beta'\right)} \tag{2.51}$$

As well-known, it is convenient to work in the standard plane of incidence and to consider the GO field components parallel ($\|$) and perpendicular ($\perp$) to it. Therefore, it results:

$$\zeta_0\underline{J}_s^* = \left(E_\perp^i - E_\perp^r - E_\perp^t\right)\cos\theta^i\hat{e}_\perp + \left(E_\|^i + E_\|^r - E_\|^t\right)\hat{t} \tag{2.52}$$

$$\underline{J}_{ms}^* = \left(E_\|^i - E_\|^r - E_\|^t\right)\cos\theta^i\hat{e}_\perp + \left(E_\perp^i + E_\perp^r - E_\perp^t\right)\hat{t} \tag{2.53}$$

wherein $E_\|^i$ and $E_\perp^i$ are the incident electric field components (at the origin) parallel and perpendicular to the ordinary plane of incidence, $\theta^i$ is the incidence angle in such a plane, $\hat{e}_\perp = \left(\hat{s}'\times\hat{y}\right)/\left|\hat{s}'\times\hat{y}\right|$ is the unit vector normal to the ordinary plane of incidence, $\hat{s}'$ being the unit vector of the incidence direction, and $\hat{t} = \hat{y}\times\hat{e}_\perp$. The reflected and transmitted field components can be expressed in terms of the incident field components by means of the reflection matrix $\underline{\underline{R}}$ and transmission matrix $\underline{\underline{T}}$, and their expressions can be found in [18].

As well-known, in the high-frequency approximation, the PO integral (2.44) extended to $S_0$ can be reduced asymptotically to a sum of ray field contributions from (isolated) interior stationary phase

points on $S_0$ and an edge diffracted field contribution. To this end, it is necessary to perform the evaluation of the following integral:

$$I_s = -\frac{jk_0}{4\pi}\cdot$$
$$\cdot\int_0^{\infty} \mathrm{e}^{jk_0 x'\sin\beta'\cos\phi'} \int_{-\infty}^{\infty} e^{-jk_0 z'\cos\beta'} \frac{e^{-jk_0\sqrt{\left|\underline{\rho}-\underline{\rho}'\right|^2+(z-z')^2}}}{\sqrt{\left|\underline{\rho}-\underline{\rho}'\right|^2+(z-z')^2}}\, dz'\, dx' \tag{2.54}$$

As reported in [19], by making the substitution $z'-z=\left|\underline{\rho}-\underline{\rho}'\right|\sinh\zeta$ and using one of the integral representations of the zeroth order Hankel function of the second kind $H_0^{(2)}$ it results:

$$\int_{-\infty}^{\infty} e^{-jk_0 z'\cos\beta'} \frac{e^{-jk_0\sqrt{\left|\underline{\rho}-\underline{\rho}'\right|^2+(z-z')^2}}}{\sqrt{\left|\underline{\rho}-\underline{\rho}'\right|^2+(z-z')^2}}\, dz' =$$
$$= -j\pi\, e^{-jk_0 z\cos\beta'}\, H_0^{(2)}\left(k_0\left|\underline{\rho}-\underline{\rho}'\right|\sin\beta'\right) \tag{2.55}$$

The involved Hankel function can be now written with the useful integral representation

$$H_0^{(2)}\left(k_0\left|\underline{\rho}-\underline{\rho}'\right|\sin\beta'\right) = \frac{1}{\pi}\int_C e^{-jk_0\left|\underline{\rho}-\underline{\rho}'\right|\sin\beta'\cos(\theta\mp\alpha)} d\alpha \tag{2.56}$$

where $C$ is the integration path in the complex $\alpha$-plane (see Fig. 2.9). The angle $\theta$ is between the illuminated face and the vector $\underline{\rho}-\underline{\rho}'$, and the sign $-$ (+) applies if $y>0$ ($y<0$). If $\rho=\left|\underline{\rho}\right|$, according to

the geometry shown in Fig. 2.10, $\left|\underline{\rho}-\underline{\rho}'\right|\sin\theta=\rho\sin\phi$ and $\left|\underline{\rho}-\underline{\rho}'\right|\cos\theta=\rho\cos\phi-x'$, so obtaining

$$H_0^{(2)}\left(k_0\left|\underline{\rho}-\underline{\rho}'\right|\sin\beta'\right)=\frac{1}{\pi}\int_C e^{-jk_0\rho\sin\beta'\cos(\alpha\mp\phi)}e^{jk_0x'\sin\beta'\cos\alpha}\,d\alpha \tag{2.57}$$

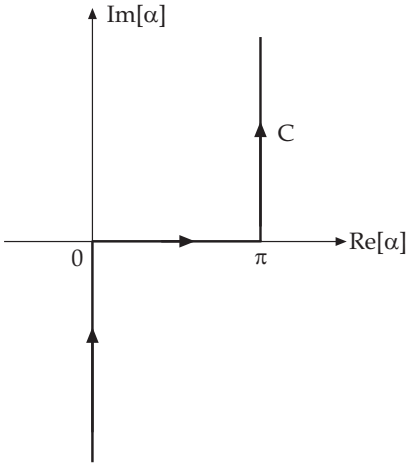


**Figure 2.9** Integration path in the complex $\alpha$-plane.

and then:

$$I_s=-\frac{k_0}{4\pi}e^{-jk_0z\cos\beta'}\cdot$$
$$\cdot\int_0^\infty\int_C e^{-jk_0\rho\sin\beta'\cos(\alpha\mp\phi)}e^{jk_0x'\sin\beta'(\cos\alpha+\cos\phi')}\,d\alpha\,dx'=$$
$$=-\frac{k_0}{4\pi}e^{-jk_0z\cos\beta'}\cdot$$
$$\cdot\int_C e^{-jk_0\rho\sin\beta'\cos(\alpha\mp\phi)}\int_0^\infty e^{jk_0x'\sin\beta'(\cos\alpha+\cos\phi')}\,dx'\,d\alpha \tag{2.58}$$

By applying the Sommerfeld-Maliuzhinets inversion formula, it results:

$$\int_0^{\infty} e^{jk_0 x' \sin\beta' \left(\cos\alpha + \cos\phi'\right)} \, dx' = \frac{-1}{jk_0 \sin\beta' \left(\cos\alpha + \cos\phi'\right)} \tag{2.59}$$

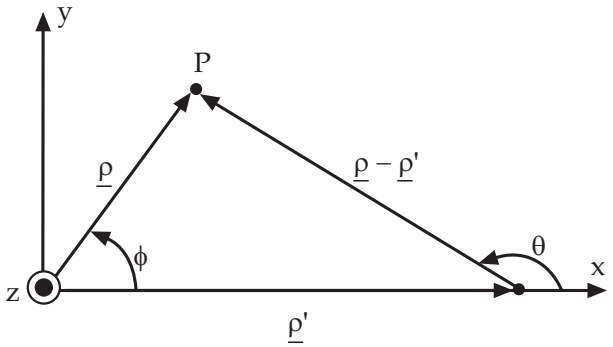


**Figure 2.10** Integration path in the complex $\alpha$ -plane.

so that

$$I_s = \frac{e^{-jk_0 z \cos\beta'}}{2\sin\beta'} \; \frac{1}{2\pi j} \int_C \frac{e^{-jk_0 \rho \sin\beta' \cos(\alpha \mp \phi)}}{\cos\alpha + \cos\phi'} \, d\alpha \tag{2.60}$$

where the sign $-$ (+) applies in the range $0 < \phi < \pi$ ($\pi < \phi < 2\pi$). Such an integral can be evaluated by using the *Steepest Descent Method* [19]. To this end, the integration path *C* is closed with the Steepest Descent Path (SDP) passing through the pertinent saddle point $\alpha_s$ as shown in Fig. 2.11. According to the Cauchy residue theorem, the contribution related to the integration along *C* (distorted for the presence of singularities in the integrand) is equivalent to the sum of the integral along the SDP and the residue contributions $\mathrm{Re}s_i\left(\alpha_p\right)$ associated with all those poles that are inside the closed path *C*+SDP, i.e.,

$$I_s(\Omega)=\frac{1}{2\pi j}\int_C g(\alpha)e^{\Omega f(\alpha)}\,d\alpha=$$
$$=\sum_i \mathrm{Re}\,s_i(\alpha_p)-\frac{1}{2\pi j}\int_{\mathrm{SDP}} g(\alpha)e^{\Omega f(\alpha)}\,d\alpha=$$
$$=\sum_i \mathrm{Re}\,s_i(\alpha_p)+I(\Omega) \tag{2.61}$$

in which

$$I(\Omega)=-\frac{1}{2\pi j}\int_{\mathrm{SDP}} g(\alpha)e^{\Omega f(\alpha)}\,d\alpha=$$
$$=-\frac{e^{\Omega f(\alpha_s)}}{2\pi j}\int_{\mathrm{SDP}} g(\alpha)e^{\Omega\left[f(\alpha)-f(\alpha_s)\right]}\,d\alpha \tag{2.62}$$

$$g(\alpha)=\frac{\mathrm{e}^{-jk_0 z\cos\beta'}}{2\sin\beta'}\frac{1}{\cos\alpha+\cos\phi'}=\frac{A}{\cos\alpha+\cos\phi'} \tag{2.63}$$

$\Omega=k_0\rho$ and $f(\alpha)=-j\sin\beta'\cos(\alpha\mp\phi)$. Note that $\Omega$ is typically large, $\alpha_p=\pi-\phi'$ and $\alpha_s=\phi$ ($\alpha_s=2\pi-\phi$) if $0<\phi<\pi$ ($\pi<\phi<2\pi$). Moreover, by putting $\alpha=\alpha'+j\alpha''$ and imposing that $\mathrm{Im}\left[f(\alpha)\right]=\mathrm{Im}\left[f(\alpha_s)\right]$ and $\mathrm{Re}\left[f(\alpha)\right]\le\mathrm{Re}\left[f(\alpha_s)\right]$, the considered SDP is described by:

$$\alpha'=\alpha_s+\mathrm{sgn}(\alpha'')\cos^{-1}\left(\frac{1}{\cosh\alpha''}\right)=\alpha_s+gd(\alpha'') \tag{2.64}$$

where $gd(\alpha'')$ is the Gudermann function. By using now the change of variable $f(\alpha)-f(\alpha_s)=-\tau^2<0$, eq. (2.62) can be written as

$$I(\Omega) = \pm \int_{-\infty}^{\infty} G(\tau)\, e^{-\Omega\tau^2} d\tau \tag{2.65}$$

wherein

$$G(\tau) = \frac{1}{2\pi j} g\left(\alpha(\tau)\right) e^{\Omega f(\alpha_s)} \frac{d\alpha}{d\tau} \tag{2.66}$$

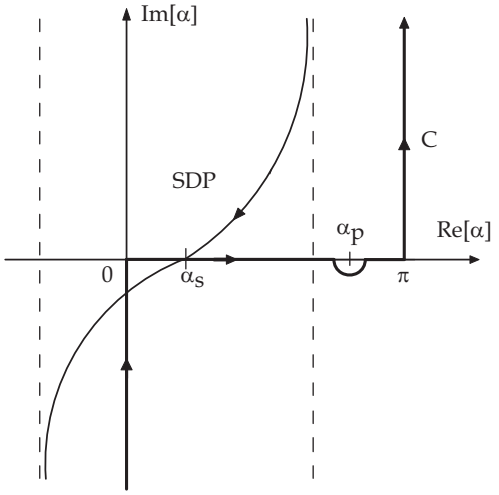


**Figure 2.11** SDP in the complex $\alpha$ -plane.

When $\alpha_p$ is approaching $\alpha_s$, the function $G(\tau)$ cannot be expanded in a Taylor series. To overcome this drawback it is convenient to regularise the integrand in (2.65) using the Multiplicative Method. It requires introducing the regularised function

$$G_p(\tau) = \left(\tau - \tau_p\right) G(\tau) \tag{2.67}$$

with

$$\tau_p^2 = f(\alpha_s) - f\left(\alpha_p\right) = -j \sin\beta' \left[1 + \cos\left(\phi \pm \phi'\right)\right] =$$

$$= -j2\sin\beta'\cos^2\left(\frac{\phi \pm \phi'}{2}\right) = -j\delta \tag{2.68}$$

and $\delta$ is a measure of the distance between $\alpha_p$ and $\alpha_s$. Accordingly,

$$I(\Omega) = \pm \int_{-\infty}^{\infty} G_p(\tau) \frac{e^{-\Omega\tau^2}}{\tau - \tau_p} d\tau \tag{2.69}$$

Since $G_p(\tau)$ is analytic near $\tau = 0$, it can be expanded in a Taylor series. By retaining only the first term (i.e., the $\Omega^{-1/2}$-order term) since $\Omega \gg 1$, it results:

$$I(\Omega) \simeq \pm\left[\sqrt{\frac{\pi}{\Omega}} \frac{G_p(0)}{(-\tau_p)} F_t\left(j\Omega\tau_p^2\right)\right] \tag{2.70}$$

in which

$$\frac{G_p(0)}{(-\tau_p)} = G(0) = \frac{1}{2\pi j} g(\alpha_s) e^{\Omega f(\alpha_s)} \left.\frac{d\alpha}{d\tau}\right|_{\tau=0} =$$
$$= \frac{1}{2\pi j} \frac{A\, e^{-j\Omega\sin\beta'}}{\cos\phi + \cos\phi'} \left[\pm\sqrt{\frac{2}{\sin\beta'}}\, e^{j\pi/4}\right] \tag{2.71}$$

and

$$F_t(\eta) = 2j\sqrt{\eta}\, e^{j\eta} \int_{\sqrt{\eta}}^{\infty} e^{-j\xi^2} d\xi \tag{2.72}$$

is the UTD transition function [2]. By substituting (2.68) and (2.71) in (2.70), the explicit form of the asymptotic evaluation of $I(\Omega)$ is:

$$I(\Omega) \simeq \frac{e^{-j\pi/4}}{2\sqrt{2\pi k_0 \rho \sin\beta'}} \frac{e^{-jk_0(\rho\sin\beta' + z\cos\beta')}}{\sin\beta'(\cos\phi + \cos\phi')} \cdot$$

$$\cdot F_t\left(2k_0\rho\sin\beta'\cos^2\left(\frac{\phi \pm \phi'}{2}\right)\right) =$$

$$= \frac{e^{-j\pi/4}}{2\sqrt{2\pi k_0}} \frac{e^{-jk_0 s}}{\sqrt{s}} \frac{1}{\sin^2\beta'(\cos\phi + \cos\phi')} \cdot$$

$$\cdot F_t\left(2k_0 s\sin^2\beta'\cos^2\left(\frac{\phi \pm \phi'}{2}\right)\right) \qquad (2.73)$$

where the identities $\rho = s\sin\beta'$ and $z = s\cos\beta'$ are used on the diffraction cone. The above analytic result contributes to the UAPO diffracted field to be added to the GO field and is referred to as a uniform asymptotic solution because $I(\Omega)$ is well-behaved when $\alpha_p \to \alpha_s$. In the GTD framework, the matrix formulation for the scattered field can be written as

$$\underline{E}^s = \begin{pmatrix} E_\beta^s \\ E_\phi^s \end{pmatrix} = \underline{\underline{M}} \begin{pmatrix} E_{\beta'}^i \\ E_{\phi'}^i \end{pmatrix} I_s \qquad (2.74)$$

As a consequence the UAPO edge diffraction contribution $\underline{E}^d$ is:

$$\underline{E}^d = \begin{pmatrix} E_\beta^d \\ E_\phi^d \end{pmatrix} = \underline{\underline{M}} \begin{pmatrix} E_{\beta'}^i \\ E_{\phi'}^i \end{pmatrix} I(\Omega) = \underline{\underline{D}} \begin{pmatrix} E_{\beta'}^i \\ E_{\phi'}^i \end{pmatrix} \frac{e^{-jk_0 s}}{\sqrt{s}} \qquad (2.75)$$

where the UAPO solution for the $2\times 2$ diffraction matrix

$$\underline{\underline{D}} = \begin{pmatrix} -D_{\beta\beta'} & -D_{\beta\phi'} \\ -D_{\phi\beta'} & -D_{\phi\phi'} \end{pmatrix} =$$

$$= \begin{pmatrix} -M_{11} & -M_{12} \\ -M_{21} & -M_{22} \end{pmatrix} \frac{1}{2\sqrt{2\pi k_0}} \frac{e^{-j\pi/4}}{\sin^2 \beta' (\cos\phi + \cos\phi')} \cdot$$
$$\cdot F_t \left( 2k_0 s \sin^2 \beta' \cos^2 \left( \frac{\phi \pm \phi'}{2} \right) \right) \tag{2.76}$$

where the sign $+(-)$ applies if $0 < \phi < \pi$ $(\pi < \phi < 2\pi)$. The explicit expression of the coefficients $M_{ij}$ $(i, j = 1, 2)$ can be found in [18]. Accordingly, the UAPO solutions have the same ease of handling of those derived in the UTD framework and, in addition, they have the inherent advantage of providing the diffracted field from the knowledge of the GO response of the structure. In other words, it is sufficient to make explicit the reflection and transmission coefficients related to the considered structure for obtaining the UAPO diffraction coefficients.

# Chapter 3

# High frequency diffraction by an arbitrary-angled dielectric wedge

The problem of diffraction by a dielectric wedge has great relevance for practical applications. The accurate path loss prediction in radio wave propagation environments requires a correct characterization of diffraction contributions arising from the presence of edges and corners. However, the research activity focused mainly on impenetrable structures at high frequency and rigorous solutions have been reported in the literature for perfectly conducting wedges or impedance wedges. Starting from these solutions, there have been some attempts to extend their validity to the penetrable structures. This methods result to be complicated and manageable just for simple configurations, so it has been necessary to build up new approaches for this kind of problems. The lack of an exact and, at the same time, computationally efficient solution which can be employed in ray tracing tools forces simplifications to be made and to apply approximate solutions.

The aim of this chapter is to provide a UAPO solution for the field diffracted by the edge of a lossless arbitrary-angled dielectric wedge in the case of normal incidence. The solution is derived by means of the decomposition of the considered scattering problem into two sub-problems relevant to external and internal regions of the wedge. For each of them, proper equivalent currents, which can be interpreted as sources for the scattered fields, are determined by taking into account the penetrable nature of the structure. Then, uniform asymptotic evaluations of the radiation integrals allow deriving closed form expressions for the diffracted field. As demonstrated by numerical examples, the here developed UAPO solution compensates the GO field discontinuities in the exterior and interior regions. Furthermore,

its accuracy is confirmed by the good agreement attained with results provided by numerical methods.

## 3.1 Diffraction by dielectric wedges: state of the art

The problem of plane wave diffraction by wedges has received great attention due to the importance of its solutions in radio propagation planning, analysis and design of radiating structures and waveguide theory. The first studies have concerned wedges with perfectly conducting surfaces [2], [6] or impedances faces [14], [20], [21]. Heuristic solutions have also been proposed in [8], [9] for solving diffraction problems in the case of dielectric structures. Although efficient, they are not based on a rigorous analytical procedure and, therefore, should be used with considerable attention.

Rawlins [22] presented an approximate solution for the field produced when an electromagnetic plane wave is diffracted by an arbitrary-angled dielectric wedge, whose refractive index is near unity. It was obtained from an application of the Kontorovich-Lebedev transform and a formal Neumann-type expansion. The results were in agreement with those derived by the same author with reference to a right-angled wedge [23]. The diffracted field of an *E*-polarized plane wave by a dielectric wedge was formulated in terms of integral equations by Bernsten in [24]. These were transformed into Fredholm integral equations and solved by iterative methods for limited values of the dielectric constant. Joo *et al.* [25] proposed an asymptotic solution for the field diffracted by a right-angled dielectric wedge based on a correction of PO approximation to the edge diffraction. The correction in the far-field zone was calculated by solving a dual series equation agreeable to simple numerical evaluation. The extension of the approach to arbitrary-angled wedges was addressed in two companion papers [26] and [27]. Burge *et al.* [28], starting from a PO version of the GTD, provided an edge coefficient for the external and internal diffraction by an arbitrary-angled dielectric wedges.

Rouviere *et al.* in [29] improved the Luebbers' heuristic solution [8] in the UTD framework [2] by adding two new terms that compensate the discontinuity created by the field transmitted through the structure. Another heuristic solution for the diffraction coefficient

of a penetrable wedge has been proposed in [30] by Bernardi *et al.*. It is obtained by a modification of the exact UTD diffraction coefficient related to the metallic wedge.

The FDTD method was applied in [31] and [32], providing numerical results for the diffraction coefficient of right-angled wedges made of perfect electrical conductor (PEC), lossless dielectric and lossy dielectric material.

Another interesting attempt to solve the problem of the diffraction by a right-angled dielectric wedge was proposed by Radlow [33]. He used multidimensional Wiener-Hopf equations to model the problem, but the factorization of these equations needs function-theoretic techniques employing two complex variables that are cumbersome to handle. Bates [34] introduced iterative formulas to obtain a set of basic wave-functions useful to represent the sources situated on the plane of symmetry of an arbitrary-angled dielectric wedge. Seo and Ra [35] proposed a remarkable methodology to evaluate the scattering from a lossy dielectric wedge: reflected and refracted GO fields are obtained by inhomogeneous plane wave tracing in the lossy medium, while PO approximation in the edge diffracted fields are accurately corrected by adding the multipole line sources at the edge of the wedge to satisfy the extinction theorem. The unknown expansion coefficients used at the tip of the wedge to make disappearing the extinction integral are evaluated numerically. Salem *et al.* [36] extended Rawlins' approach [22] to a more general form of excitation (line source) of a dielectric wedge. They expressed the Kontorovich-Lebedev transform functions as a Neumann series and represented the scattered field as a Bessel function series, so extending solutions to the case of real valued wavenumbers and arbitrarily positioned source and observer. Daniele and Lombardi [37] analyzed the problem of diffraction of an incident plane wave by an isotropic penetrable wedge in the general case of skew incidence. They used generalized Wiener-Hopf equations, and the solution is obtained using analytical and numerical-analytical approaches that reduce the Wiener-Hopf factorization to Fredholm integral equations of second kind. Vasilev *et al.* [38], [39] developed a numerical approach based on the method of integral equations to solve the problem. They represented the unknown surface currents on the dielectric wedge as a sum of uniform and non-uniform components (using the Ufimtsev's method), making

possible the derivation of the numerical solution. Budaev [40] developed a hybrid methodology to solve the problem of diffraction by a dielectric wedge in an exact sense, which combines analytical and numerical techniques.

UAPO solutions were proposed in explicit closed form in [41] and [42] for evaluating the field diffracted by right- and obtuse-angled lossless dielectric wedges in the inner and outer regions. The UAPO-based approach has been also applied to acute-angled wedges in [43] considering a specific range of incidence directions for both cases of *E*- and *H*-polarized plane wave. Then, in [44] the analysis has been extended to all possible cases of incidence direction providing generalized UAPO solutions which are valid for the diffraction by a wedge with arbitrary aperture.

## 3.2 Diffraction by an arbitrary-angled dielectric wedge

In this section the UAPO solutions for the diffracted field originated by an arbitrary-angled lossless dielectric wedge are determined for an incident plane wave. The geometry used as reference in the following is relevant to a wedge having an acute internal apex angle. This choice is justified by the complexity of the propagation mechanisms (multiple internal and external rays) which include those concerning right- and obtuse-angled wedges [41], [42], as will be demonstrated at the end of this chapter.

Let us consider the problem of the diffraction of an *E*-polarized plane-wave by the edge of an acute-angled dielectric wedge (see Fig. 3.1). Its internal apex angle is $\alpha$ and its material is lossless, non-magnetic ($\mu_r = 1$), with relative permittivity $\varepsilon_r$ and propagation constant $k_d = k_d\sqrt{\varepsilon_r}$. The wedge surfaces are denoted by $S_0$ and $S_n$. A Cartesian reference system $(x, y, z)$ is introduced with the *y*-axis normal to the face $S_0$ and the *z*-axis directed along the edge. The incidence direction is assumed perpendicular to the edge (see Fig. 3.1) and defined by the angle $\phi'$ ($\phi' = 0$ corresponds to the grazing incidence with respect to $S_0$).

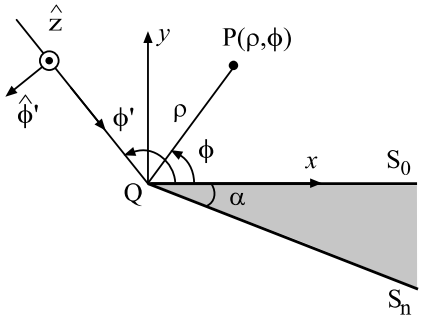


**Figure 3.1** Geometry of the diffraction problem.

The observation point is denoted by $P(\rho,\phi)$. The structure divides the space in two regions: the exterior region $(0<\phi<2\pi-\alpha)$ and the interior region $(2\pi-\alpha<\phi<2\pi)$.

### 3.2.1 GO field model for $0 < \phi' < \pi/2$

Closed form expressions for the GO response when $0<\phi'<\pi/2$ are derived in this section.

Only the face $S_0$ is directly illuminated by the incident field. A transmitted ray exists in the inner region and, in absence of total internal reflection on $S_n$, it is transmitted through this last. The reflected ray travels toward $S_0$ and gives rise to following reflection and transmission mechanisms involving $S_0$ and $S_n$. When the value of the internal angle of incidence makes to occur the inversion the rays begin to go far from the apex. Accordingly, two series of internal and external rays exist: the first contains rays (black arrows in Fig. 3.2) travelling towards the apex and the second comprises those (red arrows in Fig. 3.2) going far from the apex, as illustrated in Fig. 3.2. The external rays exist until the internal total reflection doesn't occur. The number of pre- and post-inversion rays is determined by the values of $\phi'$, $\alpha$ and $\varepsilon_r$. In order to better understand the ray propagation inside and outside the wedge, the reader can refer to Fig. 3.3. If $\theta_0^i=\pi/2-\phi'$ is the external incidence angle, the wave

penetrates into the wedge through $S_0$ with the transmission angle $\theta_{0L}^t = \sin^{-1}\left(\sin\theta^i / \sqrt{\varepsilon_r}\right)$ and propagates toward $S_n$.

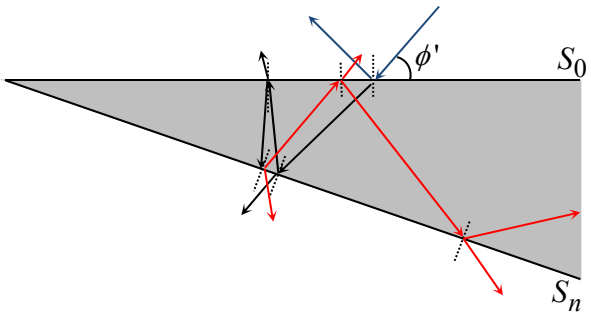


**Figure 3.2** Internal reflection and external transmission.

The ray impinges on $S_n$ with the incidence angle $\theta_1^i$ and, for the Snell's laws, it is reflected ($\theta_1^r = \theta_1^i$) and transmitted through $S_n$ with the angle $\theta_1^t$, as shown in Fig. 3.3. According to the considered values of $\phi'$ and $\varepsilon_r$, the total internal reflection can occur and no transmitted wave through $S_n$ exists. In such a case, an evanescent wave propagating along $S_n$ and attenuating in the direction normal to it arises. The condition ensuring the absence of total reflection at $P_1$ is:

$$\theta_1^i \le \theta^c = \arcsin\left(1/\sqrt{\varepsilon_r}\right) \tag{3.1}$$

where $\theta^c$ is the corresponding critical angle.

By denoting with $\hat{s}^i = (-\cos\phi', -\sin\phi', 0)$ the unit vector in the incidence direction, it results:

$$\underline{E}^i = E_0 e^{-jk_0 \hat{s}^i \cdot \underline{r}} \hat{z} = E_0 e^{jk_0 \rho \cos(\phi - \phi')} \hat{z} \tag{3.2}$$

wherein $E_0$ is the amplitude of the incident field at the origin. The field $\underline{E}^{r0}$ reflected by $S_0$ can be determined as:

$$\underline{E}^{r0} = R_0 \underline{E}^i(P_0) e^{-jk_0 dr_0} \tag{3.3}$$

where $R_0$ is the reflection coefficient at $P_0$ and $dr_0$ is the distance

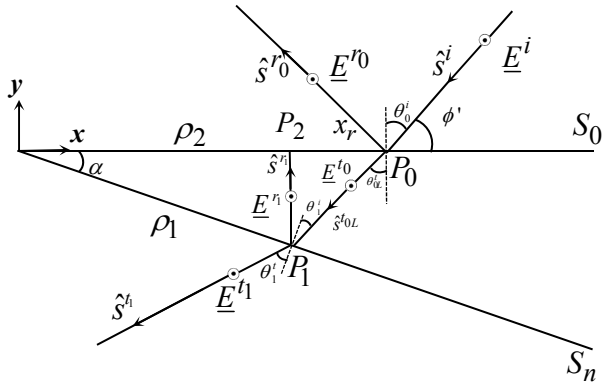


**Figure 3.3** Rays transmissions/reflections through the wedge

from $P_0$ to $P$ along the reflected ray:

$$dr_0 = -\rho\cos(\phi+\phi') + x_r\cos\phi' \tag{3.4}$$

in which $x_r$ is the coordinate of $P_0$. As a result, eq. (3.3) reads as:

$$\underline{E}^{r0} = R_0 E_0 e^{jk_0\rho\cos(\phi+\phi')}\hat{z} \tag{3.5}$$

As regards the field $\underline{E}^{t0L}$ transmitted through $S_0$, it results:

$$\underline{E}^{t0L} = T_0 \underline{E}^i(P_0) e^{-jk_0 dt_0} \tag{3.6}$$

$T_0$ being the transmission coefficient at $P_0$ and $dt_0$ is the distance from $P_0$ to $P$ along the transmitted ray:

$$dt_0 = -\rho \sin\left(\phi + \theta_{0L}^t\right) + x_r \sin\theta_{0L}^t \tag{3.7}$$

As a consequence, it results:

$$\underline{E}^{t0L} = T_0 E_0 e^{jk_0 x_r\left(\cos\phi' - \sqrt{\varepsilon_r}\sin\theta_{0L}^t\right)} e^{jk_d \rho \sin\left(\phi + \theta_{0L}^t\right)} \hat{z} = \\ = T_0 E_0 e^{jk_d \rho \sin\left(\phi + \theta_{0L}^t\right)} \hat{z} \tag{3.8}$$

The field $\underline{E}^{r1}$ transmitted through $S_0$ and then reflected at $P_1(\rho_1, \phi_1)$ on $S_n$ with $\phi_1 = 2\pi - \alpha$ is given by:

$$\underline{E}^{r1} = R_1 \underline{E}^{t0L}\left(P_1\right) e^{-jk_d dr_1} \tag{3.9}$$

wherein $R_1$ is the reflection coefficient at $P_1$ and $dr_1$ is the distance from $P_1$ to $P$ along the ray reflected from $S_n$:

$$dr_1 = \rho_1 \sin\theta_1^i + \rho \sin\left(\phi + \alpha - \theta_1^i\right) \tag{3.10}$$

Now, it is simple to verify that

$$\theta_1^i = \theta_{0L}^t - \alpha \tag{3.11}$$

and so eq. (3.9) reads as

$$\underline{E}^{r1} = R_1 T_0 E_0 e^{-jk_d \rho \sin\left(\phi + \alpha - \theta_1^i\right)} \hat{z} \tag{3.12}$$

If $\theta_1^i \le \theta^c$, the field $\underline{E}^{t1}$ transmitted through $S_n$ can be evaluated as:

$$\underline{E}^{t_1} = T_1 \underline{E}^{t_0}(P_1) e^{-jk_0 dt_1} \tag{3.13}$$

wherein $T_1$ is the transmission coefficient at $P_1$ and $dt_1$ is the distance from $P_1$ to $P$ along the transmitted ray:

$$dt_1 = \rho_1 \sin\theta_1^t - \rho \sin\left(\phi + \alpha + \theta_1^t\right) \tag{3.14}$$

where $\theta_1^t = \sin^{-1}\left(\sqrt{\varepsilon_r}\sin\theta_1^i\right)$ is the transmission angle at $P_1$. Therefore, eq. (3.13) reads as:

$$\underline{E}^{t_1} = T_1 T_0 E_0 e^{jk_0 \rho \sin\left(\phi+\alpha+\theta_1^t\right)} \hat{z} \tag{3.15}$$

The field $\underline{E}^{r_2}$ reflected at $P_2(\rho_2, \phi_2)$ on $S_0$ with $\phi_2 = 0$ is given by:

$$\underline{E}^{r_2} = R_2 \underline{E}^{r_1}(P_2) e^{-jk_d dr_2} \tag{3.16}$$

wherein $R_2$ is the reflection coefficient at $P_2$ and $dr_2$ is the distance from $P_2$ to $P$ along the reflected ray:

$$dr_2 = \rho_2 \sin\theta_2^i - \rho \sin\left(\phi + \theta_2^i\right) \tag{3.17}$$

where $\theta_2^i = \theta_{0L}^t - 2\alpha$. It can be easily verified that:

$$\underline{E}^{r_2} = R_2 R_1 T_0 E_0 e^{jk_d \rho \sin\left(\phi+\theta_2^i\right)} \hat{z} \tag{3.18}$$

If $\theta_2^i \le \theta^c$, the field $\underline{E}^{t_2}$ transmitted through $S_0$ can be evaluated as:

$$\underline{E}^{t2} = T_2 \underline{E}^{\eta} \left( P_2 \right) e^{-jk_0 dt_2} \tag{3.19}$$

wherein $T_2$ is the transmission coefficient at $P_2$ and $dt_2$ is the distance from $P_2$ to $P$ along the transmitted ray:

$$dt_2 = \rho_2 \sin\theta_2^t + \rho \sin\left(\phi - \theta_2^t\right) \tag{3.20}$$

Since $\theta_2^t = \sin^{-1}\left(\sqrt{\varepsilon_r}\sin\theta_2^i\right)$ eq. (3.19) reads as:

$$\underline{E}^{t2} = T_2 R_1 T_0 E_0 e^{-jk_0\rho\sin\left(\phi-\theta_2^t\right)}\hat{z} \tag{3.21}$$

The ray transmitted through $S_0$ travels toward the apex undergoing $N_i = \mathrm{Int}\left[\theta_{0L}^t/\alpha\right]$ reflections/transmissions ( $\mathrm{Int}[\cdot]$ denotes the integer part of the argument) before moving away from it. Accordingly, $\theta_n^i = \theta_n^r = \theta_{0L}^t - n\,\alpha$ for $n = 1,2,...,N_i$ and the total internal reflection doesn't happen if $\theta_n^i \le \theta^c$.

With reference to the first set of rays propagating towards the apex, the field contributions for $n = 3,...,N_i$ can be evaluated by reiterating the previous approach. The expressions of the corresponding internal ( $\underline{E}_L^{in}$ ) and external ( $\underline{E}_L^{ext}$ ) GO fields are:

$$\underline{E}_L^{in} = \underline{E}^{t0L} + \sum_{n=1}^{N} \underline{E}^{rn} =$$

$$= E_0 T_0 \left\{ e^{jk_d\rho\sin\left(\phi+\theta_{0L}^t\right)} + \sum_{\substack{n=1 \\ n\,even}}^{N} \left( \prod_{p=1}^{n} R_p \right) e^{jk_d\rho\sin\left(\phi+\theta_n^i\right)} + \right.$$

$$+\sum_{\substack{n=1\\ n\,odd}}^{N}\left(\prod_{p=1}^{n}R_p\right)e^{-jk_d\rho\sin\left(\phi+\alpha-\theta_n^i\right)}\Bigg\}\hat{z} \tag{3.22}$$

and

$$\begin{aligned}
\underline{E}_L^{ext} &= \underline{E}^i + \underline{E}^{r_0} + \sum_{n=1}^{N+1}\underline{E}^{t_n} = \\
&= E_0 e^{jk_0\rho\cos(\phi-\phi')}\hat{z}W(0,\pi+\phi') + \\
&+R_0E_0e^{jk_0\rho\cos(\phi+\phi')}\hat{z}W(0,\pi-\phi') + \\
&+\Bigg[E_0T_0\sum_{\substack{n=1\\ n\,odd}}^{N+1}\left(\prod_{p=1}^{n-1}R_p\right)T_n e^{jk_0\rho\sin\left(\phi+\alpha+p\theta_n^t\right)}\cdot \\
&\cdot W\left(\frac{3}{2}\pi-\alpha-p\theta_n^t,2\pi-\alpha\right)U\left(\theta_c-\theta_n^i\right)\Bigg]\hat{z} + \\
&+E_0T_0\sum_{\substack{n=1\\ n\,even}}^{N+1}\left(\prod_{p=1}^{n-1}R_p\right)T_n e^{-jk_0\rho\sin\left(\phi-q\theta_n^t\right)}W\left(0,\frac{\pi}{2}+q\theta_n^t\right)U\left(\theta_c-\theta_n^i\right)\hat{z}
\end{aligned} \tag{3.23}$$

where

$$N=\begin{cases}N_i & if\ N_i\ odd\\ N_i+1 & if\ N_i\ even\end{cases} \tag{3.24}$$

the function $W()$ is defined as:

$$W\left(\phi_1,\phi_2\right)=\begin{cases}1 & \text{if } \phi_1<\phi<\phi_2\\ 0 & \text{elsewhere}\end{cases} \tag{3.25}$$

$U()$ is the unit step function:

$$U\left(\theta^c-\theta_n^i\right)=\begin{cases}1 & \theta^c>\theta_n^i\\ 0 & \text{elsewhere}\end{cases} \tag{3.26}$$

and the parameters $p$ and $q$ have been defined as:

$$p=\begin{cases}-1 & \text{if } n=N\\ 1 & \text{elsewhere}\end{cases} \tag{3.27}$$

$$q=\begin{cases}-1 & \text{if } n=N+1\\ 1 & \text{elsewhere}\end{cases} \tag{3.28}$$

The expression (3.24) allows one to keep in account both the possible cases of inversion so that (3.22) and (3.23) are generally valid, the unit step function $W()$ is useful to keep into account the shadow boundaries and the parameters $p$ and $q$ have been introduced to have similar expressions for the two sets of interaction points, as will be shown in the following.

A crucial interaction point is the $(N+1)$-th one which corresponds to the internal incidence angle $\theta_{N+1}^i=(N+1)\alpha-\theta_{0L}^t$. The inversion occurs at this point and the ray travels far from the apex, as illustrated in Fig. 3.4. The use of the parameters $p$ (eq. 3.27) and $q$ (eq. 3.28) allows one to consider the first contribution of this set as arising from $S_0$. Then, it is opportune to describe this series of interactions starting from this ray. The angle $\theta_{0R}^t=\theta_{N+1}^r=\theta_{N+1}^i$ plays now the role of $\theta_{0L}^t$ for evaluating the field contributions. The number of interaction points of the ray propagating far from the apex is

$$M = \mathrm{Int}\left[\frac{\frac{\pi}{2} - \theta_{0R}^{t}}{\alpha}\right] \tag{3.29}$$

Accordingly, the overall number of internal reflections is given by $N + M + 1$ and the internal incidence/reflection angles after the inversion are: $\theta_m^i = \theta_m^r = \theta_{0R}^t + m\alpha$ for $m = 1, 2, ..., M$.

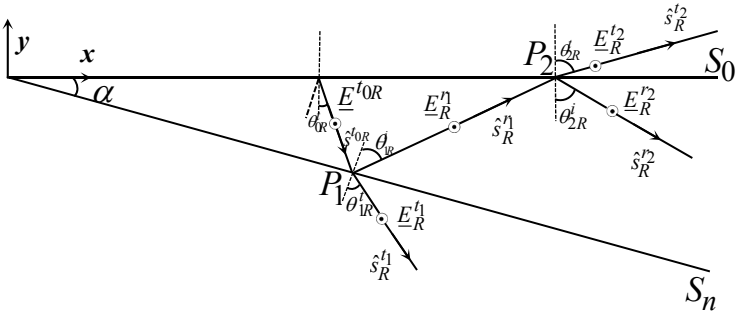


**Figure 3.4** Rays transmissions/reflections after the inversion

The first ray reflected from the internal face of $S_0$ after the inversion is $\underline{E}^{t0R}$ and it is simple to verify that:

$$\underline{E}^{t0R} = \underline{E}^{rN+1} = E_0 T_0 \Gamma(N) e^{jk_d \sin(\phi - \theta_{0R}^t)} \hat{z} \tag{3.30}$$

where

$$\Gamma(N) = \begin{cases} \prod_{p=1}^{N+1} R_p & \text{if } N_i \text{ odd} \\ U\left(\frac{\pi}{2} - \theta_n^i - \alpha\right) \prod_{p=1}^{N+1} R_p & \text{if } N_i \text{ even} \end{cases} \tag{3.31}$$

The function $\Gamma(N)$ defined in (3.31) is useful to keep in account the cumulative product of the reflection coefficients related to the previous interaction points.

Accordingly, with reference to the second set of rays propagating far from the apex, the expressions of the corresponding internal ( $\underline{E}_R^{in}$ ) and external ( $\underline{E}_R^{ext}$ ) GO fields are:

$$\begin{aligned}\underline{E}_R^{in} &= \underline{E}^{t_{0R}} + \sum_{m=1}^{M} \underline{E}^{r_m} = \\ &= E_0 T_0 \Gamma(N) \Bigg[ e^{jk_d \rho \sin\left(\phi - \theta_{0R}^t\right)} + \\ &+ \sum_{\substack{m=1 \\ m\,even}}^{M} \left( \prod_{p=1}^{m} R_p \right) e^{jk_d \rho \sin\left(\phi - \theta_m^i\right)} + \\ &+ \sum_{\substack{m=1 \\ m\,odd}}^{M} \left( \prod_{p=1}^{m} R_p \right) e^{-jk_d \rho \sin\left(\phi + \alpha + \theta_m^i\right)} \Bigg] \hat{z}\end{aligned} \tag{3.32}$$

and

$$\begin{aligned}\underline{E}_R^{ext} &= \sum_{m=1}^{M} \underline{E}^{t_m} = \\ &= E_0 T_0 \Gamma(N) \cdot \\ &\cdot \Bigg\{ \Bigg[ \sum_{\substack{m=1 \\ m\,odd}}^{M} \left( \prod_{p=1}^{m-1} R_p \right) T_m e^{jk_0 \rho \sin\left(\phi + \alpha - \theta_m^t\right)} \cdot\end{aligned}$$

$$\cdot W\left(\frac{3}{2}\pi-\alpha+\theta_m^t, 2\pi-\alpha\right)U\left(\theta_c-\theta_m^i\right)\Bigg]+$$

$$+\sum_{\substack{m=1\\ m\,even}}^{M}\left(\prod_{p=1}^{m-1}R_p\right)T_m e^{-jk_0\rho\sin\left(\phi+\theta_m^t\right)}W\left(0,\frac{\pi}{2}-\theta_m^t\right)U\left(\theta_c-\theta_m^i\right)\Bigg\}\hat{z} \tag{3.33}$$

Then, the overall GO field expressions for the external and internal regions are:

$$\underline{E}^{in}=\underline{E}_L^{in}+\underline{E}_R^{in}=\underline{E}^{t_0L}+\sum_{n=1}^{N}\underline{E}^{r_n}+\underline{E}^{t_0R}+\sum_{m=1}^{M}\underline{E}^{r_m} \tag{3.34}$$

$$\underline{E}^{ext}=\underline{E}_L^{ext}+\underline{E}_R^{ext}=\underline{E}^{i}+\underline{E}^{r_0}+\sum_{n=1}^{N+1}\underline{E}^{t_n}+\sum_{m=1}^{M}\underline{E}^{t_m} \tag{3.35}$$

## 3.2.2 Equivalent problems

In this Section, suitable integral representations for the scattered field by an object in the exterior and interior regions are derived by using the equivalence principle. Let us consider the scattering problem depicted in Fig. 3.5(a) wherein a scatterer is illuminated by an electromagnetic source. The field in the exterior region is given by the superposition of the incident field $\underline{E}^i$ and the field $\underline{E}_{ext}^s$ scattered by the object, whereas $\underline{E}_{in}^s$ is the field scattered into the wedge.

As well-known, the boundary conditions for the considered problem are given by:

$$\hat{n}\times\left(\underline{E}^{i}+\underline{E}^{s}_{ext}\right)\Big|_{S}=\hat{n}\times\left(\underline{E}^{s}_{in}\right)\Big|_{S} \tag{3.36}$$

$$\hat{n}\times\left(\underline{H}^{i}+\underline{H}^{s}_{ext}\right)\Big|_{S}=\hat{n}\times\left(\underline{H}^{s}_{in}\right)\Big|_{S} \tag{3.37}$$

i.e., the tangential components of the fields are continuous across the interface *S*. In addition, radiation boundary conditions must be satisfied at infinity.

Let us consider now the problem in Fig. 3.5(b) wherein the field inside the scatterer is null and the field outside is originated by equivalent electric $\underline{J}^{ext}_{s}$ and magnetic $\underline{J}^{ext}_{ms}$ surface currents on *S*. The problem in Fig. 3.5(b) is equivalent to the original problem (Fig. 3.5 (a)) for evaluating the scattered field in the exterior region $\underline{E}^{s}$ as long as the aforementioned surface currents equal the discontinuities of the tangential components of the electric and magnetic fields, namely:

$$\underline{J}^{ext}_{s}=\hat{n}^{ext}\times\left(\underline{H}^{i}+\underline{H}^{s}_{ext}\right)\Big|_{S} \tag{3.38}$$

$$\underline{J}^{ext}_{ms}=-\hat{n}^{ext}\times\left(\underline{E}^{i}+\underline{E}^{s}_{ext}\right)\Big|_{S} \tag{3.39}$$

In a similar way, the problem in Fig. 3.5(c) is equivalent to the one in Fig. 3.5(a) for determining the scattered field inside the wedge being:

$$\underline{J}^{in}_{s}=\hat{n}^{in}\times\left(\underline{H}^{s}_{in}\right)\Big|_{S} \tag{3.40}$$

$$\underline{J}^{in}_{ms}=-\hat{n}^{in}\times\left(\underline{E}^{s}_{in}\right)\Big|_{S} \tag{3.41}$$

It must be stressed that the major difficulty encountered when evaluating the currents (3.38)-(3.41) is the lack of exact expressions for the tangential components of the fields. As a consequence, only “approximate” surface currents can be easily evaluated.

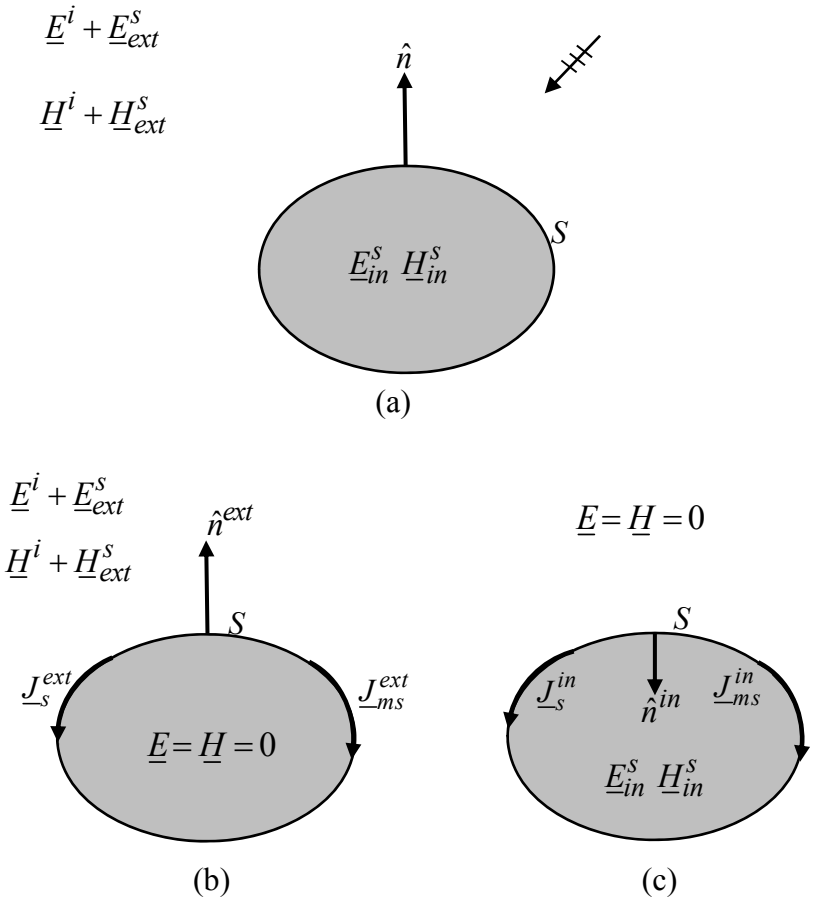


**Figure 3.5** Original scattering problem (a). External problem (b). Internal problem (c).

Let us consider now the problem of plane wave scattering by an acute-angled dielectric wedge shown in Fig. 3.6(a). In light of the previous discussion, the problem can be decomposed into an external problem (Fig. 3.6 (b)) and an internal problem (Fig. 3.6 (c)).
For each of them, proper equivalent electric and magnetic surface currents are introduced on $S_0$ and $S_n$ in accordance with eqns. (3.38)-(3.41).

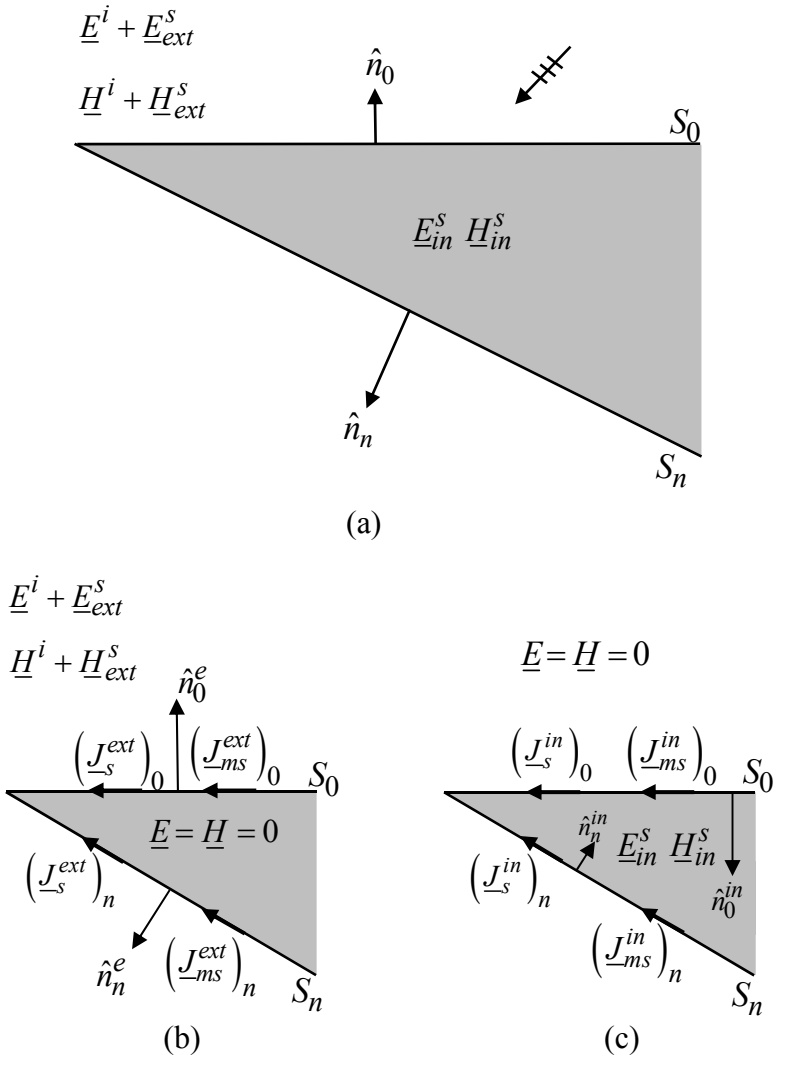


**Figure 3.6** Scattering by a dielectric wedge (a). External problem (b). Internal problem (c).

The field scattered by the wedge in the external and internal regions can be expressed as:

$$\underline{E}^{s}_{ext,in} = \left(\underline{E}^{s}_{ext,in}\right)_0 + \left(\underline{E}^{s}_{ext,in}\right)_n \tag{3.42}$$

wherein $\left(\underline{E}^{s}_{ext,in}\right)_0$ and $\left(\underline{E}^{s}_{ext,in}\right)_n$ are the contributions to the scattered field in the external/internal region associated to $S_0$ and $S_n$, respectively and can be written as:

$$\left(\underline{E}^{s}_{ext}\right)_{0,n} = -jk_0 \cdot$$
$$\cdot \iint_{S_{0,n}} \left[\left(\underline{\underline{I}} - \hat{R}\hat{R}\right)\zeta_0 \left(\underline{J}^{ext}_{s}\right)_{0,n} + \left(\underline{J}^{ext}_{ms}\right)_{0,n} \times \hat{R}\right] G\left(\underline{r}, \underline{r}'\right) dS_{0,n} \tag{3.43}$$

$$\left(\underline{E}^{s}_{in}\right)_{0,n} = -jk_d \cdot$$
$$\cdot \iint_{S_{0,n}} \left[\left(\underline{\underline{I}} - \hat{R}\hat{R}\right)\zeta_d \left(\underline{J}^{in}_{s}\right)_{0,n} + \left(\underline{J}^{in}_{ms}\right)_{0,n} \times \hat{R}\right] G\left(\underline{r}, \underline{r}'\right) dS_{0,n} \tag{3.44}$$

### 3.2.3 Diffracted field: UAPO solutions for $0 < \phi' < \pi/2$

In this Section, closed form expressions for the field diffracted by the edge of a lossless acute-angled dielectric wedge are derived in both the external and the internal region (see Fig. 3.6(b) and 3.6(c)) by using the methodologies presented in Sec. 2.5 and Subsec. 3.2.2. For each region, the two series of contributions, towards and far from the apex, are considered separately to simplify reader's understanding.

#### External problem

In reference to the space surrounding the wedge it results

$$\left(\underline{E}^{s}_{ext}\right)_0 = -jk_0 \iint_{S_0} \left[ \left(\underline{\underline{I}} - \hat{R}\hat{R}\right)\zeta_0 \left(\underline{J}^{ext}_{s}\right)_0 + \left(\underline{J}^{ext}_{ms}\right)_0 \times \hat{R} \right] G\left(\underline{r}, \underline{r}'\right) dS_0 \tag{3.45}$$

$$\left(\underline{E}^{s}_{ext}\right)_n = -jk_0 \iint_{S_n} \left[ \left(\underline{\underline{I}} - \hat{R}\hat{R}\right)\zeta_0 \left(\underline{J}^{ext}_{s}\right)_n + \left(\underline{J}^{ext}_{ms}\right)_n \times \hat{R} \right] G\left(\underline{r}, \underline{r}'\right) dS_n \tag{3.46}$$

Being present two series of rays, pre- and post-inversion, they are treated separately and only the main results are reported.

The explicit evaluation of the equivalent currents in the radiation integrals (3.45), (3.46) is carried out in Appendix A.

## Pre-inversion contributions

By substituting eqns. (A.8), (A.9) and using the approximation $\hat{R} \cong \hat{s} = (\cos\phi, \sin\phi, 0)$ ($\hat{s}$ is the unit vector of the diffraction direction) into eq. (3.45), it is possible to rewrite this last as follows:

$$\left(\underline{E}^{s}_{ext}\right)^{L}_0 = \left[\left(\underline{E}^{s}_{ext}\right)^{L}_0\right]_{I+R} + \sum_{\substack{n=1 \\ n\,even}}^{N+1} \left[\left(\underline{E}^{s}_{ext}\right)^{L}_0\right]_{T_n} =$$

$$= E_0 \left\{ \left[\sin\phi'\left(1 - R_0\right) - \sin\phi\left(1 + R_0\right)\right] I_0 + \right.$$

$$\left. -T_0 \sum_{\substack{n=1 \\ n\,even}}^{N+1} \left( \prod_{p=1}^{n-1} R_p \right) T_n \left(\sin\phi + \cos\theta^t_n\right) U\left(\theta^c - \theta^i_n\right) I_{0_n} \right\} \hat{z} = \tag{3.47}$$

where

$$I_0 = \frac{-jk_0}{4\pi}\int_0^{+\infty} e^{jk_0 x'\cos\phi'}\int_{-\infty}^{+\infty}\frac{e^{-jk_0\sqrt{(x-x')^2+y^2+(z-z')^2}}}{\sqrt{(x-x')^2+y^2+(z-z')^2}}dz'dx' \quad (3.48)$$

$$I_{0_n} = \frac{-jk_0}{4\pi}\int_0^{+\infty} e^{jk_0 x'\sin q\theta_n^t}\int_{-\infty}^{+\infty}\frac{e^{-jk_0\sqrt{(x-x')^2+y^2+(z-z')^2}}}{\sqrt{(x-x')^2+y^2+(z-z')^2}}dz'dx' \quad (3.49)$$

According to Subsec. 2.5, and taking into account that $\beta' = \beta = \pi/2$ the integral $I_0$ can be rewritten as:

$$I_0 = \frac{1}{4\pi j}\int_C \frac{e^{-jk_0\rho\cos(\alpha_c+q_0\phi)}}{\cos\alpha_c+\cos\phi'}d\alpha_c \quad (3.50)$$

where

$$q_0 = \begin{cases} 1 & 0<\phi<\pi \\ -1 & \pi<\phi<2\pi-\alpha \end{cases} \quad (3.51)$$

and $C$ is the integration path in Fig. 2.9. By applying the steepest descent method and performing a uniform asymptotic evaluation ( $k_0\rho \gg 1$) of the integral (3.48) along the SDP, it is possible to determine the following expression of the UAPO diffracted field contribution related to $I_0$:

$$\left[\left(\underline{E}_{ext}^{d}\right)_0^L\right]_{I+R} = E_0\left[\sin\phi'(1-R_0)-\sin\phi(1+R_0)\right]\frac{e^{-j\pi/4}}{2\sqrt{2\pi k_0}}\cdot \cdot\frac{F_t\left[2k_0\rho\cos^2\left(\frac{\phi\pm\phi'}{2}\right)\right]}{\cos\phi+\cos\phi'}\frac{e^{-jk_0\rho}}{\sqrt{\rho}}\hat{z} \quad (3.52)$$

in which the sign + applies in the interval ($0 < \phi < \pi$) and the sign − applies in the interval ($\pi < \phi < 2\pi$). In the same way, the integrals $I_{0_n}$ can be rewritten as:

$$I_{0_n} = \frac{1}{4\pi j}\int_C \frac{e^{-jk_0\rho\cos\left[\alpha+q_0\left(\frac{\pi}{2}-q\theta_n^t\right)\right]}}{\cos\alpha+\cos\left(\frac{\pi}{2}-q\theta_n^t\right)}d\alpha \tag{3.53}$$

and so the following expression of the UAPO diffracted field contributions originated by $I_{0_n}$ are:

$$\sum_{\substack{n=1\\ n\,even}}^{N+1}\left[\left(\underline{E}_{ext}^d\right)_0^L\right]_{T_n} = -E_0T_0\sum_{\substack{n=1\\ n\,even}}^{N+1}\left(\prod_{p=1}^{n-1}R_p\right)T_n\left(\sin\phi+\cos\theta_n^t\right)U\left(\theta^c-\theta_n^i\right)\cdot$$
$$\cdot\frac{F_t\left[2k_0\rho\cos^2\left(\frac{\phi\pm\left(\pi/2-q\theta_n^t\right)}{2}\right)\right]}{\cos\phi+\cos\left(\pi/2-q\theta_n^t\right)}\frac{e^{-j\pi/4}}{2\sqrt{2\pi k_0}}\frac{e^{-jk_0\rho}}{\sqrt{\rho}}\hat{z} \tag{3.54}$$

in which the sign + applies in the interval ($0 < \phi < \pi$) and the sign − applies in the interval ($\pi < \phi < 2\pi - \alpha$). Therefore, the UAPO diffracted field pre-inversion contribution originated by $S_0$ can be determined by means of eqns. (3.53), (3.54) as:

$$\left(\underline{E}_{ext}^d\right)_0^L = \left[\left(\underline{E}_{ext}^d\right)_0^L\right]_{I+R} + \sum_{\substack{n=1\\ n\,even}}^{N+1}\left[\left(\underline{E}_{ext}^d\right)_0^L\right]_{T_n} \tag{3.55}$$

For what concerns the integral on $S_n$ in eq. (3.46), it can be rewritten as:

$$\left(\underline{E}^{s}_{ext}\right)^{L}_{n} = T_0 E_0 \cdot$$

$$\cdot \sum_{\substack{n=1 \\ n\,odd}}^{N+1} \left( \prod_{p=1}^{n-1} R_p \right) T_n \left[ \sin\left(\phi+\alpha\right) - \cos p\theta^{t}_{n} \right] U\left(\theta^{c} - \theta^{i}_{n}\right) I_{n_n}\, \hat{z} \quad (3.56)$$

where

$$I_{n_n} = \frac{-jk_0}{4\pi} \int_{0}^{+\infty} e^{jk_0\rho'\sin q\theta^{t}_{n}} \int_{-\infty}^{+\infty} \frac{e^{-jk_0\sqrt{(\rho-\rho')^2+(z-z')^2}}}{\sqrt{(\rho-\rho')^2+(z-z')^2}} dz'\, d\rho' \quad (3.57)$$

The integral $I_{n_n}$ can be rewritten in the equivalent form:

$$I_{n_n} = \frac{1}{4\pi j} \int_{C} \frac{e^{-jk_0\rho\cos\left\{\alpha_c + q_n\left[\phi+(2\pi-\alpha)\right]\right\}}}{\cos\alpha_c + \cos\left(\pi/2 - q\theta^{t}_{n}\right)} d\alpha_c \quad (3.58)$$

where

$$q_n = \begin{cases} -1 & 0 < \phi < \pi - \alpha \\ 1 & \pi - \alpha < \phi < 2\pi - \alpha \end{cases} \quad (3.59)$$

By applying the steepest descent method and performing a uniform asymptotic evaluation ($k_0\rho \gg 1$) of the integral (3.58) along the SDP, the following expression for the UAPO diffracted field contribution due to $S_n$ can be obtained:

$$\left(\underline{E}^{d}_{ext}\right)^{L}_{n} = E_0 T_0 \frac{e^{-j\pi/4}}{2\sqrt{2\pi k_0}} \sum_{\substack{n=1 \\ n\,odd}}^{N+1} \left( \prod_{p=1}^{n-1} R_p \right) T_n \left[ \sin\left(\phi+\alpha\right) - \cos p\theta^{t}_{n} \right] \cdot$$

$$\cdot\frac{F_t\left[2k_0\rho\cos^2\left(\frac{\left(\phi+\alpha\right)\pm\left(\pi/2-p\theta_n^t\right)}{2}\right)\right]}{\cos\left(\phi+\alpha\right)+\cos\left(\pi/2-p\theta_n^t\right)}\frac{e^{-jk_0\rho}}{\sqrt{\rho}}U\left(\theta^c-\theta_n^i\right)\hat{z} \tag{3.60}$$

in which the sign + applies in the interval $\left(\pi-\alpha<\phi<2\pi-\alpha\right)$ and the sign − applies in the interval $\left(0<\phi<\pi-\alpha\right)$.

## Post-inversion contributions

By substituting eqns. (A.21), (A.22) and using the approximation $\hat{R}\cong\hat{s}=(\cos\phi,\sin\phi,0)$ into eq. (3.45), it is possible to rewrite this last as follows:

$$\left(\underline{E}_{ext}^s\right)_0^R=-E_0T_0\Gamma(N)\cdot$$
$$\cdot\sum_{\substack{m=1\\ m\,even}}^{M}\left(\prod_{p=1}^{m-1}R_p\right)T_m\left(\sin\phi+\cos\theta_m^t\right)U\left(\theta^c-\theta_m^i\right)I_{0_m}\hat{z} \tag{3.61}$$

where

$$I_{0_m}=\frac{-jk_0}{4\pi}\int_0^{+\infty}e^{-jk_0x'\sin\theta_m^t}\int_{-\infty}^{+\infty}\frac{e^{-jk_0\sqrt{(x-x')^2+y^2+(z-z')^2}}}{\sqrt{(x-x')^2+y^2+(z-z')^2}}dz'dx' \tag{3.62}$$

The integral $I_{0_m}$ can be rewritten in the equivalent form:

$$I_{0_m} = \frac{1}{4\pi j}\int_C \frac{e^{-jk_0\rho\cos(\alpha+q_0\phi)}}{\cos\alpha+\cos\left(\frac{\pi}{2}+\theta_m^t\right)}d\alpha \tag{3.63}$$

where $C$ is the integration path in Fig. 2.9. By applying the steepest descent method and performing a uniform asymptotic evaluation ( $k_0\rho \gg 1$) of the integral (3.63) along the SDP, it is possible to determine the following expression of the UAPO diffracted field contribution originated by $S_0$:

$$\left(\underline{E}_{ext}^{d}\right)_0^R = -E_0T_0\Gamma(N)\left[\sum_{\substack{m=1\\ m\,even}}^{M}\left(\prod_{p=1}^{m-1}R_p\right)T_m\left(\sin\phi+\cos\theta_m^t\right)\right]\frac{e^{-j\pi/4}}{2\sqrt{2\pi k_0}}\cdot$$
$$\cdot\frac{F_t\left[2k_0\rho\cos^2\left(\frac{\phi\pm\left(\pi/2+\theta_m^t\right)}{2}\right)\right]}{\cos\phi+\cos\left(\pi/2+\theta_m^t\right)}\frac{e^{-jk_0\rho}}{\sqrt{\rho}}U\left(\theta^c-\theta_m^i\right)\hat{z} \tag{3.64}$$

in which the sign + applies in the interval $0<\phi<\pi$ and the sign − applies in the interval $\pi<\phi<2\pi-\alpha$ .

For what concerns the integral on $S_n$ in eq. (3.46), it can be rewritten as:

$$\left(\underline{E}_{ext}^{s}\right)_n^R = T_0E_0\Gamma(N)\cdot$$
$$\cdot\sum_{\substack{m=1\\ m\,odd}}^{M}\left(\prod_{p=1}^{m-1}R_p\right)T_m\left[\sin\left(\phi+\alpha\right)-\cos\theta_m^t\right]U\left(\theta^c-\theta_m^i\right)I_{n_m}\hat{z} \tag{3.65}$$

where

$$I_{n_m} = \frac{-jk_0}{4\pi} \int_0^{+\infty} e^{-jk_0\rho'\sin\theta_m^t} \int_{-\infty}^{+\infty} \frac{e^{-jk_0\sqrt{(\rho-\rho')^2+(z-z')^2}}}{\sqrt{(\rho-\rho')^2+(z-z')^2}} dz'\,d\rho' \tag{3.66}$$

wherein the integral $I_{n_m}$ can be rewritten in the equivalent form:

$$I_n = \frac{1}{4\pi j} \int_C \frac{e^{-jk\rho\cos\left\{\alpha+q\left[\phi+(2\pi-\alpha)\right]\right\}}}{\cos\alpha+\cos(\pi/2+\theta)} d\alpha_c \tag{3.67}$$

where

$$q_0 = \begin{cases} 1 & 0<\phi<\pi-\alpha \\ -1 & \pi-\alpha<\phi<2\pi-\alpha \end{cases} \tag{3.68}$$

By applying the steepest descent method and performing a uniform asymptotic evaluation ($k_0\rho \gg 1$) of the integral (3.67) along the SDP, the following expression for the UAPO diffracted field contribution due to $S_n$ can be obtained:

$$\left(\underline{E}_{ext}^d\right)_n^R = E_0 T_0 \Gamma(N) \frac{e^{-j\pi/4}}{2\sqrt{2\pi k_0}} \sum_{\substack{m=1 \\ m\,odd}}^{M} \left(\prod_{p=1}^{m-1} R_p\right) T_m\left[\sin(\phi+\alpha)-\cos\theta_m^t\right] \cdot$$
$$\cdot \frac{F_t\left[2k_0\rho\cos^2\left(\frac{(\phi+\alpha)\pm(\pi/2+\theta_m^t)}{2}\right)\right]}{\cos(\phi+\alpha)+\cos(\pi/2+\theta_m^t)} \frac{e^{-jk_0\rho}}{\sqrt{\rho}} U\left(\theta^c-\theta_m^i\right)\hat{z} \tag{3.69}$$

in which the sign − applies in the interval $\pi-\alpha<\phi<2\pi-\alpha$ and the sign + applies in the interval $0<\phi<\pi-\alpha$.

Then, as for the GO field, the total diffracted field in the region external to the wedge is given by the superposition of the pre-inversion contributions (eqns. (3.55), (3.60)) with the post-inversion ones (eqns. (3.64), (3.69)).

$$\underline{E}^d_{ext} = \left(\underline{E}^d_{ext}\right)^L_0 + \left(\underline{E}^d_{ext}\right)^L_n + \left(\underline{E}^d_{ext}\right)^R_n + \left(\underline{E}^d_{ext}\right)^R_0 \tag{3.70}$$

## Internal problem

For what concerns the internal region the scattered field contributions are:

$$\left(\underline{E}^s_{in}\right)_0 = -jk_d \iint_{S_0} \left[\left(\underline{\underline{I}} - \hat{R}\hat{R}\right)\zeta_d \left(\underline{J}^{in}_s\right)_0 + \left(\underline{J}^{in}_{ms}\right)_0 \times \hat{R}\right] G\left(\underline{r}, \underline{r}'\right) dS_0 \tag{3.71}$$

$$\left(\underline{E}^s_{in}\right)_n = -jk_d \iint_{S_n} \left[\left(\underline{\underline{I}} - \hat{R}\hat{R}\right)\zeta_d \left(\underline{J}^{in}_s\right)_n + \left(\underline{J}^{in}_{ms}\right)_n \times \hat{R}\right] G\left(\underline{r}, \underline{r}'\right) dS_n \tag{3.72}$$

Also for this problem, the pre- and post-inversion contributions are evaluated separately.

## Pre-inversion contributions

The currents involved in eqns. (3.71), (3.72) are reported in Appendix A (see eqns. (A.12)-(A.15)). As regards $\left(\underline{E}^s_{in}\right)^L_0$, the substitution of eqns. (A.12), (A.13) in the integral (3.70) leads to:

$$\left(\underline{E}^s_{in}\right)^L_0 = T_0 E_0 \left\{ \left(\sin\phi - \cos\theta^t_{0L}\right) I_0 + \right.$$

$$+\sum_{\substack{n=1\\ n\,even}}^{N}\left(\prod_{p=1}^{n-1}R_p\right)\left[\left(1+R_n\right)\sin\phi+\left(1-R_n\right)\cos\theta_n^i\right]I_{0_n}\Bigg\}\hat{z}=$$

$$=\left[\left(\underline{E}_{in}^{s}\right)_0\right]_{T_0}^{L}+\sum_{\substack{n=1\\ n\,even}}^{N+1}\left[\left(\underline{E}_{in}^{s}\right)_0\right]_{R_n}^{L} \tag{3.73}$$

where

$$I_0=\frac{-jk_d}{4\pi}\int_0^{+\infty}e^{jk_dx'\sin\theta_{0L}^t}\int_{-\infty}^{+\infty}\frac{e^{-jk_d\sqrt{(x-x')^2+y^2+(z-z')^2}}}{\sqrt{(x-x')^2+y^2+(z-z')^2}}dz'dx' \tag{3.74}$$

$$I_{0_n}=\frac{-jk_d}{4\pi}\int_0^{+\infty}e^{jk_dx'\sin\theta_n^i}\int_{-\infty}^{+\infty}\frac{e^{-jk_d\sqrt{(x-x')^2+y^2+(z-z')^2}}}{\sqrt{(x-x')^2+y^2+(z-z')^2}}dz'dx' \tag{3.75}$$

The integral $I_0$ can be rewritten in the equivalent form:

$$I_0=\frac{1}{4\pi j}\int_C\frac{e^{-jk_d\rho\cos(\alpha+\phi)}}{\cos\alpha+\cos\left(\pi/2-\theta_{0L}^t\right)}d\alpha \tag{3.76}$$

After performing a uniform asymptotic evaluation of the integral (3.76) along SDP, the following expression for the first contribution of UAPO diffracted field originated by $S_0$ can be obtained:

$$\left[\left(\underline{E}_{in}^{d}\right)_0^L\right]_{T_0}=T_0E_0\frac{e^{-j\pi/4}}{2\sqrt{2\pi k_d}}\left(\sin\phi-\cos\theta_{0L}^t\right)\cdot$$

$$\cdot \frac{F_t\left[2k_d\rho\cos^2\left(\frac{\phi+\left(\pi/2-\theta_{0L}^t\right)}{2}\right)\right]}{\cos\phi+\cos\left(\pi/2-\theta_{0L}^t\right)}\frac{e^{-jk_d\rho}}{\sqrt{\rho}}\hat{z} \tag{3.77}$$

The integrals $I_{0_n}$ can be rewritten in the equivalent form:

$$I_{0_n}=\frac{1}{4\pi j}\int_C \frac{e^{-jk_d\rho\cos(\alpha+\phi)}}{\cos\alpha+\cos\left(\pi/2-\theta_n^i\right)}d\alpha \tag{3.78}$$

After performing a uniform asymptotic evaluation of the integral (3.78) along SDP, the following expression for the second contribution of UAPO diffracted field originated by $S_0$ can be obtained:

$$\sum_{\substack{n=1\\ n\,even}}^{N+1}\left[\left(\underline{E}_{in}^d\right)_0^L\right]_{R_n}=T_0E_0\frac{e^{-j\pi/4}}{2\sqrt{2\pi k_d}}\frac{e^{-jk_d\rho}}{\sqrt{\rho}}\cdot$$

$$\cdot\sum_{\substack{n=1\\ n\,even}}^{N}\left(\prod_{p=1}^{n-1}R_p\right)\left[\left(1+R_n\right)\sin\phi+\left(1-R_n\right)\cos\theta_n^i\right]\cdot$$

$$\cdot\frac{F_t\left[2k_d\rho\cos^2\left(\frac{\phi+\left(\pi/2-\theta_n^i\right)}{2}\right)\right]}{\cos\phi+\cos\left(\pi/2-\theta_n^i\right)}\hat{z} \tag{3.79}$$

Therefore the UAPO diffracted field contribution originated by $S_0$ can be determined by means of eqns. (3.77), (3.79) as:

$$\left(\underline{E}_{in}^{d}\right)_0^L = \left[\left(\underline{E}_{in}^{d}\right)_0^L\right]_{T_0} + \sum_{\substack{n=1 \\ n\,even}}^{N+1}\left[\left(\underline{E}_{in}^{d}\right)_0^L\right]_{R_n} \tag{3.80}$$

With reference to the contribution $\left(\underline{E}_{in}^{s}\right)_n^L$, let us substitute the currents (A.14), (A.15) in the integral (3.72). Accordingly, it results:

$$\left(\underline{E}_{in}^{s}\right)_n^L = T_0 E_0 \sum_{\substack{n=1 \\ n\,odd}}^{N}\left(\prod_{p=1}^{n-1} R_p\right)\left[\left(1-R_n\right)\cos\theta_n^i - \left(1+R_n\right)\sin\left(\phi+\alpha\right)\right] I_{n_n}\hat{z} \tag{3.81}$$

where

$$I_{n_n} = \frac{-jk_d}{4\pi}\int_0^{+\infty} e^{jk_d\rho'\sin\theta_n^i}\int_{-\infty}^{+\infty}\frac{e^{-jk_d\sqrt{(\rho-\rho')^2+(z-z')^2}}}{\sqrt{(\rho-\rho')^2+(z-z')^2}}dz'\,d\rho' \tag{3.82}$$

It is possible to rewrite $I_{n_n}$ as a line integral in the complex $\alpha$-plane:

$$I_{n_n} = \frac{1}{4\pi j}\int_C \frac{e^{-jk_d\rho\cos\left[\alpha_c+\phi+\left(2\pi-\alpha\right)\right]}}{\cos\alpha_c+\cos\left(\pi/2-\theta_n^i\right)}d\alpha_c \tag{3.83}$$

A uniform asymptotic evaluation of (3.83) leads to the following expression for the UAPO diffracted field contribution originated by $S_n$:

$$\left(\underline{E}_{in}^{d}\right)_n^L = E_0 T_0 \sum_{\substack{n=1 \\ n\,odd}}^{N}\left(\prod_{p=1}^{n-1} R_p\right)\left[\left(1-R_n\right)\cos\theta_n^i - \left(1+R_n\right)\sin\left(\phi+\alpha\right)\right]\cdot$$

$$\cdot \frac{F_t\left[2k_d\rho\cos^2\left(\frac{(\phi+\alpha)+\left(\pi/2-\theta_n^i\right)}{2}\right)\right]}{\cos(\phi+\alpha)+\cos\left(\pi/2-\theta_n^i\right)} \frac{e^{-j\pi/4}}{2\sqrt{2\pi k_d}} \frac{e^{-jk_d\rho}}{\sqrt{\rho}}\hat{z} \tag{3.84}$$

## Post-inversion contributions

The currents involved in eqns. (3.71), (3.72) are reported in Appendix A (see eqns. (A.25)-(A.28)). As regards $\left(\underline{E}_{in}^s\right)_0^R$, the substitution of eqns. (A. 25), (A.26) in the integral (3.71) leads to:

$$\left(\underline{E}_{in}^s\right)_0^R = T_0 E_0 \Gamma(N)\left\{\left(\sin\phi-\cos\theta_{0R}^t\right)I_0 + \right.$$

$$\left. + \sum_{\substack{m=1\\ m\,even}}^{M}\left(\prod_{p=1}^{m-1}R_p\right)\left[\left(1+R_m\right)\sin\phi+\left(1-R_m\right)\cos\theta_m^i\right]I_{0_m}\right\}\hat{z} =$$

$$= \left[\left(\underline{E}_{in}^s\right)_0^R\right]_{T_0} + \sum_{\substack{m=1\\ m\,even}}^{M}\left[\left(\underline{E}_{in}^s\right)_0^R\right]_{R_m} \tag{3.85}$$

where

$$I_0 = \frac{-jk_d}{4\pi}\int_0^{+\infty} e^{jk_d x'\sin\theta_{0R}^t}\int_{-\infty}^{+\infty}\frac{e^{-jk_d\sqrt{(x-x')^2+y^2+(z-z')^2}}}{\sqrt{(x-x')^2+y^2+(z-z')^2}}dz'dx' \tag{3.86}$$

$$I_{0_m} = \frac{-jk_d}{4\pi} \int_0^{+\infty} e^{jk_d x' \sin\theta_m^i} \int_{-\infty}^{+\infty} \frac{e^{-jk_d\sqrt{(x-x')^2+y^2+(z-z')^2}}}{\sqrt{(x-x')^2+y^2+(z-z')^2}} dz'dx' \tag{3.87}$$

The integral $I_0$ can be rewritten in the equivalent form:

$$I_0 = \frac{1}{4\pi j} \int_C \frac{e^{-jk_d\rho\cos(\alpha+\phi)}}{\cos\alpha+\cos\left(\pi/2+\theta_{0R}^t\right)} d\alpha \tag{3.88}$$

After performing a uniform asymptotic evaluation of the contribution of the integral (3.88) along SDP, the following expression for the first contribution of UAPO diffracted field originated by $S_0$ can be obtained:

$$\left[\left(\underline{E}_{in}^d\right)_0^R\right]_{T_0} = T_0 E_0 \Gamma(N) \frac{e^{-j\pi/4}}{2\sqrt{2\pi k_d}} \left(\sin\phi - \cos\theta_{0R}^t\right) \cdot \frac{F_t\left[2k_d\rho\cos^2\left(\frac{\phi+\left(\pi/2+\theta_{0R}^t\right)}{2}\right)\right]}{\cos\phi+\cos\left(\pi/2+\theta_{0R}^t\right)} \frac{e^{-jk_d\rho}}{\sqrt{\rho}} \hat{z} \tag{3.89}$$

The integral $I_{0_m}$ can be rewritten as:

$$I_{0_m} = \frac{1}{4\pi j} \int_C \frac{e^{-jk_d\rho\cos(\alpha+\phi)}}{\cos\alpha+\cos\left(\pi/2+\theta_m^i\right)} d\alpha \tag{3.90}$$

After performing a uniform asymptotic evaluation of the contribution of the integral (3.90) along SDP, the following expression for the second contribution of UAPO diffracted field originated by $S_0$ can be obtained:

$$\sum_{\substack{m=1\\ m\,even}}^{M}\left[\left(\underline{E}_{in}^{d}\right)_{0}^{R}\right]_{R_m}=T_0E_0\Gamma(N)\frac{e^{-j\pi/4}}{2\sqrt{2\pi k_d}}\cdot$$

$$\cdot\left\{\sum_{\substack{m=1\\ m\,even}}^{M}\left(\prod_{p=1}^{m-1}R_p\right)\left[\left(1+R_m\right)\sin\phi+\left(1-R_m\right)\cos\theta_m^i\right]\cdot\right.$$

$$\left.\cdot\frac{F_t\left[2k_d\rho\cos^2\left(\dfrac{\phi+\left(\pi/2+\theta_m^i\right)}{2}\right)\right]}{\cos\phi+\cos\left(\pi/2+\theta_m^i\right)}\right\}\frac{e^{-jk_d\rho}}{\sqrt{\rho}}\hat{z}\qquad(3.91)$$

Therefore the UAPO diffracted field post-inversion contribution originated by $S_0$ can be determined by means of eqns. (3.89), (3.91) as:

$$\left(\underline{E}_{in}^{d}\right)_{0}^{R}=\left[\left(\underline{E}_{in}^{d}\right)_{0}^{R}\right]_{T_0}+\sum_{\substack{m=1\\ m\,even}}^{M}\left[\left(\underline{E}_{in}^{d}\right)_{0}^{R}\right]_{R_m}\qquad(3.92)$$

With reference to the contribution $\left(\underline{E}_{in}^{s}\right)_{n}^{R}$, let us substitute the currents (A.27), (A.28) in the integral (3.72). Accordingly, it results:

$$\left(\underline{E}_{in}^{s}\right)_{n}^{R}=T_0E_0\Gamma(N)\cdot$$

$$\cdot\sum_{\substack{m=1\\ m\,odd}}^{M}\left(\prod_{p=1}^{m-1}R_p\right)\left[\left(1-R_m\right)\cos\theta_m^i-\left(1+R_m\right)\sin\left(\phi+\alpha\right)\right]I_{n_m}\hat{z}\qquad(3.93)$$

where

$$I_{n_m} = \frac{-jk_d}{4\pi} \int_0^{+\infty} e^{jk_d \rho' \sin\theta_m^i} \int_{-\infty}^{+\infty} \frac{e^{-jk_d\sqrt{(\rho-\rho')^2+(z-z')^2}}}{\sqrt{(\rho-\rho')^2+(z-z')^2}} dz' d\rho' \tag{3.94}$$

It is possible to rewrite $I_{n_m}$ as a line integral in the complex $\alpha$-plane:

$$I_{n_m} = \frac{1}{4\pi j} \int_C \frac{e^{-jk_d \rho \cos\left[\alpha_c + \phi + (2\pi - \alpha)\right]}}{\cos\alpha_c + \cos\left(\pi/2 + \theta_m^i\right)} d\alpha_c \tag{3.95}$$

A uniform asymptotic evaluation of (3.95) leads to the following expression for the UAPO diffracted field contribution originated by $S_n$:

$$\left(\underline{E}_{in}^d\right)_n^R = E_0 T_0 \Gamma(N) \frac{e^{-j\pi/4}}{2\sqrt{2\pi k_d}} \cdot$$
$$\cdot \sum_{\substack{m=1 \\ m\,odd}}^{M} \left( \prod_{p=1}^{m-1} R_p \right) \left[ \left(1 - R_m\right)\cos\theta_m^i - \left(1 + R_m\right)\sin\left(\phi + \alpha\right) \right] \cdot$$
$$\cdot \frac{F_t\left[ 2k_d \rho \cos^2\left( \frac{\left(\phi + \alpha\right) + \left(\pi/2 + \theta_m^i\right)}{2} \right) \right]}{\cos\left(\phi + \alpha\right) + \cos\left(\pi/2 + \theta_m^i\right)} \frac{e^{-jk_d\rho}}{\sqrt{\rho}} \hat{z} \tag{3.96}$$

Consequently, the total diffracted field in the region internal to the wedge is given by the superposition of the pre-inversion contributions (eqns. (3.80) and (3.84)) with the post-inversion ones (eqns. (3.92) and (3.96)).

$$\underline{E}_{in}^{d} = \left(\underline{E}_{in}^{d}\right)_0^L + \left(\underline{E}_{in}^{d}\right)_n^L + \left(\underline{E}_{in}^{d}\right)_0^R + \left(\underline{E}_{in}^{d}\right)_n^R \tag{3.97}$$

### 3.2.4 Formulation of the problem for $\pi/2 < \phi' < \pi-\alpha$

The geometry of the problem is the same of Fig. 3.1 and the values of $\phi'$ are here considered in the range from $\pi/2$ to $\pi-\alpha$ so that only the face $S_0$ is directly illuminated by the incident field. A transmitted ray exists in the inner region and, in absence of total internal reflection, it is partially transmitted at the interface $S_n$. Then, a series of internal and external rays propagating far from the apex arises as illustrated in Fig. 3.7. The external rays exist until the total reflection doesn't occur.

By matching Fig 3.7 with Fig 3.2 it is evident that this ray-tracing is the same of that related to the post-inversion case. Consequently, the contributions to GO and diffracted field are the same of the post-inversion series of rays.

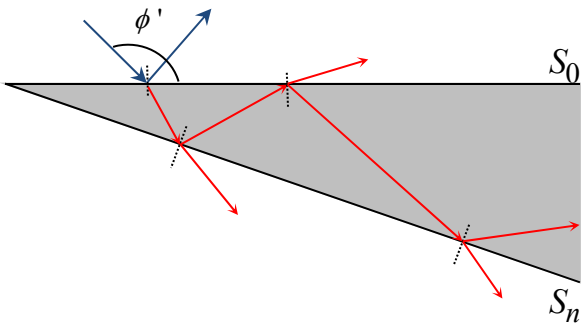


**Figure 3.7** Internal reflection and external transmission.

Under the assumption that surface wave effects can be neglected, the total field at any observation point $P(\rho,\phi)$ can be expressed as the superposition of the GO fields present in each region and the edge diffracted field.

## GO field model for $\pi/2 < \phi' < \pi-\alpha$

Closed form expressions for the GO response when $\pi/2 < \phi' < \pi - \alpha$ are shown in this section. The physical mechanism of ray propagation inside and outside the wedge is depicted in Fig. 3.8. As can be seen, the incident ray undergoes a double transmission through the interfaces $S_0$ and $S_n$, respectively. If $\theta^i = \phi' - \pi/2$ is the external incidence angle, the waves penetrate into the wedge through $S_0$ with the transmission angle $\theta_{0R}^t = \sin^{-1}\left(\sin\theta_0^i / \sqrt{\varepsilon_r}\right)$ and undergoes multiple reflections in the internal region until the reflection angle $\theta_m^r = \theta_m^i = m\,\alpha + \theta_{0R}^t$ at the $m$-th interaction becomes greater than $\pi/2 - \alpha$. As a consequence, the number of total internal reflections is $M = \mathrm{Int}\left[\left(\pi/2 - \theta_{0R}^t\right)/\alpha\right]$, where $\mathrm{Int}[\cdot]$ denotes the integer part of the argument.

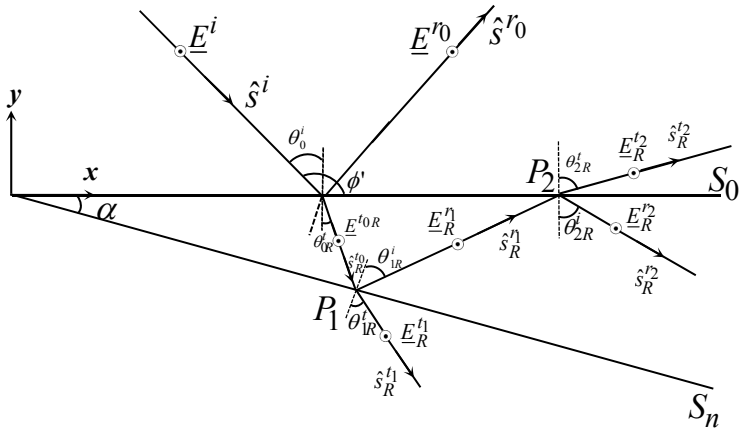


**Figure 3.8** Rays transmissions/reflections through the wedge.

Transmitted waves through $S_0$ and $S_n$ exist until the total reflection occurs inside the wedge, i.e., when $\theta_m^i > \theta_c = \sin^{-1}\left(1/\sqrt{\varepsilon_r}\right)$, and

define shadow boundaries fixed by the angles $\theta_m^t = \sin^{-1}\left(\sqrt{\varepsilon_r}\sin\theta_m^i\right)$ in the space surrounding the wedge.The unit vectors relevant to the propagation direction of the rays incident and reflected at the interfaces $S_0$ are:

$$\hat{s}^i = \left(\sin\theta_0^i, -\cos\theta_0^i, 0\right);\ \ \hat{s}^{r0} = \left(\sin\theta_0^i, \cos\theta_0^i, 0\right) \tag{3.98}$$

and the expressions (3.2), (3.3) for the incident electric field $\underline{E}^i$ and the field reflected from $S_0$, still hold.

As regards the field $\underline{E}^{t0R}$ transmitted through $S_0$, it can be expressed as:

$$\underline{E}^{t0R} = E_0 T_0 e^{jk_d \sin(\phi-\theta_{0R}^t)}\hat{z} \tag{3.99}$$

and the likeness with (3.30) is evident, except for the absence of function $\Gamma(N)$.

For the next interaction points, by taking advantage of the analogy of ray-tracing with the post-inversion case, the expressions of the GO fields are equal to (3.32) (3.33), excluding the function $\Gamma(N)$. Consequently, the overall expressions of the internal and external GO fields are:

$$\underline{E}^{in} = \left[\underline{E}_{0R}^t + \sum_{m=1}^{M}\underline{E}^{r_m}\right] =$$

$$= E_0 T_0 \left[ e^{jk_d \rho \sin(\phi-\theta_{0R}^t)} + \right.$$

$$\left. + \sum_{\substack{m=1 \\ m\,even}}^{M}\left(\prod_{p=1}^{m} R_p\right) e^{jk_d \rho \sin\left(\phi-\theta_m^i\right)} + \right.$$

$$+\sum_{\substack{m=1\\ m\,odd}}^{M}\left(\prod_{p=1}^{m}R_p\right)e^{-jk_d\rho\sin\left(\phi+\alpha+\theta_m^i\right)}\Bigg]\hat{z} \tag{3.100}$$

and

$$\begin{aligned}
&\underline{E}^{ext}=\underline{E}^{i}+\underline{E}^{r_0}+\sum_{m=1}^{M}\underline{E}^{t_m}=\\
&=E_0e^{jk_0\rho\cos(\phi-\phi')}\hat{z}W(0,\pi+\phi')+\\
&+R_0E_0e^{jk_0\rho\cos(\phi+\phi')}\hat{z}W(0,\pi-\phi')+\\
&+E_0T_0\Bigg[\sum_{\substack{m=1\\ m\,odd}}^{M}\left(\prod_{p=1}^{m-1}R_p\right)T_me^{jk_0\rho\sin\left(\phi+\alpha-\theta_m^t\right)}\cdot\\
&\cdot W\left(\frac{3}{2}\pi-\alpha+\theta_m^t,2\pi-\alpha\right)U\left(\theta_c-\theta_m^i\right)+\\
&+\sum_{\substack{m=1\\ m\,even}}^{M}\left(\prod_{p=1}^{m-1}R_p\right)T_me^{-jk_0\rho\sin\left(\phi+\theta_m^t\right)}W\left(0,\frac{\pi}{2}-\theta_m^t\right)U\left(\theta_c-\theta_m^i\right)\Bigg]\hat{z}
\end{aligned} \tag{3.101}$$

where $W()$ is defined in (3.25) and $U()$ is defined in (3.26).

## Diffracted field: UAPO solutions for $\pi/2 < \phi' < \pi-\alpha$

The closed form expressions for the field diffracted by the edge of a lossless acute-angled dielectric wedge when $\pi/2<\phi'<\pi-\alpha$ are here presented in both the external and the internal region (see Fig. 3.6(b) and 3.6(c)). The methodology used to obtain them is the same described in Subsec. 3.2.3 and only the final results are reported here, because of the evident analogy with the post-inversion case. In fact, as

direct consequence of the equality of the GO fields expression with the post-inversion ones (aside from the absence of $\Gamma(N)$), also the expressions of the equivalent electric $\underline{J}_s^{ext,in}$ and magnetic $\underline{J}_{ms}^{ext,in}$ surface currents, defined in (3.38)-(3.41) and reported in the post-inversion section of Appendix A, still hold.

As regards the external problem, the field scattered by the wedge in the surrounding space is represented by the radiation integral (3.43) and consequently by the (3.45) and (3.46). The field scattered inside the wedge (internal problem) can be evaluated by the (3.44) and therefore by solving (3.71) and (3.72).

## External problem

The UAPO diffracted field contribution originated by $S_0$ can be expressed as:

$$\left(\underline{E}_{ext}^{d}\right)_0 = \left[\left(\underline{E}_{ext}^{d}\right)_0\right]_{I+R} + \sum_{\substack{m=1 \\ m\,even}}^{M} \left[\left(\underline{E}_{ext}^{d}\right)_0\right]_{T_m} \tag{3.102}$$

where

$$\left[\left(\underline{E}_{ext}^{d}\right)_0\right]_{I+R} = E_0\left[\sin\phi'\left(1-R_0\right)-\sin\phi\left(1+R_0\right)\right]\frac{e^{-j\pi/4}}{2\sqrt{2\pi k_0}}\cdot \cdot\frac{F_t\left[2k_0\rho\cos^2\left(\dfrac{\phi\pm\phi'}{2}\right)\right]}{\cos\phi+\cos\phi'}\frac{e^{-jk_0\rho}}{\sqrt{\rho}}\hat{z} \tag{3.103}$$

and

$$\sum_{\substack{m=1\\ m\,even}}^{M}\left[\left(\underline{E}_{ext}^{d}\right)_0\right]_{T_m}=-E_0T_0\left[\sum_{\substack{m=1\\ m\,even}}^{M}\left(\prod_{p=1}^{m-1}R_p\right)T_m\left(\sin\phi+\cos\theta_m^t\right)\right]\cdot$$
$$\cdot\frac{F_t\left[2k_0\rho\cos^2\left(\dfrac{\phi\pm\left(\pi/2+\theta_m^t\right)}{2}\right)\right]}{\cos\phi+\cos\left(\pi/2+\theta_m^t\right)}\frac{e^{-j\pi/4}}{2\sqrt{2\pi k_0}}\frac{e^{-jk_0\rho}}{\sqrt{\rho}}U\left(\theta^c-\theta_m^i\right)\hat{z} \tag{3.104}$$

in both expression the sign + applies in the interval $\left(0<\phi<\pi\right)$ and the sign − applies in the interval $\left(\pi<\phi<2\pi-\alpha\right)$.

The UAPO diffracted field contribution due to $S_n$ is:

$$\left(\underline{E}_{ext}^{d}\right)_n=E_0T_0\frac{e^{-j\pi/4}}{2\sqrt{2\pi k_0}}\left\{\sum_{\substack{m=1\\ m\,odd}}^{M}\left(\prod_{p=1}^{m-1}R_p\right)T_m\left[\sin\left(\phi+\alpha\right)-\cos\theta_m^t\right]\right\}\cdot$$
$$\cdot\frac{F_t\left[2k_0\rho\cos^2\left(\dfrac{\left(\phi+\alpha\right)\pm\left(\pi/2+\theta_m^t\right)}{2}\right)\right]}{\cos\left(\phi+\alpha\right)+\cos\left(\pi/2+\theta_m^t\right)}\frac{e^{-jk_0\rho}}{\sqrt{\rho}}U\left(\theta_c-\theta_m^i\right)\hat{z} \tag{3.105}$$

in which the sign - applies in the interval $\left(\pi-\alpha<\phi<2\pi-\alpha\right)$ and the sign + applies in the interval $\left(0<\phi<\pi-\alpha\right)$.

Then, the total diffracted field in the region external to the wedge is given by the superposition of the contributions (3.102) and (3.105)

$$E_{ext}^{d}=\left(\underline{E}_{ext}^{d}\right)_0+\left(\underline{E}_{ext}^{d}\right)_n \tag{3.106}$$

## Internal problem

The UAPO diffracted field contribution originated by $S_0$ can be expressed as:

$$\left(\underline{E}_{in}^{d}\right)_0 = \left[\left(\underline{E}_{in}^{d}\right)_0\right]_{T_0} + \sum_{\substack{m=1 \\ m\,even}}^{M}\left[\left(\underline{E}_{in}^{d}\right)_0\right]_{R_m} \tag{3.107}$$

where

$$\left[\left(\underline{E}_{in}^{d}\right)_0\right]_{T_0} = T_0 E_0 \frac{e^{-j\pi/4}}{2\sqrt{2\pi k_d}}\left(\sin\phi - \cos\theta_{0R}^{t}\right)\cdot \cdot \frac{F_t\left[2k_d\rho\cos^2\left(\frac{\phi+\left(\pi/2+\theta_{0R}^{t}\right)}{2}\right)\right]}{\cos\phi+\cos\left(\pi/2+\theta_{0R}^{t}\right)}\frac{e^{-jk_d\rho}}{\sqrt{\rho}}\hat{z} \tag{3.108}$$

and

$$\sum_{\substack{m=1 \\ m\,even}}^{M}\left[\left(\underline{E}_{in}^{d}\right)_0\right]_{R_m} = T_0 E_0 \cdot \cdot \sum_{\substack{m=1 \\ m\,even}}^{M}\left(\prod_{p=1}^{m-1} R_p\right)\left[\left(1+R_m\right)\sin\phi+\left(1-R_m\right)\cos\theta_m^{i}\right]\cdot \cdot \frac{F_t\left[2k_d\rho\cos^2\left(\frac{\phi+\left(\pi/2+\theta_m^{i}\right)}{2}\right)\right]}{\cos\phi+\cos\left(\pi/2+\theta_m^{i}\right)}\frac{e^{-j\pi/4}}{2\sqrt{2\pi k_d}}\frac{e^{-jk_d\rho}}{\sqrt{\rho}}\hat{z} \tag{3.109}$$

The expression of the UAPO diffracted field contribution originated by $S_n$ is:

$$\left(\underline{E}_{in}^{d}\right)_n = E_0 T_0 \sum_{\substack{m=1 \\ m\,odd}}^{M} \left( \prod_{p=1}^{m-1} R_p \right) \left[ \left(1 - R_m\right) \cos\theta_m^i - \left(1 + R_m\right) \sin\left(\phi + \alpha\right) \right] \cdot$$
$$\cdot \frac{F_t\left[ 2k_d \rho \cos^2\left( \frac{\left(\phi + \alpha\right) + \left(\pi/2 + \theta_m^i\right)}{2} \right) \right]}{\cos\left(\phi + \alpha\right) + \cos\left(\pi/2 + \theta_m^i\right)} \frac{e^{-j\pi/4}}{2\sqrt{2\pi k_d}} \frac{e^{-jk_d\rho}}{\sqrt{\rho}} \hat{z} \tag{3.110}$$

So, the total diffracted field in the region internal to the wedge is given by the superposition of the contributions (3.107) and (3.110).

$$\underline{E}_{in}^{d} = \left(\underline{E}_{in}^{d}\right)_0 + \left(\underline{E}_{in}^{d}\right)_n \tag{3.111}$$

## 3.2.5 Numerical results

In this Section, numerical results are reported in order to prove the validity and accuracy of the UAPO solution for the field diffracted by the edge of an acute-angled and lossless dielectric wedge developed in Subsecs. 3.2.1, 3.2.3 and 3.2.4. For what concerns simulations in Figs. 3.9-3.12, the considered wedge is characterized by $\alpha = 20°$ and $\varepsilon_r = 3$ and the field amplitude is evaluated over a circular path having radius $\rho = 4\lambda_0$. Numerical results shown in Figs. 3.9 and 3.10 are relevant to an *E*-polarized plane wave having $E_0 = 1$ V/m illuminating only the face $S_0$ and propagating in the direction $\phi' = 35°$. These values produce $N = 1$ pre-inversion interaction point and other $M = 3$ points associated to the post-inversion series. Therefore, the complete number of internal reflection is $N + M + 1 = 5$, but the total internal reflection occurs at the fourth interaction. Consequently, in addition to

the boundaries related to the incident and specular reflection directions, three transmission boundaries exist in the external region.

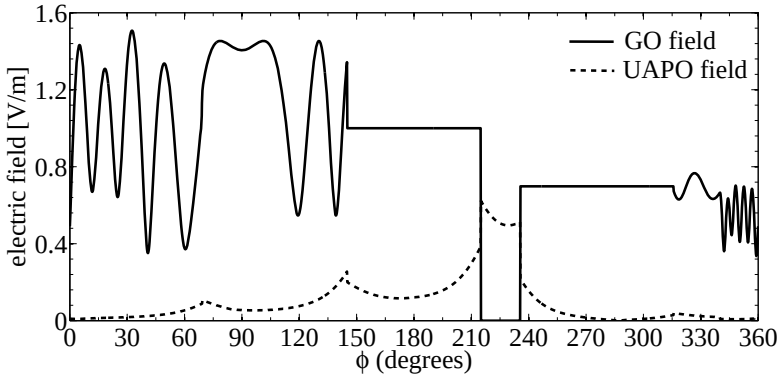


**Figure 3.9** Amplitude of the z-component of the GO and UAPO diffracted field: $\phi' = 35°$.

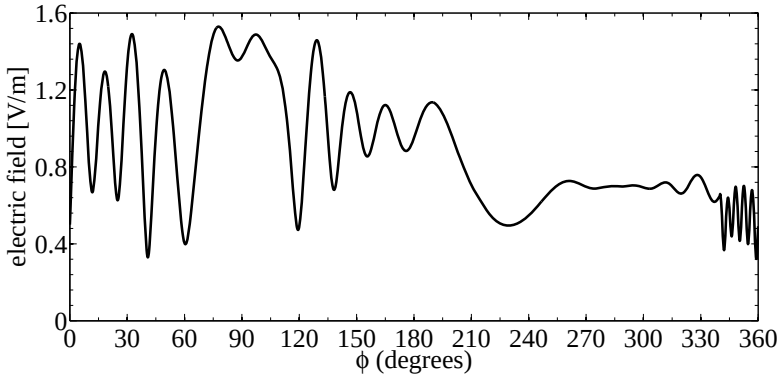


**Figure 3.10** Amplitude of the z-component of the total field: $\phi' = 35°$.

As can be seen, the GO pattern in Fig. 3.9 is discontinuous in correspondence of the shadow boundaries: $\phi_{RB_0} = 145°$, $\phi_{SB_0} = 215°$, $\phi_{TB_n-1} = 235.6°$, $\phi_{TB_0-1} = 69.3°$, $\phi_{TB_n-2} = 315.7°$. However, the UAPO diffracted field is significant at these boundaries and perfectly compensates the GO field discontinuities (see Fig. 3.10).

Figs. 3.11 and 3.12 are relevant to *E*-polarized plane wave having $E_0 = 1$ V/m propagating in the direction $\phi' = 110°$. In this case, the GO field boundaries are located at $\phi_{RB_0} = 70°$, $\phi_{SB_0} = 290°$ and

$\phi_{TB_n-1} = 314.4°$ since the total internal reflection occurs at the second interaction (see Fig. 3.11). The developed UAPO solution removes also in this case the discontinuities at the shadow boundaries (see Fig. 3.12).

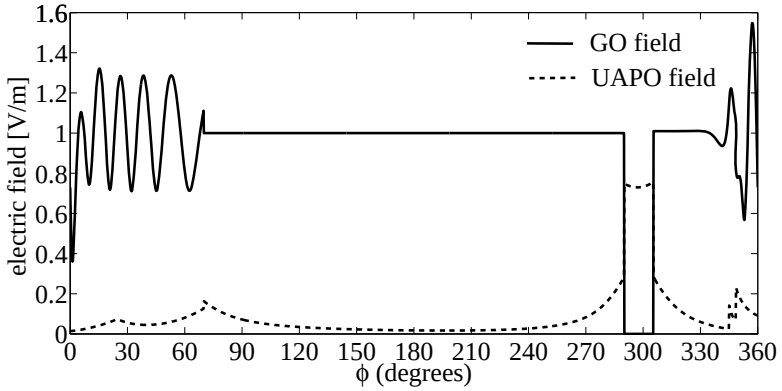


**Figure 3.11** Amplitude of the z-component of the GO and UAPO diffracted field: $\phi' = 110°$.

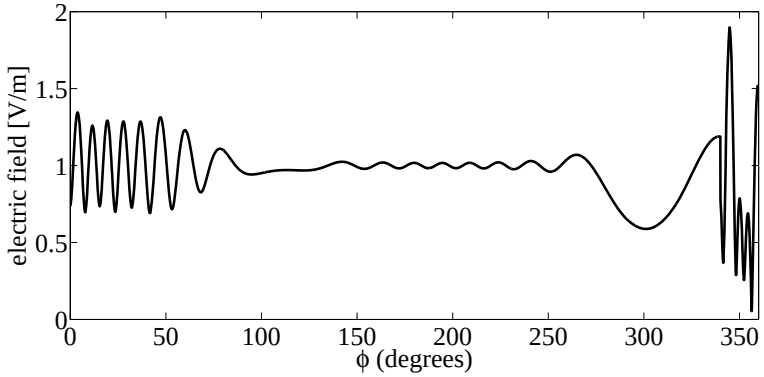


**Figure 3.12** Amplitude of the z-component of the total field: $\phi' = 110°$.

It is opportune to point out that the compensation of the GO field discontinuities indicates only the consistency of the UAPO solution. On the other hand, an exact and reliable reference solution is needed to test its accuracy. To this end, numerical simulations are performed by using two reliable numerical solvers. The former is the

radiofrequency module of *Comsol Multiphysics*, a commercial tool based on FEM. The latter is an in-house code based on FDTD technique [45]. Such a code implements the total field/scattered field technique to generate an accurate incident numerical plane wave. The outer boundaries of the computational domain are terminated with a Uniaxial Perfectly Matched Layer (UPML) [46] backed with a perfect electric conductor wall. As well-known, UPML's function is able to absorb the incoming electromagnetic waves with very low retro reflections in the simulation region.

Comparison between the UAPO and numerical results are shown in Figs. 3.13-3.16. They refer to lossless wedges characterized by $\varepsilon_r = 2$ and $\alpha = 15°, 30°, 45°, 60°$ illuminated by an *E*-polarized plane wave having $E_0 = 1$ V/m and impinging at $\phi' = 110°$.

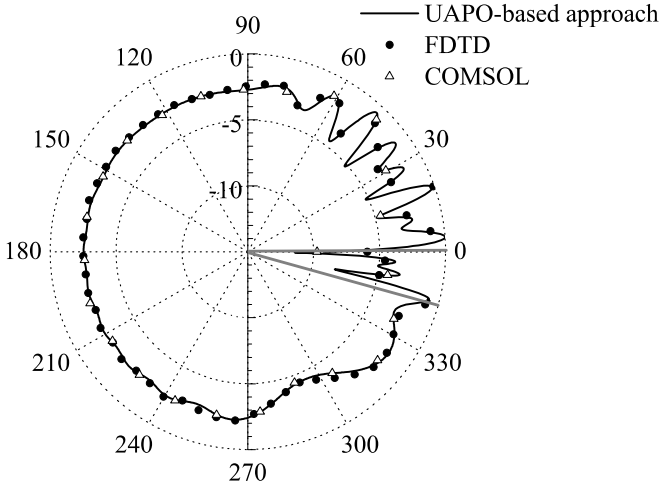


**Figure 3.13** The *z*-component of the electric field when $\alpha = 15°$.

The field magnitude (normalized to the peak value and expressed in decibel) is collected on a circular path with $\rho = 4\lambda_0$. Fig. 3.13 is relevant to $\alpha = 15°$, so that $M = 5$. In addition to the boundaries related to the incident and specular reflection directions, two boundaries exist in the external region since the total internal reflection occurs at the third interaction. As can be seen, a remarkably good agreement is attained with both the COMSOL solution and the FDTD-based results. In particular, the UAPO solution accuracy is

confirmed not only outside the wedge but also inside it. Analogous considerations can be drawn from the results in Figs. 3.14, 3.15 and 3.16 relevant to higher values of $\alpha$. Note that Fig. 3.14 refers to the case $\alpha = 30°$ ($M = 2$) with one transmission contribution through $S_n$ in addition to the incident and specular reflection contributions. Finally, Figs. 3.15 and 3.16 are relevant to cases for which no transmission contributions exist in the external region since the total internal reflection occurs at the one and only interaction on the internal face of $S_n$.

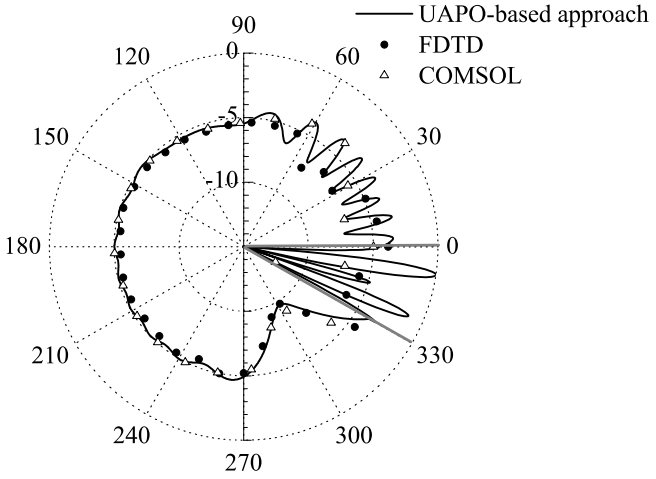


**Figure 3.14** The *z*-component of the electric field when $\alpha = 30°$.

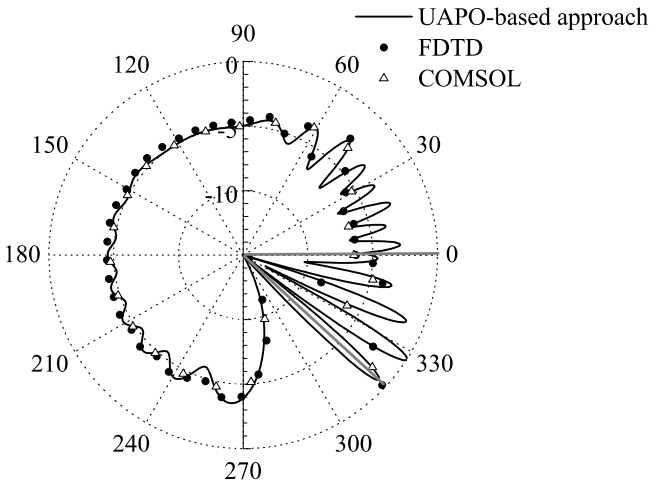


**Figure 3.15** The *z*-component of the electric field when $\alpha = 45°$.

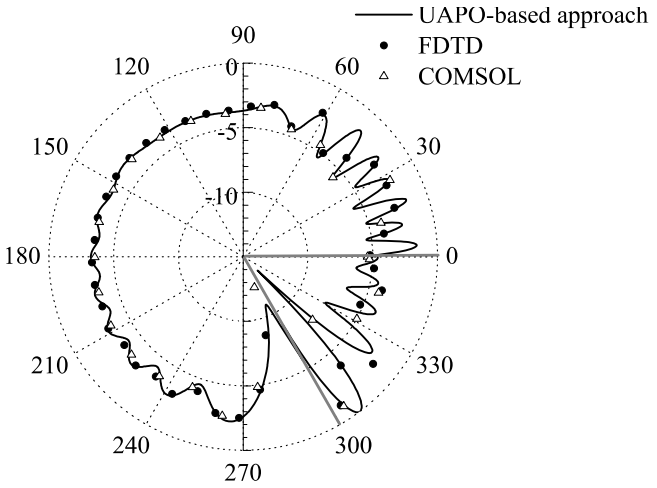


**Figure 3.16** The *z*-component of the electric field when $\alpha = 60°$.

The proposed UAPO solutions are characterized by some limitations due to the use of the PO approximation in the radiation integral. By looking at Figs. 3.10 and 3.12 it is evident the fact that they break the boundary condition at the dielectric interfaces. This limitation can be appreciated also in the case of dielectric constant going to infinity for simulating a perfectly conducting wedge.

Moreover, the UAPO solutions give unreliable results in the case of grazing incidence as demonstrated in [47].

### 3.2.6 Formulation of the problem for *H*-polarized plane waves

In Subsecs. 3.2.1, 3.2.3 and 3.2.4 the effects of an *E*-polarized plane wave impinging on a dielectric acute-angled wedge have been analyzed. The aim of this section is to provide UAPO solutions for the field diffracted by the same wedge now illuminated by a *H*-polarized plane wave. Being the problem almost similar to the previous ones, only the simplest case of one series of rays has been considered and just the final results have been reported in the following.

The geometry of the problem is the same of Fig. 3.1 with the difference that the uniform plane wave illuminating the wedge has the magnetic field $\underline{H}$ directed along $\hat{z}$, as shown in Fig. 3.17. The direction of propagation is still fixed by the angle $\phi'$ and its values are here considered in the range from $\pi/2$ to $\pi-\alpha$ so that only the face $S_0$ is directly illuminated by the incident field. As for the *E*-polarization case, a series of internal and external rays propagating far from the apex arises (Fig. 3.17) and the external rays exist until the total reflection doesn't occur.

By matching Fig 3.17 with Figs. 3.8 and 3.4 it is evident that this ray-tracing is the same of those related to the *E*-polarization case apart for the magnetic field $\underline{H}$ directed along $\hat{z}$. Consequently, the contributions to GO magnetic fields are analogous to those related to the GO electric fields in the *E*-polarization case.

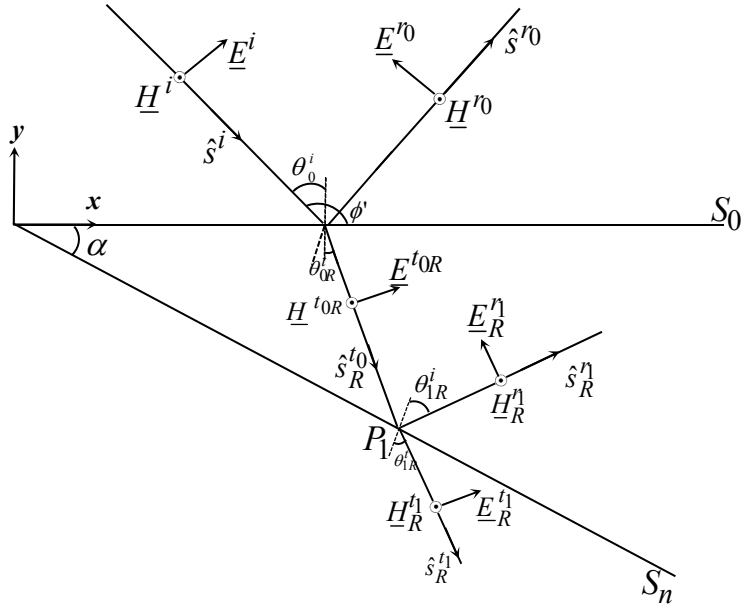


**Figure 3.17** Rays transmissions/reflections through the wedge

The expressions for GO electric fields in the *H*-polarization case can be simply obtained by applying the property of plane wave.

Then, the whole expressions of the GO response for the electric field are:

$$\underline{E}^{ext} = \underline{E}^i + \underline{E}^{r_0} + \sum_{m=1}^{M} \underline{E}^{t_m} =$$

$$= \zeta_0 H_0 \left\{ e^{jk_0\rho\cos(\phi-\phi')}\left(-\cos\phi'\hat{x}+\sin\phi'\hat{y}\right) + \right.$$

$$+ R_0 e^{jk_0\rho\cos(\phi+\phi')}\left(-\sin\phi'\hat{x}-\cos\phi'\hat{y}\right) +$$

$$+ T_0 \sum_{\substack{m=1 \\ m\,even}}^{M} \left( \prod_{p=1}^{m-1} R_p \right) T_m e^{-jk_0\rho\sin\left(\phi+\theta_m^t\right)} \left(-\cos\theta_m^t\hat{x}+\sin\theta_m^t\hat{y}\right) +$$

$$+T_0 \sum_{\substack{m=1 \\ m\,odd}}^{M} \left( \prod_{p=1}^{m-1} R_p \right) T_m e^{jk_0 \rho \sin\left(\phi+\alpha-\theta_m^t\right)} \left[ \cos(\theta_m^t - \alpha)\hat{x} + \sin(\theta_m^t - \alpha)\hat{y} \right] \Bigg\} \tag{3.112}$$

and

$$\underline{E}^{in} = \underline{E}_{0R}^{t} + \sum_{m=1}^{M} \underline{E}^{r_m} =$$

$$= \zeta_d H_0 T_0 \Bigg\{ e^{jk_d \sin(\phi-\theta_{0R}^t)} \left( \cos\theta_{0R}^t \hat{x} + \sin\theta_{0R}^t \hat{y} \right) +$$

$$+ \sum_{\substack{m=1 \\ m\,even}}^{M} \left( \prod_{p=1}^{m} R_p \right) e^{jk_d \rho \sin\left(\phi-\theta_m^i\right)} \left( \cos\theta_m^i \hat{x} + \sin\theta_m^i \hat{y} \right) +$$

$$+ \sum_{\substack{m=1 \\ m\,odd}}^{M} \left( \prod_{p=1}^{m} R_p \right) e^{-jk_d \rho \sin\left(\phi+\alpha+\theta_m^i\right)} \left[ -\cos\left(\theta_m^i + \alpha\right)\hat{x} + \sin\left(\theta_m^i + \alpha\right)\hat{y} \right] \Bigg\} \tag{3.113}$$

It must be stressed that now the expression of the coefficients of reflection and transmission present in eqns. (3.112) and (3.113) are relative to the *H*-polarization case.

The closed form expressions for the electric field diffracted by the edge of the wedge in both the external and the internal region (see Fig. 3.6(b) and 3.6(c)) have been obtained following the same approach of Subsecs. 3.2.3 and 3.2.4. The expression of the diffracted magnetic field can be easily obtained by the relationship:

$$\underline{H}^d = \frac{1}{\zeta} \hat{s} \times \underline{E}^d \tag{3.114}$$

The expressions of the equivalent electric $\underline{J}_s^{ext,in}$ and magnetic $\underline{J}_{ms}^{ext,in}$ surface currents, defined in (3.38)-(3.41) are reported in the *H*-polarization section of Appendix A.

As regards the external problem, the field scattered by the wedge in the surrounding space is represented by the radiation integral (3.43) and consequently by the (3.45) and (3.46). The field scattered inside the wedge (internal problem) can be evaluated by the (3.44) and therefore by solving (3.71) and (3.72). The corresponding magnetic fields can be found by (3.114).

## External problem

By defining the unit vector $\hat{\phi} = (-\sin\hat{x}, \cos\hat{y}, 0)$, the UAPO diffracted electric field contribution originated by $S_0$ can be expressed as:

$$\left(\underline{E}_{ext}^{d}\right)_0 = \left[\left(\underline{E}_{ext}^{d}\right)_0\right]_{I+R} + \sum_{\substack{m=1 \\ m\,even}}^{M} \left[\left(\underline{E}_{ext}^{d}\right)_0\right]_{T_m} \tag{3.115}$$

where

$$\left[\left(\underline{E}_{ext}^{d}\right)_0\right]_{I+R} = \zeta_0 H_0 \left[\sin\phi'\left(1-R_0\right) - \sin\phi\left(1+R_0\right)\right] \cdot \frac{F_t\left[2k_0\rho\cos^2\left(\frac{\phi \pm \phi'}{2}\right)\right]}{\cos\phi + \cos\phi'} \frac{e^{-jk_0\rho}}{\sqrt{\rho}} \frac{e^{-j\pi/4}}{2\sqrt{2\pi k_0}}\hat{\phi} \tag{3.116}$$

and

$$\sum_{\substack{m=1\\ m\,even}}^{M}\left[\left(\underline{E}_{ext}^{d}\right)_0\right]_{T_m}=-\zeta_0 H_0 T_0\left[\sum_{\substack{m=1\\ m\,even}}^{M}\left(\prod_{p=1}^{m-1}R_p\right)T_m\left(\sin\phi+\cos\theta_m^t\right)\right]\cdot$$
$$\cdot\frac{F_t\left[2k_0\rho\cos^2\left(\dfrac{\phi\pm\left(\pi/2+\theta_m^t\right)}{2}\right)\right]}{\cos\phi+\cos\left(\pi/2+\theta_m^t\right)}\frac{e^{-j\pi/4}}{2\sqrt{2\pi k_0}}\frac{e^{-jk_0\rho}}{\sqrt{\rho}}U\left(\theta_c-\theta_m^i\right)\hat{\phi} \tag{3.117}$$

in both expression the sign + applies in the interval $(0<\phi<\pi)$ and the sign − applies in the interval $(\pi<\phi<2\pi-\alpha)$.

The UAPO diffracted electric field contribution due to $S_n$ is:

$$\left(\underline{E}_{ext}^{d}\right)_n=\zeta_0 H_0 T_0\frac{e^{-j\pi/4}}{2\sqrt{2\pi k_0}}\left\{\sum_{\substack{m=1\\ m\,odd}}^{M}\left(\prod_{p=1}^{m-1}R_p\right)T_m\left[\sin\left(\phi+\alpha\right)-\cos\theta_m^t\right]\right\}\cdot$$
$$\cdot\frac{F_t\left[2k_0\rho\cos^2\left(\dfrac{\left(\phi+\alpha\right)\pm\left(\pi/2+\theta_m^t\right)}{2}\right)\right]}{\cos\left(\phi+\alpha\right)+\cos\left(\pi/2+\theta_m^t\right)}\frac{e^{-jk_0\rho}}{\sqrt{\rho}}U\left(\theta_c-\theta_m^i\right)\hat{\phi} \tag{3.118}$$

in which the sign − applies in the interval $(\pi-\alpha<\phi<2\pi-\alpha)$ and the sign + applies in the interval $(0<\phi<\pi-\alpha)$. Then, the total diffracted electric field in the region external to the wedge is given by the superposition of the contributions (3.115) and (3.118).

$$\underline{E}_{ext}^{d}=\left(\underline{E}_{ext}^{d}\right)_0+\left(\underline{E}_{ext}^{d}\right)_n \tag{3.119}$$

The corresponding diffracted magnetic field $\underline{H}_{ext}^{d}$ can be found by (3.114) and it results to be directed along the z-axis.

## Internal problem

The UAPO diffracted electric field contribution originated by $S_0$ can be expressed as:

$$\left(\underline{E}_{in}^{d}\right)_0 = \left[\left(\underline{E}_{in}^{d}\right)_0\right]_{T_0} + \sum_{\substack{m=1 \\ m\,even}}^{M}\left[\left(\underline{E}_{in}^{d}\right)_0\right]_{R_m} \tag{3.120}$$

where

$$\left[\left(\underline{E}_{in}^{d}\right)_0\right]_{T_0} = \zeta_0 H_0 T_0 \frac{e^{-j\pi/4}}{2\sqrt{2\pi k_d}}\left(\sin\phi - \cos\theta_{0R}^{t}\right)\cdot \cdot \frac{F_t\left[2k_d\rho\cos^2\left(\dfrac{\phi+\left(\pi/2+\theta_{0R}^{t}\right)}{2}\right)\right]}{\cos\phi+\cos\left(\pi/2+\theta_{0R}^{t}\right)}\frac{e^{-jk_d\rho}}{\sqrt{\rho}}\hat{\phi} \tag{3.121}$$

and

$$\sum_{\substack{m=1 \\ m\,even}}^{M}\left[\left(\underline{E}_{in}^{d}\right)_0\right]_{R_m} =$$

$$= \zeta_0 H_0 T_0 \sum_{\substack{m=1 \\ m\,even}}^{M}\left(\prod_{p=1}^{m-1} R_p\right)\left[\left(1+R_m\right)\sin\phi + \left(1-R_m\right)\cos\theta_m^{i}\right]\cdot$$

$$\cdot \frac{F_t\left[2k_d\rho\cos^2\left(\frac{\phi+\left(\pi/2+\theta_m^i\right)}{2}\right)\right]}{\cos\phi+\cos\left(\pi/2+\theta_m^i\right)} \frac{e^{-j\pi/4}}{2\sqrt{2\pi k_d}} \frac{e^{-jk_d\rho}}{\sqrt{\rho}}\hat{\phi} \quad (3.122)$$

The expression of the UAPO diffracted field contribution originated by $S_n$ is:

$$\left(\underline{E}_{in}^d\right)_n = \zeta_0 H_0 T_0 \cdot$$
$$\cdot \sum_{\substack{m=1 \\ m\,odd}}^{M} \left(\prod_{p=1}^{m-1} R_p\right)\left[\left(1-R_m\right)\cos\theta_m^i - \left(1+R_m\right)\sin\left(\phi+\alpha\right)\right]\cdot$$
$$\cdot \frac{F_t\left[2k_d\rho\cos^2\left(\frac{\left(\phi+\alpha\right)+\left(\pi/2+\theta_m^i\right)}{2}\right)\right]}{\cos\left(\phi+\alpha\right)+\cos\left(\pi/2+\theta_m^i\right)} \frac{e^{-j\pi/4}}{2\sqrt{2\pi k_d}} \frac{e^{-jk_d\rho}}{\sqrt{\rho}}\hat{\phi} \quad (3.123)$$

So, the total diffracted field in the region internal to the wedge is given by the superposition of the contributions (3.120) and (3.123).

$$\underline{E}_{in}^d = \left(\underline{E}_{in}^d\right)_0 + \left(\underline{E}_{in}^d\right)_n \quad (3.124)$$

The corresponding diffracted magnetic field $\underline{H}_{in}^d$ can be found by (3.114) and it results to be directed along z-axis.

By matching the expressions (3.119) and (3. 124) of the UAPO diffracted electric fields for an *H*-polarized plane wave with those found in the *E*-polarization hypothesis (eqns. (3.106) and (3.111)), it is possible to notice a strong and useful analogy that have to be underlined. In fact, if the diffracted electric field for the *H*-polarization is written as

$$\underline{E}^{d}_{int,ext}(P) = D^{int,ext}_{\phi\phi'} \frac{e^{-jk_{d,0}\rho}}{\sqrt{\rho}} E_0 \hat{\phi} \tag{3.125}$$

then

$$D^{int,ext}_{\phi\phi'} = -D^{int,ext}_{zz} \tag{3.126}$$

where $D^{int,ext}_{zz}$ is the diffraction coefficient for the *E*-polarization, on the condition to use the appropriate Fresnel reflection and transmission coefficients (see also [41]-[43]).

## 3.3 Particular cases: right- and obtuse-angled dielectric wedges

In Subsec. 3.2.3 UAPO solutions for the diffracted field originated by an acute-angled lossless dielectric wedge have been determined for an *E*-polarized incident plane wave and for values of $\phi'$ in the range from 0 to $\pi/2$. By matching these solutions with those proposed for a right- and an obtuse-angled wedges [41], [42] it is evident that a high correspondence exists between them. The aim of this section it to show that the UAPO solutions for the diffracted field found in Subsec. 3.2.3 have general validity and can be applied to a wedge with arbitrary apex angle. The Subsecs. 3.3.1 and 3.3.2 are devoted to demonstrate that such solutions include those proposed for a right- and obtuse-angled wedges as particular cases.

### 3.3.1 Comparisons with a right-angled dielectric wedge

Let us consider the problem of plane-wave diffraction by the edge of a right-angled dielectric wedge, which solutions for GO fields and UAPO diffracted fields are well-known [41]. By considering the geometry of Fig. 3.1, the expressions of UAPO diffracted fields (3.55), (3.60), (3.64), (3.69), (3.80), (3.84), (3.92) and (3.96) found in

Subsec. 3.2.3 lead to the same solutions of [41], if made particular for $\alpha = \pi/2$. In fact, being $0 < \theta_{0L}^{t} < \pi/2$ it results:

$$N_i = \mathrm{Int}\left[\frac{\theta_{0L}^{t}}{\alpha}\right] = \mathrm{Int}\left[\frac{\theta_{0L}^{t}}{\pi/2}\right] = 0 \tag{3.127}$$

As a consequence, $N = N_i + 1 = 1$ and so the function $\Gamma(N)$ defined in eq. (3.31) becomes:

$$\Gamma(1) = U\left(\frac{\pi}{2} - \theta_1^{i} - \frac{\pi}{2}\right)\prod_{p=1}^{2} R_p = 0 \tag{3.128}$$

Therefore, the expression of the external UAPO diffracted fields become:

$$\underline{E}_{ext}^{d} = \left(\underline{E}_{ext}^{d}\right)_0 + \left(\underline{E}_{ext}^{d}\right)_n = E_0 \frac{e^{-j\pi/4}}{2\sqrt{2\pi k_0}} \frac{e^{-jk_0\rho}}{\sqrt{\rho}} \hat{z} \cdot$$

$$\cdot\left\{\left[\sin\phi'\left(1 - R_0\right) - \sin\phi\left(1 + R_0\right)\right]\frac{F_t\left[2k_0\rho\cos^2\left(\dfrac{\phi \pm \phi'}{2}\right)\right]}{\cos\phi + \cos\phi'} + \right.$$

$$+ T_0 T_1\left(\cos\phi - \cos\theta_1^{t}\right) \cdot$$

$$\left. \cdot\frac{F_t\left[2k_0\rho\cos^2\left(\dfrac{\left(\phi + \pi/2\right) \pm \left(\pi/2 + \theta_1^{t}\right)}{2}\right)\right]}{\cos\left(\phi + \pi/2\right) + \cos\left(\pi/2 + \theta_1^{t}\right)} U\left(\theta^{c} - \theta_1^{i}\right)\right\} \tag{3.129}$$

In eq. (3.129), in the first term the sign + applies in the interval $\left(0<\phi<\pi\right)$ and the sign − applies in the interval $\left(\pi<\phi<\frac{3}{2}\pi\right)$ and in the second term the sign + applies in the interval $\left(0<\phi<\frac{\pi}{2}\right)$ and the sign − applies in the interval $\left(\frac{\pi}{2}<\phi<\frac{3}{2}\pi\right)$. The expression of the UAPO internal diffracted field becomes:

$$\underline{E}_{in}^{d}=\left(\underline{E}_{in}^{d}\right)_0+\left(\underline{E}_{in}^{d}\right)_n=$$

$$=E_0T_0\frac{e^{-j\pi/4}}{2\sqrt{2\pi k_0}}\left\{\left(\sin\phi-\cos\theta_{0L}^{t}\right)\frac{F_t\left[2k_d\rho\cos^2\left(\frac{\phi+\left(\pi/2-\theta_{0L}^{t}\right)}{2}\right)\right]}{\cos\phi+\cos\left(\pi/2-\theta_{0L}^{t}\right)}+\right.$$

$$+\left[\left(1-R_1\right)\sin\theta_{0L}^{t}-\left(1+R_1\right)\cos\phi\right]\cdot$$

$$\left.\cdot\frac{F_t\left[2k_d\rho\cos^2\left(\frac{\left(\phi+\pi/2\right)+\left(\pi/2-\theta_1^{i}\right)}{2}\right)\right]}{\cos\left(\phi+\pi/2\right)-\cos\theta_{0L}^{t}}\right\}\frac{e^{-jk_0\rho}}{\sqrt{\rho}}\hat{z}\qquad(3.130)$$

The expressions (3.129) and (3.130) agree with those reported in [41] and so the available solutions of UAPO diffracted fields for a right-angled dielectric wedge can be considered as particular solutions of those relative to an acute-angled dielectric wedge, reported in Subsec. 3.2.3.

### 3.3.2 Comparisons with an obtuse-angled dielectric wedge

In this subsection the solutions for the plane-wave diffraction by the edge of an obtuse-angled dielectric wedge reported in [42] are taken as reference. Starting from the geometry of Fig. 3.1, the expressions of UAPO diffracted fields (3.55), (3.60), (3.64), (3.69), (3.80), (3.84), (3.92) and (3.96) found in Subsec. 3.2.3 are considered for values of the aperture of the wedge $\alpha$ greater than $\pi/2$. By following the same approach of [42], two separated cases, relative to different ranges of values of the internal transmission angle $\theta_{0L}^{t}$ have been studied. In the first case the values of $\theta_{0L}^{t}$ are such to avoid the illumination of the internal face of $S_n$. In the second one it is illuminated by the ray transmitted through $S_0$ giving arise to a further reflected/transmitted ray.

**CASE 1**: $S_n$ not illuminated ($\theta_{0L}^{t} < \alpha - \pi/2$)

Being $\theta_{0L}^{t} < \alpha - \pi/2$ and $\alpha > \pi/2$ it results $N_i = \mathrm{Int}\left[\theta_{0L}^{t}/\alpha\right] = 0$ and so $N = N_i + 1 = 1$. Then, the function $\Gamma(N)$ defined in (3.31) becomes:

$$\Gamma(1) = U\left(\frac{\pi}{2} - \theta_1^i - \alpha\right)\prod_{p=1}^{2} R_p = 0 \qquad (3.131)$$

Therefore, the expression of the external UAPO diffracted field becomes:

$$\underline{E}_{ext}^{d} = \left(\underline{E}_{ext}^{d}\right)_0 + \left(\underline{E}_{ext}^{d}\right)_n = E_0 \frac{e^{-j\pi/4}}{2\sqrt{2\pi k_0}} \frac{e^{-jk_0\rho}}{\sqrt{\rho}} \cdot$$

$$\cdot\left[\sin\phi'\left(1-R_0\right)-\sin\phi\left(1+R_0\right)\right]\frac{F_t\left[2k_0\rho\cos^2\left(\dfrac{\phi\pm\phi'}{2}\right)\right]}{\cos\phi+\cos\phi'}\hat{z} \tag{3.132}$$

in which the sign + applies in the interval $\left(0<\phi<\pi\right)$ and the sign − applies in the interval $\left(\pi<\phi<2\pi-\alpha\right)$. The expression for the UAPO internal diffracted field becomes:

$$\underline{E}_{in}^{d}=\left(\underline{E}_{in}^{d}\right)_0+\left(\underline{E}_{in}^{d}\right)_n=E_0T_0\frac{e^{-j\pi/4}}{2\sqrt{2\pi k_0}}\frac{e^{-jk_0\rho}}{\sqrt{\rho}}$$
$$\cdot\left(\sin\phi-\cos\theta_{0L}^{t}\right)\frac{F_t\left[2k_d\rho\cos^2\left(\dfrac{\phi+\left(\pi/2-\theta_{0L}^{t}\right)}{2}\right)\right]}{\cos\phi+\cos\left(\pi/2-\theta_{0L}^{t}\right)}\hat{z} \tag{3.133}$$

The expressions (3.132) and (3.133) match with solutions reported in [42] for the range $0<\theta_{0L}^{t}<\alpha-\pi/2$.

**CASE 2**: $S_n$ illuminated ($\theta_{0L}^{t}>\alpha-\pi/2$)

Being $\theta_{0L}^{t}>\alpha-\pi/2$ and $\alpha>\pi/2$ it results $N_i=\mathrm{Int}\left[\theta_{0L}^{t}/\alpha\right]=0$ and so $N=N_i+1=1$. Then, the function $\Gamma\left(N\right)$ defined in (3.31) becomes:

$$\Gamma\left(1\right)=U\left(\frac{\pi}{2}-\theta_1^{i}-\alpha\right)\prod_{p=1}^{2}R_p=0 \tag{3.134}$$

Therefore, the expression of the external UAPO diffracted fields becomes:

$$\underline{E}_{ext}^{d}=\left(\underline{E}_{ext}^{d}\right)_0+\left(\underline{E}_{ext}^{d}\right)_n=E_0\frac{e^{-j\pi/4}}{2\sqrt{2\pi k_0}}\frac{e^{-jk_0\rho}}{\sqrt{\rho}}\Bigg\{$$

$$\left[\sin\phi'\left(1-R_0\right)-\sin\phi\left(1+R_0\right)\right]\frac{F_t\left[2k_0\rho\cos^2\left(\dfrac{\phi\pm\phi'}{2}\right)\right]}{\cos\phi+\cos\phi'}+$$

$$+T_0T_1\left[\sin\left(\phi+\alpha\right)-\cos\theta_1^t\right]\cdot$$

$$\cdot\frac{F_t\left[2k_0\rho\cos^2\left(\dfrac{\left(\phi+\alpha\right)\pm\left(\pi/2+\theta_1^t\right)}{2}\right)\right]}{\cos\left(\phi+\alpha\right)+\cos\left(\pi/2+\theta_1^t\right)}U\left(\theta^c-\theta_1^i\right)\Bigg\}\hat{z}\qquad(3.135)$$

In eq. (3.135) in the first term the sign + applies in the interval $\left(0<\phi<\pi\right)$ and the sign − applies in the interval $\left(\pi<\phi<2\pi-\alpha\right)$ and in the second term the sign + applies in the interval $\left(0<\phi<\pi-\alpha\right)$ and the sign − applies in the interval $\left(\pi-\alpha<\phi<2\pi-\alpha\right)$. The expression for the UAPO internal diffracted field becomes:

$$\underline{E}_{in}^{d}=\left(\underline{E}_{in}^{d}\right)_0+\left(\underline{E}_{in}^{d}\right)_n=E_0T_0\frac{e^{-j\pi/4}}{2\sqrt{2\pi k_0}}\frac{e^{-jk_0\rho}}{\sqrt{\rho}}\Bigg\{$$

$$\left(\sin\phi-\cos\theta_{0L}^t\right)\frac{F_t\left[2k_d\rho\cos^2\left(\dfrac{\phi+\left(\pi/2-\theta_{0L}^t\right)}{2}\right)\right]}{\cos\phi+\cos\left(\pi/2-\theta_{0L}^t\right)}+$$

$$+\left[\left(1-R_1\right)\cos\left(\theta_{0L}^t-\alpha\right)-\left(1+R_1\right)\sin\left(\phi+\alpha\right)\right]\cdot$$

$$\cdot \frac{F_t\left[2k_d\rho\cos^2\left(\frac{(\phi+\alpha)+\left(\alpha-\theta_{0L}^t\right)}{2}\right)\right]}{\cos(\phi+\alpha)+\cos\left(\alpha-\theta_{0L}^t\right)}\Bigg\}\hat{z} \qquad (3.136)$$

The expressions (3.135) and (3.136) are equal to solutions reported in [42] for the case of $\theta_{0L}^t > \alpha - \pi/2$.

Therefore, the expressions (3.132), (3.133), (3.135) (3.136) are identical to those described in [42] and so the available solutions of the UAPO diffracted fields for an obtuse-angled dielectric wedge can be considered as particular solutions of those relative to an acute-angled dielectric wedge, reported in Subsec. 3.2.3.

In conclusion, basing on how much shown in Subsecs. 3.3.1 and 3.3.2, it is possible to consider the solutions of the UAPO diffracted fields found in Subsec. 3.2.3 as relative to an arbitrary-angled dielectric wedge.

## Chapter 4

# Time Domain solutions for diffraction by dielectric wedges

TD electromagnetic scattering problems are currently receiving great attention from both the research community and industry because of the widespread use of ultra-wide band (UWB) communication and radar systems. Actually, the large bandwidth of the UWB signals makes natural and more convenient to directly study the transient electromagnetic wave propagation phenomena rather than processing the FD data. In fact, the TD analysis allows one to determine all the necessary parameters in an UWB communication system as number of multipath, power, time delay, and distortion. Furthermore, the analysis of transient scattering phenomena is of importance for predicting the effects of electromagnetic pulses on civil and military structures. Many analytical TD solutions were proposed for predicting diffraction phenomena mainly concerning PEC objects. In this framework, the TD versions of GTD and UTD for a straight edge in PEC structures were developed by Veruttipong [48]. Rousseau and Pathak [49] proposed a TD-UTD solution applicable to the more general problem of diffraction by an arbitrarily curved PEC wedge which may contain curved faces and/or a curved edge. The TD-UTD formulation furnishes a simple physical representation for radiation and scattering phenomena since it uses the same rays (incident, reflected, and diffracted contributions) as the FD-UTD one. The available solutions were derived by means of analytical inversions of the corresponding high-frequency asymptotic expressions, so that they are valid for an observation time close to the arrival times of the various wave fronts. Note that TD-UTD is applicable for short pulse wave excitations.

A TD version of the physical theory of diffraction (TD-PTD) was derived by Johansen in [50]. He added the field predicted by the TD equivalent edge currents to the TD physical optics (TD-PO) field [51] in order to correct it. A TD-UTD solution for describing the transient

electromagnetic scattering from a smooth convex PEC surface excited by a general time impulsive astigmatic ray field was presented in [52]. The transient radiation and surface fields of elemental pulsed antennas placed on a smooth perfectly conducting, arbitrary convex surface were studied in [53]. With reference to the propagation of UWB signals, the two-dimensional multiple-diffraction by an arbitrary number of obstacles was solved in [54]. The proposed TD solution accounts for different types of objects along the propagation path. The scattering of an electromagnetic time dependent plane wave by the edge of an impedance wedge was considered by Pelosi *et al.* in [55], and suitable expressions for the surface currents induced on the faces of the wedge were determined. Gennarelli *et al.* presented in [56] a TD version of the UAPO solution for the field diffracted by the edge of a non-penetrable half-plane characterized by an anisotropic impedance boundary condition. The diffraction by a junction formed by two thin layers consisting of highly conducting non-magnetic dielectrics was considered in [57].

In this chapter the diffraction phenomenon of plane waves by dielectric wedges is studied in TD framework. TD diffraction by penetrable wedges is a challenging problem from an analytical point of view, and no solutions are available in closed form apart from those concerning right- and obtuse-angled lossless wedges [58], [59]. The authors transformed the UAPO diffraction coefficients proposed in [41], [42] into TD by taking advantage of their UTD-like nature. In the same way, in this chapter the diffraction problems related to a penetrable acute-angled wedge are tackled and solved in TD by exploiting the knowledge of the corresponding FD-UAPO solutions found in Sec. 3.2. In particular, closed form TD-UAPO solutions for the diffraction coefficients in the dielectric region and the surrounding space are derived in the case of impulse function plane wave. Then, the diffraction response to an arbitrary incident field is found via a convolution technique. The methodology may be successfully employed to determine responses to medium/high frequency incident fields since the FD-UAPO solution is asymptotic.

# 4.1 Time Domain diffraction by an acute-angled dielectric wedge

This section concerns the computation of the TD-UAPO field diffracted by a lossless dielectric wedge with an acute apex angle when it is excited by an impulse function plane wave. This last impinges at normal incidence with respect to the edge, which is assumed coincident with the z-axis of the coordinate system (see Fig. 4.1). Both cases of *E*- and *H*-polarization for the incident plane wave are considered. The key point is the analytical evaluation of the TD-UAPO diffraction coefficients related to the dielectric region and the surrounding space. They are determined here according to [48] via an inverse Laplace transform of the corresponding FD counterparts reported in Sec. 3.2, where the expressions of the FD-UAPO diffraction coefficients have been obtained in terms of the Fresnel reflection and/or transmission coefficients of the structure and the UTD transition function [2].

## 4.1.1 Formulation of the problem for $0 < \phi' < \pi/2$

The considered canonical structure is a wedge having acute apex angle $\alpha$ and consisting of a lossless non-magnetic ($\mu_r = 1$) dielectric with relative permittivity $\varepsilon_r$, which is assumed independent on the frequency. The wedge-shaped region is bounded by the surfaces $S_0$ and $S_n$, and surrounded by the free-space. The angle $\phi'$ fixes the incidence direction in a polar coordinate system perpendicular to the edge (see Fig. 4.1), and its values are assumed to range from 0 to $\pi/2$ as in Subsec. 3.2.1 so that only $S_0$ is illuminated by the incident plane wave and two series of internal and external rays arise: a first one propagating towards the apex and another one which goes far from the apex after the inversion (see Fig. 3.2). Therefore, by defining the incidence angle $\theta^i = \phi' - \pi/2$, the wave penetrates into the wedge according to the transmission angle $\theta_0^t = \sin^{-1}\left(\sin\theta^i / \sqrt{\varepsilon_r}\right)$. The ray

transmitted through $S_0$ travels toward the apex undergoing $N_i = \mathrm{Int}\left[\theta_{0L}^t / \alpha\right]$ reflections/transmissions before moving away from it. This series of $N_i$ internal incidence/reflection angles can be evaluated as $\theta_n^i = \theta_n^r = \theta_{0L}^t - n\,\alpha$ for $n = 1, 2, ..., N_i$. The corresponding transmitted waves through $S_0$ and $S_n$ exist until the total reflection occurs inside the wedge, i.e., when $\theta_n^i > \theta_c = \sin^{-1}\left(1/\sqrt{\varepsilon_r}\right)$, and define the shadow boundaries fixed by the angles $\theta_n^t = \sin^{-1}\left(\sqrt{\varepsilon_r}\,\sin\theta_n^i\right)$ in the space surrounding the wedge. As already illustrated in 3.2.1, at the ($N$+1)-th interaction point the inversion happens and so the rays travel far from the apex and another series of points of internal reflection/external transmission occurs (see Fig. 3.4). The value $\theta_{0R}^t = (N+1) - \theta_{0L}^t$ is the angle of the first ray reflected from $S_0$ after the inversion. By this way, $M$ interaction points of the rays propagating far from the apex exist, with $M$ defined in (3.29). The internal incidence/reflection angles after the inversion are: $\theta_m^i = \theta_m^r = \theta_{0R}^t + m\,\alpha$ for $m = 1, 2, ..., M$.

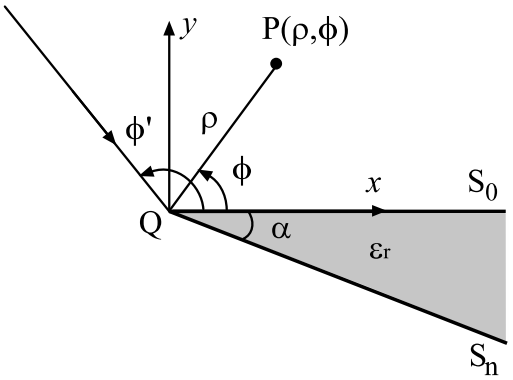


**Figure 4.1** Geometry of the diffraction problem.

The integer $M^* = \mathrm{Int}\left[\left(\theta_c - \theta_{0R}^t\right)/\alpha\right] \le M$ fixes the total number of transmission contributions.

The propagation mechanisms are the same of the FD case, then the statements of Subsec. 3.2.1 about GO field contributions are still valid. According to Subsec. 3.2.3, the FD-UAPO diffracted field $\underline{E}^d$ to be considered together with the FD-GO field at $P$ can be expressed as:

$$\underline{E}^d(P) = \begin{pmatrix} E_z^d(P) \\ E_\phi^d(P) \end{pmatrix} = \begin{pmatrix} D_{zz} & 0 \\ 0 & D_{\phi\phi'} \end{pmatrix} \begin{pmatrix} E_z^i(Q) \\ E_{\phi'}^i(Q) \end{pmatrix} \frac{\mathrm{e}^{-jk\rho}}{\sqrt{\rho}} =$$

$$= \underline{\underline{D}}\, \underline{E}^i(Q) \frac{\mathrm{e}^{-jk\rho}}{\sqrt{\rho}} = \left[ \underline{\underline{D}}_0 + \underline{\underline{D}}_n \right] \underline{E}^i(Q) \frac{\mathrm{e}^{-jk\rho}}{\sqrt{\rho}} \qquad (4.1)$$

wherein $\underline{\underline{D}}_0$ and $\underline{\underline{D}}_n$ denote the $2\times 2$ diagonal matrices of the FD-UAPO diffraction coefficients related to $S_0$ and $S_n$, respectively, $k$ is the propagation constant in the observation region, and $\underline{E}^i$, indicating the incident field at the diffraction point $Q$ is defined in eq. (3.2). The analytical expressions of $\underline{\underline{D}}_0$ and $\underline{\underline{D}}_n$ elements for both series of rays have been derived in Subsec. 3.2.3 by considering two separate scattering problems relevant to the wedge region and the surrounding space. The corresponding radiation integrals have been formulated in terms of electric and magnetic equivalent PO surface currents lying on the internal and external faces of the wedge. For each observation domain, analytical manipulations and calculations completed by uniform asymptotic evaluations of the resulting integrals have been performed for obtaining closed form expressions. Note that the FD-UAPO diffraction coefficients found in in Subsec. 3.2.3 do not take into account surface waves. The TD counterpart of $\underline{E}^d$ can be calculated by using the following convolution integral:

$$\underline{e}^d(P,t) = \frac{1}{\sqrt{\rho}} \int_{t_0}^{t-\rho/c} \underline{\underline{d}}\left( t - \frac{\rho}{c} - \tau \right) \underline{e}^i(Q,\tau)\, \mathrm{d}\tau \quad \text{if} \quad t - \frac{\rho}{c} > t_0 \qquad (4.2)$$

in which $\underline{e}^i$ is the incident field (forcing function) turned on at $t=t_0$ and $c$ is the speed of light in the considered observation region. The entries of the TD-UAPO diffraction matrix $\underline{\underline{d}}$ are determined according to [48] by performing the inverse Laplace transform of the corresponding elements of $\underline{\underline{D}}$, and their expressions are reported in the next Section accounting for observation region and wedge surface contributions.

## 4.1.2 Time Domain UAPO diffraction coefficients

In this section the nonzero entries of the TD-UAPO diffraction matrix $\underline{\underline{d}}$ are made explicit according to [48] by performing the inverse Laplace transform of the corresponding elements of $\underline{\underline{D}}$ found in Subsec. 3.2.3. According to approach of Sec. 3.2, two separate scattering problems relevant to the wedge (internal region) and the surrounding space (external region) are addressed, and for each problem the two series of rays (pre- and post- inversion) are evaluated distinctly.

### External problem

### Pre-inversion contributions

The total diffracted field in the region external to the wedge is given by the superposition of the contributions related to $S_0$ and $S_n$ which are expressed by (3.55) and (3.60) in the FD. By performing the inverse Laplace transform to them it results in the TD:

$$\left(d_{zz}^{ext}\right)^L = \left(d_{zz}^{ext}\right)_0^L + \left(d_{zz}^{ext}\right)_n^L \tag{4.3}$$

where:

$$\left(d_{zz}^{ext}\right)_0^L = \frac{1}{2\sqrt{2\pi}}\Bigg\{ \frac{\left(1-R_0\right)\sin\phi' - \left(1+R_0\right)\sin\phi}{\cos\phi+\cos\phi'} g\left(2\rho\cos^2\left(\frac{\phi\pm\phi'}{2}\right),t\right) + -T_0 \sum_{\substack{n=1 \\ n\ even}}^{N+1} T_n \left(\prod_{p=1}^{n-1} R_p\right) \frac{\sin\phi+\cos\theta_n^t}{\cos\phi+\cos(\pi/2-q\theta_n^t)} \cdot \cdot g\left(2\rho\cos^2\left(\frac{\phi\pm(\pi/2-q\theta_n^t)}{2}\right),t\right)\Bigg\} \tag{4.4}$$

and

$$\left(d_{zz}^{ext}\right)_n^L = \frac{1}{2\sqrt{2\pi}} T_0 \sum_{\substack{n=1 \\ n\ odd}}^{N+1} T_n \left(\prod_{p=1}^{n-1} R_p\right) \frac{\sin\left(\phi+\alpha\right)-\cos p\theta_n^t}{\cos(\phi+\alpha)+\cos(\pi/2-p\theta_n^t)} \cdot \cdot g\left(2\rho\cos^2\left(\frac{(\phi+\alpha)\pm(\pi/2-p\theta_n^t)}{2}\right),t\right) \tag{4.5}$$

In eq. (4.4) the sign + applies in the interval $\left(0<\phi<\pi\right)$ and the sign − applies in the interval $\left(\pi<\phi<2\pi-\alpha\right)$. In eq. (4.5) the sign + applies in the interval $\left(\pi-\alpha<\phi<2\pi-\alpha\right)$ and the sign − applies in the interval $\left(0<\phi<\pi-\alpha\right)$. The function $g(\cdot)$ used in the above expressions is so defined:

$$g\left(X,t\right) = \frac{X}{\sqrt{\pi ct}\left(t+X/c\right)} \tag{4.6}$$

## Post-inversion contributions

The total diffracted field in the region external to the wedge after the inversion is given by the superposition of the contributions related to $S_0$ and $S_n$ which are expressed by (3.64) and (3.69) in the FD. As a consequence, in the TD it results:

$$\left(d_{zz}^{ext}\right)^R = \left(d_{zz}^{ext}\right)_0^R + \left(d_{zz}^{ext}\right)_n^R \tag{4.7}$$

where:

$$\left(d_{zz}^{ext}\right)_0^R = \frac{1}{2\sqrt{2\pi}} T_0 - \Gamma(N) \sum_{\substack{m=1 \\ m\ even}}^{M^*} T_m \left( \prod_{p=1}^{m-1} R_p \right) \frac{\sin\phi + \cos\theta_m^t}{\cos\phi + \cos(\theta_m^t + \pi/2)} \cdot$$
$$\cdot g\left( 2\rho\cos^2\left( \frac{\phi \pm (\theta_m^t + \pi/2)}{2} \right), t \right) \tag{4.8}$$

and

$$\left(d_{zz}^{ext}\right)_n^R = T_0\, \Gamma(N) \sum_{\substack{m=1 \\ m\ odd}}^{M^*} T_m \left( \prod_{p=1}^{m-1} R_p \right) \frac{\sin(\phi+\alpha) - \cos\theta_m^t}{\cos(\phi+\alpha) + \cos(\theta_m^t + \pi/2)} \cdot$$
$$\cdot g\left( 2\rho\cos^2\left( \frac{(\phi+\alpha) \pm (\theta_m^t + \pi/2)}{2} \right), t \right) \frac{1}{2\sqrt{2\pi}} \tag{4.9}$$

where the function $g(\cdot)$ is defined in eq. (4.6). In eq. (4.12) the sign + applies in the interval $(0 < \phi < \pi)$ and the sign − applies in the interval $(\pi < \phi < 2\pi - \alpha)$. In eq. (4.13) the sign − applies in the interval $(\pi - \alpha < \phi < 2\pi - \alpha)$ and the sign + applies in the interval $(0 < \phi < \pi - \alpha)$.

Then, the total diffracted field in the region external to the wedge is given by the superposition of the pre- inversion contributions (eq. (4.3)) with the post-inversion ones (eq. (4.7))

$$d_{zz}^{ext} = \left(d_{zz}^{ext}\right)_0^L + \left(d_{zz}^{ext}\right)_n^L + \left(d_{zz}^{ext}\right)_0^R + \left(d_{zz}^{ext}\right)_n^R \tag{4.10}$$

## Internal problem

## Pre-inversion contributions

The total diffracted field in the region internal to the wedge is given by the superposition of the contributions related to $S_0$ and $S_n$ which are reported in FD eqns. (3.80) and (3.84). Then, applying the inverse Laplace transform to them it results in TD:

$$\left(d_{zz}^{in}\right)^L = \left(d_{zz}^{in}\right)_0^L + \left(d_{zz}^{in}\right)_n^L \tag{4.11}$$

where:

$$\left(d_{zz}^{in}\right)_0^L = \frac{1}{2\sqrt{2\pi}} T_0 \Bigg\{ \frac{\sin\phi - \cos\theta_{0L}^t}{\cos\phi + \cos(\pi/2 - \theta_{0L}^t)} g\left(2\rho\cos^2\left(\frac{\phi + (\pi/2 - \theta_{0L}^t)}{2}\right), t\right) + \sum_{\substack{n=1 \\ n\ even}}^{N} \left(\prod_{p=1}^{n-1} R_p\right) \frac{(1+R_n)\sin\phi + (1-R_n)\cos\theta_n^i}{\cos\phi + \cos(\pi/2 - \theta_n^i)} \cdot g\left(2\rho\cos^2\left(\frac{\phi + (\pi/2 - \theta_n^i)}{2}\right), t\right) \Bigg\} \tag{4.12}$$

and

$$\left(d_{zz}^{in}\right)_n^L = T_0 \left\{ \sum_{\substack{n=1 \\ n\ odd}}^{N} \left( \prod_{p=1}^{n-1} R_p \right) \frac{(1-R_n)\cos\theta_n^i - (1+R_n)\sin(\phi+\alpha)}{\cos(\phi+\alpha)+\cos(\pi/2-\theta_n^i)} \cdot \right.$$
$$\left. \cdot g\left( 2\rho\cos^2\left( \frac{(\phi+\alpha)+(\pi/2-\theta_n^i)}{2} \right), t \right) \right\} \frac{1}{2\sqrt{2\pi}} \qquad (4.13)$$

where the function $g(\cdot)$ is defined in eq. (4.6).

## Post-inversion contributions

The total diffracted field in the region internal to the wedge in the FD is given by the superposition of the contributions (3.92) and (3.96). Therefore, in the TD it results:

$$\left(d_{zz}^{in}\right)^R = \left(d_{zz}^{in}\right)_0^R + \left(d_{zz}^{in}\right)_n^R \qquad (4.14)$$

where:

$$\left(d_{zz}^{in}\right)_0^R = T_0\Gamma(N) \left\{ \sum_{\substack{m=1 \\ m\ even}}^{M} \left( \prod_{p=1}^{m-1} R_p \right) \frac{(1+R_m)\sin\phi + (1-R_m)\cos\theta_m^i}{\cos\phi + \cos(\theta_m^i + \pi/2)} \cdot \right.$$
$$\left. g\left( 2\rho\cos^2\left( \frac{\phi+(\theta_m^i+\pi/2)}{2} \right), t \right) \right\} \frac{1}{2\sqrt{2\pi}} \qquad (4.15)$$

and

$$\left(d_{zz}^{in}\right)_n^R = \Gamma(N)T_0 \left\{ \sum_{\substack{m=1 \\ m\ odd}}^{M} \left( \prod_{p=1}^{m-1} R_p \right) \frac{(1-R_m)\cos\theta_m^i - (1+R_m)\sin(\phi+\alpha)}{\cos(\phi+\alpha)+\cos(\theta_m^i+\pi/2)} \cdot \right.$$

$$\cdot g\left( 2\rho\cos^2\left( \frac{\phi-(2\pi-\alpha)+(\theta_m^i+\pi/2)}{2} \right), t \right) \Bigg\} \frac{1}{2\sqrt{2\pi}} \qquad (4.16)$$

Then, the total diffracted field into the wedge is given by the superposition of the pre- inversion contributions (eq. (4.11)) with the post-inversion ones (eqns. (4.14))

$$d_{zz}^{in} = \left(d_{zz}^{in}\right)_0^L + \left(d_{zz}^{in}\right)_n^L + \left(d_{zz}^{in}\right)_0^R + \left(d_{zz}^{in}\right)_n^R \qquad (4.17)$$

According to the property of eq. (3.126) found in Subsec. 3.2.6 (and to [41]-[43]), in the hypothesis of an *H*-polarized plane wave impinging on a dielectric wedge, it result

$$\left(d_{\phi\phi'}\right)^{in,ext} = -\left(d_{zz}\right)^{in,ext} \qquad (4.18)$$

where $\left(d_{\phi\phi'}\right)^{in,ext}$ is the TD diffraction coefficient for the *H*-polarization case. As for the FD, eq. (4.18) is valid only if the Fresnel reflection and transmission coefficients used in it are those related to parallel polarization.

### 4.1.3 Numerical examples

Previous formulas have been implemented in a computer code to evaluate the TD field evolution at a fixed observation point. The first three sets of examples are relevant to a *z*-polarized incident electric field turned on at $t_0 = 0$. The first set of figures is useful to show the typical behavior of the TD-UAPO diffracted field in correspondence of a shadow boundary; it refers to a wedge characterized by $\alpha = 30°$ and $\varepsilon_r = 3$ when excited by a given function plane wave (the main waveform in Figs. 4.2-4.5) impacting at $\phi' = 135°$. The sequence from Fig. 4.2 to Fig. 4.5 displays the waveform contributions arriving at $P(\rho,\phi)$ when it moves on a circular path ($\phi = 30°, 44°, 46°, 60°$) having radius $\rho = 2$ m and crossing the boundary for the specular

reflection (SR) from $S_0$ located at $\phi_{RB_0} = 45°$. It is possible to recognize the incident and SR waveforms (solid line) and the diffraction one (dashed line). The arrival time of the diffracted field at *P* does not change of course, but the waveform magnitude varies depending on the angular distance from the SR boundary as expected. Figure 4.2 makes evident that no liaison exists between the SR waveform and the diffraction one if the position of *P* ($\phi = 30°$) is far from $\phi_{RB_0} = 45°$. On the contrary, a strong relationship is manifest in Fig. 4.3, where SR and diffraction waveforms arrive practically together at *P* ($\phi = 44°$) since this last is very close to SR boundary.

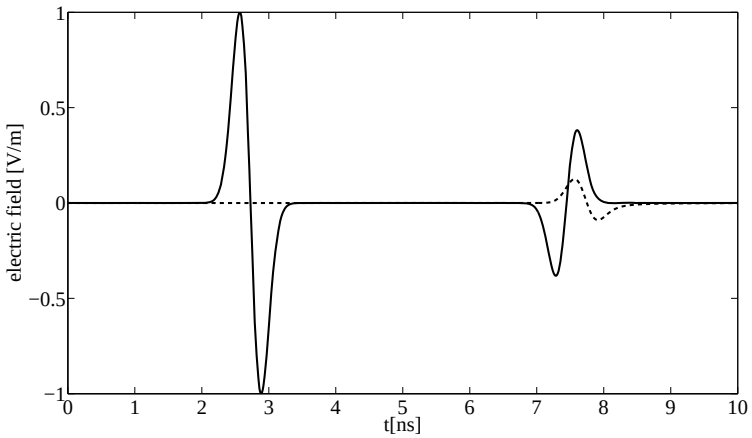


**Figure 4.2** GO (solid line) and UAPO diffraction (dashed line) contributions.
Test case data: $\alpha = 30°$, $\varepsilon_r = 3$, $\phi' = 135°$ and $\rho = 2$ m, $\phi = 30°$.

Figs. 4.4 and 4.5 show the inversion of the diffraction waveform when *P* is beyond SR boundary and the reduction of its contribution when the angular distance from SR boundary increases.

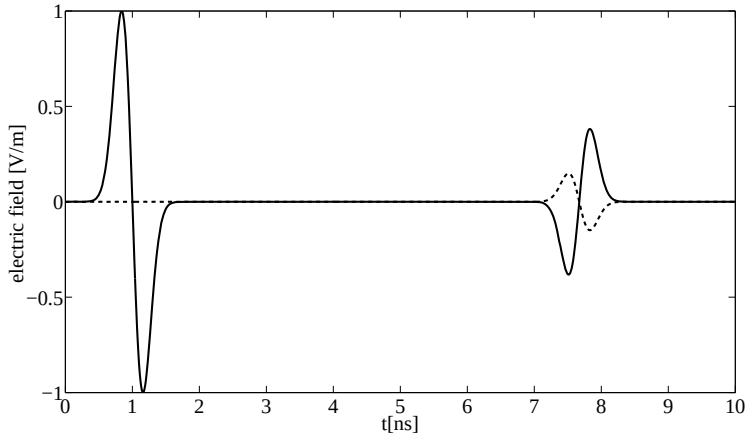


**Figure 4.3** GO (solid line) and UAPO diffraction (dashed line) contributions.
Test case data: $\alpha = 30°$, $\varepsilon_r = 3$, $\phi' = 135°$ and $\rho = 2$ m, $\phi = 44°$.

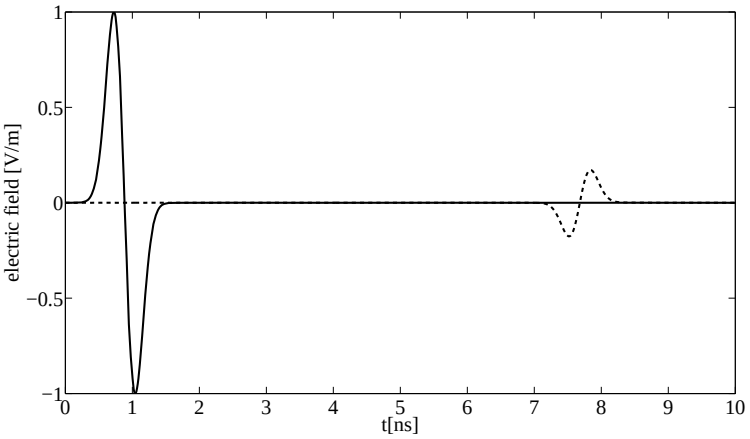


**Figure 4.4** GO (solid line) and UAPO diffraction (dashed line) contributions.
Test case data: $\alpha = 30°$, $\varepsilon_r = 3$, $\phi' = 135°$ and $\rho = 2$ m, $\phi = 46°$.

Obviously, the SR waveform vanishes when *P* is beyond the SR boundary and the incident waveform moves on the left of the box when growing $\phi$. The incident field is not displayed in Fig. 4.5 since it arrives at *P* before reaching *Q*.

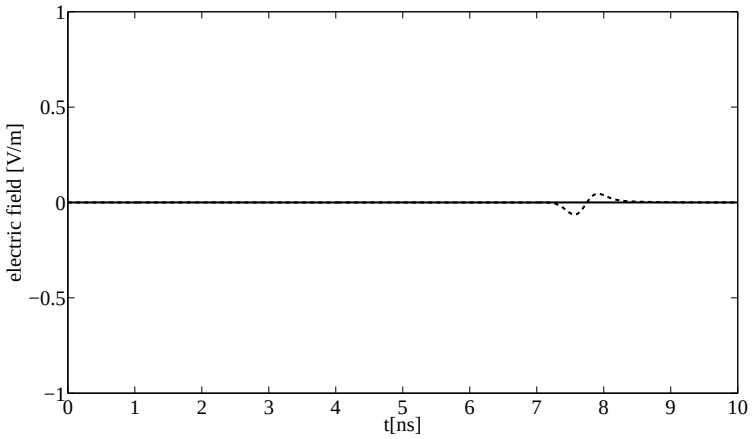


**Figure 4.5** GO (solid line) and UAPO diffraction (dashed line) contributions.
Test case data: $\alpha = 30°$, $\varepsilon_r = 3$, $\phi' = 135°$ and $\rho = 2$ m, $\phi = 60°$.

The second set of numerical results deals with a wedge described by $\alpha = 15°$ and $\varepsilon_r = 2$ when excited by a function plane wave with incidence direction fixed by $\phi' = 110°$. According to the chosen values, $M = 5$ and two further GO contributions ($M^* = 2$) must be considered in the space surrounding the wedge, i.e., the transmission-transmission (TT) outgoing waveform from $S_n$ and the transmission-reflection-transmission (TRT) outgoing waveform from $S_0$. The field contributions resulting by setting $\phi = 10°$ are shown in Fig. 4.6, where it is possible to identify the incident, SR and TRT waveforms in order of arrival. The TRT contribution arrives together the diffraction one as expected since the position of *P* is very close to the TRT shadow boundary. Analogously, the TT and diffraction waveforms reach *P* jointly if $\phi = 300°$ (see Fig. 4.7). Figure 4.8 is relevant to $\phi = 350°$: six contributions exist at *P*, but only the transmission and transmission-reflection waveforms are easy to detect. The other ones resulting from multiple internal reflections appear too close together to be completely identified.

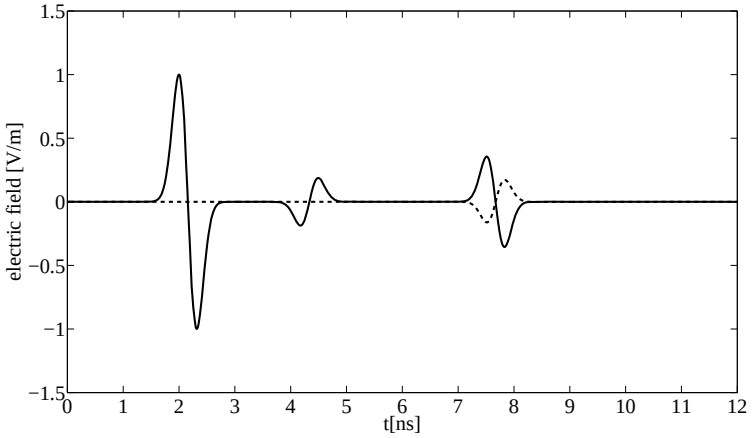


**Figure 4.6** GO (solid line) and UAPO diffraction (dashed line) contributions.
Test case data: $\alpha = 15°$, $\varepsilon_r = 2$, $\phi' = 110°$ and $\rho = 2$ m, $\phi = 10°$.

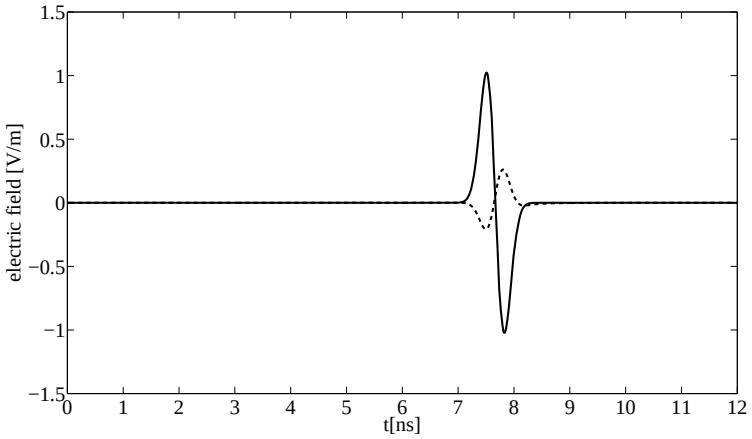


**Figure 4.7** GO (solid line) and UAPO diffraction (dashed line) contributions.
Test case data: $\alpha = 15°$, $\varepsilon_r = 2$, $\phi' = 110°$ and $\rho = 2$ m, $\phi = 300°$.

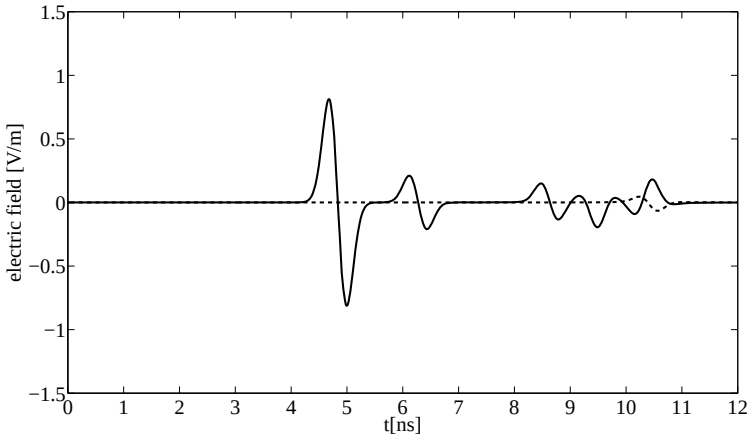


**Figure 4.8** GO (solid line) and UAPO diffraction (dashed line) contributions.
Test case data: $\alpha = 15°$, $\varepsilon_r = 2$, $\phi' = 110°$ and $\rho = 2$ m, $\phi = 350°$.

The third set of figures is relevant to an acute-angled wedge characterized by $\varepsilon_r = 3$ and $\alpha = 20°$ when the electric field arrives at $\phi' = 35°$. Being $0 < \phi' < \pi/2$ two series of internal reflections/external transmission are present into the wedge and the surrounding space. Fig. 4.9 shows the evolution of the electric field at $P(3\text{m}, 144°)$. In order of arrival, it is possible to identify the GO contributions (solid line) and the diffraction one (dashed line). This last arrives at the same time of the SR waveform since *P* is very close to the corresponding shadow boundary. SR, TRT and diffraction waveforms at $P(3\text{m}, 69°)$ are reported in Fig. 4.10. Note that *P* is very close to the TRT boundary and the incident field is not displayed since it arrives at *P* before reaching *Q* ($t = 0$). Fig. 4.11 shows the observed waveforms at $\phi = 316°$: TT, transmission-reflection-reflection-transmission (TRRT) and diffraction ones. As expected, TRRT waveform is lower than TT one and diffraction contribution arrives at the same time of TRRT. Figure 4.12 is relevant to $\phi = 350°$. Being $N + M + 1 = 5$, five GO contributions exist at *P*: the first is related to the transmission waveform and the next are related to the transmission-multiple reflections waveforms.

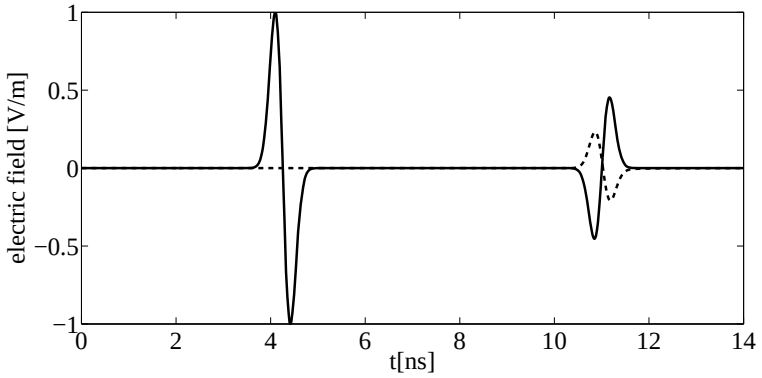


**Figure 4.9** GO (solid line) and UAPO diffraction (dashed line) contributions.
Test case data: $\alpha = 20°$, $\varepsilon_r = 3$, $\phi' = 35°$ and $\rho = 3\,\mathrm{m}$, $\phi = 144°$.

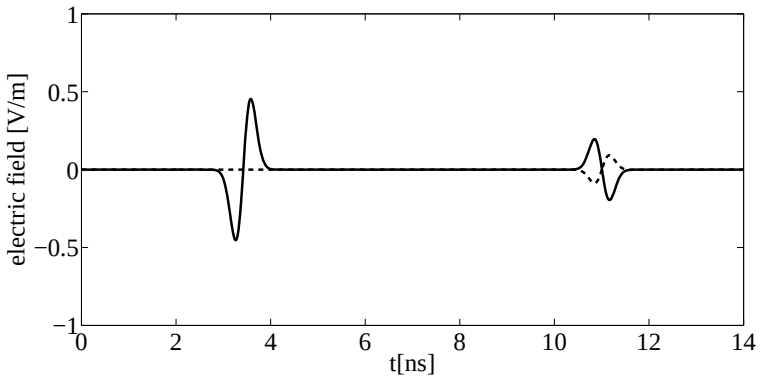


**Figure 4.10** GO (solid line) and UAPO diffraction (dashed line) contributions.
Test case data: $\alpha = 20°$, $\varepsilon_r = 3$, $\phi' = 35°$ and $\rho = 3\,\mathrm{m}$, $\phi = 69°$.

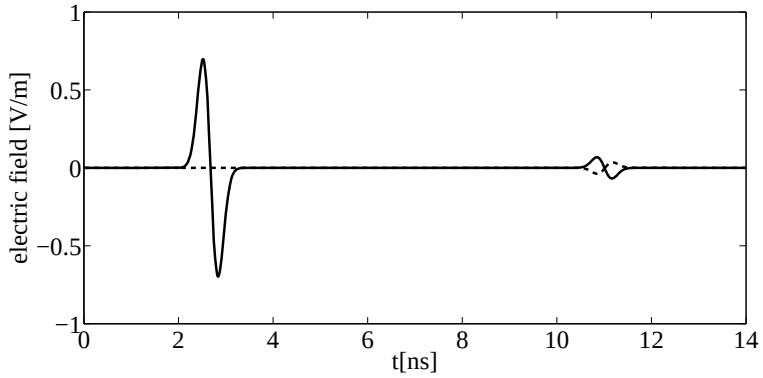


**Figure 4.11** GO (solid line) and UAPO diffraction (dashed line) contributions.
Test case data: $\alpha = 20°$, $\varepsilon_r = 3$, $\phi' = 35°$ and $\rho = 3\,\text{m}$, $\phi = 316°$.

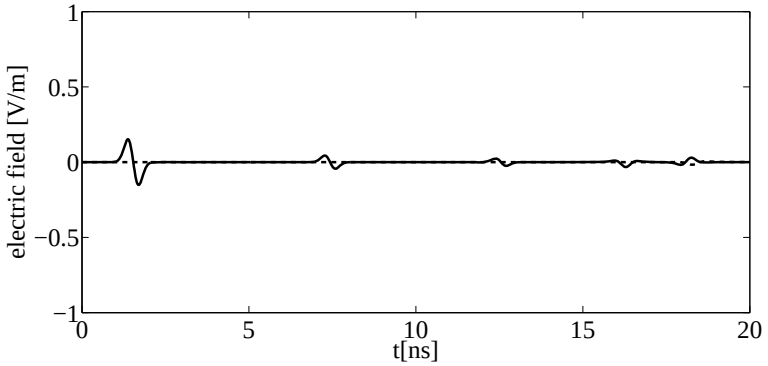


**Figure 4.12** GO (solid line) and UAPO diffraction (dashed line) contributions.
Test case data: $\alpha = 20°$, $\varepsilon_r = 3$, $\phi' = 35°$ and $\rho = 3\,\text{m}$, $\phi = 350°$.

The TD-UAPO formulation has the same advantages and limitations of the TD-UTD one. In addition, it retains the FD-UAPO limitations arising from the use of a PO approximation in the evaluation of the electric and magnetic equivalent surface currents located on the internal and external faces of the wedge-shaped dielectric region. Anyway, at the present time, the TD-UAPO formulation is the only one able to provide analytical wave solutions to TD scattering problems involving penetrable wedges. Obviously, it

is necessary to know the corresponding FD-UAPO diffraction coefficients to achieve the goal.

# Chapter 5

# Conclusions and future works

## 5.1 Summary

Approximate but quite accurate UAPO solutions for several diffraction problems involving dielectric wedges have been developed in this dissertation.

A solution to the problem of plane wave diffraction by the edge of an acute-angled dielectric wedge has been presented in Chapter 3 for both the polarization (perpendicular and parallel). As a first step, the GO response of the structure has been obtained. For the first range of values of the incidence angle two series of rays (pre- and post-inversion) are present and have been evaluated via GO investigations. Then, this last has been used to determine the equivalent electric and magnetic PO currents in the radiation integral. The considered scattering problem has been solved by considering two sub-problems, respectively external and internal to the wedge region. Then, uniform asymptotic evaluations of the radiation integrals have allowed obtaining a closed form expressions for the diffracted field. They are given in terms of the standard UTD transition function and the GO response of the wedge. The derived solution removes the GO field discontinuities and its accuracy is confirmed by the excellent agreement with numerical results in both the internal and external region. For the second range of values of the incidence angle just one series of rays is present. It is practically identical to the post-inversion series of the previous case, so it can be considered as its particular case.

In Sec. 3.7 the UAPO solutions found for the diffracted field by an acute-angled dielectric wedge have been matched with those well-

known for a right- and an obtuse-angled wedge. By using values of the internal angle of the wedge equal to $\pi/2$ and greater than $\pi/2$ the UAPO solution become identical to those reported in literature. Therefore, it has been proved that they are valid for an arbitrary-angled dielectric wedge.

In Chapter 4 the problem of diffraction of plane wave by a penetrable arbitrary-angled dielectric wedge has been addressed in the TD framework. The TD-UAPO diffraction coefficients have been determined in closed form, starting from the knowledge of the FD-UAPO counterparts, found in Cap.3. In particular, the inverse Laplace transform has been applied to the UAPO diffraction coefficients valid for the internal region of the wedge and the surrounding space. The transient diffracted field originated by an arbitrary function plane wave has been evaluated via a convolution integral. Diffraction by penetrable wedges in the TD framework is a challenging problem from the analytical point of view, and no other expressions are available in closed form for the diffraction coefficients associated with the considered problem.

Although approximate, the developed UAPO solutions are very appealing from the engineering point of view, since they provide reliable and accurate results, are computationally efficient and easy to handle. Accordingly, they can be surely useful in all the applications wherein truncation effects are not negligible.

## 5.2 Future studies

In many modern EM applications such as the design of antennas, UWB communication and radar systems, a correct characterization of the diffraction contributions due to the finite dimensions of the structures is essential. Although numerical techniques could be employed to solve problems having dimensions moderately large in terms of wavelength, they are not efficient and poorly convergent at high frequencies. As a consequence, the availability of simple, closed form and quite accurate diffraction coefficients is desirable. To this end, the developed UAPO solutions can be surely useful to describe the scattering phenomena for many canonical configurations under plane wave illumination. Areas of further investigations include:

- Generalization of the UAPO solutions to cylindrical and spherical wave illumination and other types of sources (electric dipole, etc.).
- Generalization of the UAPO solution for the arbitrary-angled dielectric wedge to the case of skew incidence.
- Evaluation of the field diffracted by composite structures (adjacent metallic and dielectric wedges) using the UAPO approach.

## Appendix A

# Acute angled wedge: equivalent surface currents

In this Appendix the equivalent surface currents in the radiation integrals (3.43), (3.44) are determined by means of a PO approximation, in both cases of $\underline{E}$- and $\underline{H}$-polarization.

## *E*-polarization

### Pre-inversion GO magnetic fields

To calculate the equivalent currents it has been necessary to determine preliminarily the GO magnetic fields corresponding to electric fields found in Subsec. 3.2.1. The magnetic fields for the first series of rays propagating towards the apex can be simply obtained by applying the property of plane wave:

$$\underline{H}^{i} = \frac{1}{\zeta_0}\hat{s}^{i} \times \underline{E}^{i} = \frac{E_0}{\zeta_0} e^{jk_0\rho\cos(\phi-\phi')}\left(-\sin\phi'\,\hat{x} + \cos\phi'\,\hat{y}\right) \quad \text{(A.1)}$$

$$\underline{H}^{r_0} = \frac{1}{\zeta_0}\hat{s}_0^{r} \times \underline{E}^{r_0} = \frac{R_0 E_0}{\zeta_0} e^{jk_0\rho\cos(\phi+\phi')}\left(\sin\phi'\,\hat{x} + \cos\phi'\,\hat{y}\right) \quad \text{(A.2)}$$

$$\underline{H}^{t_{0L}} = \frac{1}{\zeta_d}\hat{s}_{0L}^{t} \times \underline{E}^{t_{0L}} = \frac{1}{\zeta_d} T_0 E_0 e^{jk_d\rho\cos\left(\phi+\theta_{0L}^{t}\right)}\left(-\cos\theta_{0L}^{t}\,\hat{x} + \sin\theta_{0L}^{t}\,\hat{y}\right) \quad \text{(A.3)}$$

$$\underset{n\,even}{\underline{H}^{r_n}} = \frac{1}{\zeta_d}\hat{s}_n^r \times \underline{E}^{r_n} =$$

$$= \frac{T_0 E_0}{\zeta_d}\left(\prod_{p=1}^{n} R_p\right) e^{jk_d\rho\sin\left(\phi+\theta_n^i\right)}\left(-\cos\theta_n^i\hat{x} + \sin\theta_n^i\hat{y}\right) \qquad \text{(A.4)}$$

$$\underset{n\,odd}{\underline{H}^{r_n}} = \frac{1}{\zeta_d}\hat{s}_n^r \times \underline{E}^{r_n} =$$

$$= \frac{T_0 E_0}{\zeta_d}\left(\prod_{p=1}^{n} R_p\right) e^{jk_d\rho\sin\left(\phi+\alpha-\theta_n^i\right)}\left(\cos\theta_{n+1}^i\hat{x} + \sin\theta_{n+1}^i\hat{y}\right) \qquad \text{(A.5)}$$

$$\underset{n\,even}{\underline{H}^{t_n}} = \frac{1}{\zeta_0}\hat{s}_n^t \times \underline{E}^{t_n} =$$

$$= \frac{T_0 E_0}{\zeta_0}\left(\prod_{p=1}^{n-1} R_p\right) T_m e^{-jk_0\rho\sin\left(\phi-\theta_n^t\right)}\left(\cos\theta_n^t\hat{x} + \sin\theta_n^t\hat{y}\right) \qquad \text{(A.6)}$$

$$\underset{n\,odd}{\underline{H}^{t_n}} = \frac{1}{\zeta_0}\hat{s}_n^t \times \underline{E}^{t_n} =$$

$$= \frac{T_0 E_0}{\zeta_0}\left(\prod_{p=1}^{n-1} R_p\right) T_m e^{jk_0\rho\sin\left(\phi+\alpha+\theta_n^t\right)}\left(-\cos(\alpha+\theta_n^t)\hat{x} + \sin(\alpha+\theta_n^t)\hat{y}\right) \qquad \text{(A.7)}$$

wherein $\zeta_d$ is the wedge impedance, $\hat{s}_0^r = \left(-\cos\phi', \sin\phi', 0\right)$ is the unit vector along the ray reflected from the external face of $S_0$, $\hat{s}_{0L}^t = \left(-\sin\theta_{0L,}^t, -\cos\theta_{0L,}^t, 0\right)$ is the unit vector along the ray transmitted through $S_0$, $\hat{s}_n^r = \left(-\sin\theta_n^i, -\cos\theta_n^i, 0\right)$ for $n$ even is the unit vector along the rays reflected from the internal face of $S_0$,

$\hat{s}_n^r = \left(-\sin\theta_{n+1}^i, \cos\theta_{n+1}^i, 0\right)$ for $n$ odd is the unit vector along the rays reflected from the internal face of $S_n$, $\hat{s}_n^t = \left(-\sin\theta_{n,}^t \cos\theta_{n,}^t 0\right)$ for $n$ even is the unit vector along the ray transmitted through $S_0$, and $\hat{s}_n^t = \left[-\sin(\alpha+\theta_n^t), -\cos(\alpha+\theta_n^t), 0\right]$ for $n$ odd is the unit vector along the ray transmitted through $S_n$.

Now, the equivalent currents in the radiation integrals (3.43), (3.44) are determined by means of a PO approximation.

## External problem

By using eqns. (A.1), (A.2), (A.6) and (3.23) it results on $S_0$:

$$\left(\underline{J}_s^{ext}\right)_0^L = \hat{n}_0^{ext} \times \left(\underline{H}^+\right)^L\Big|_{S_0} = \hat{y} \times \left( \underline{H}^i + \underline{H}^{r_0} + \sum_{\substack{n=1 \\ n\,even}}^{N+1} \underline{H}^{t_n} \right)\Big|_{S_0} \Rightarrow$$

$$\Rightarrow \zeta_0 \left(\underline{J}_s^{ext}\right)_0^L = E_0 \Big[ \sin\phi'\left(1-R_0\right) e^{jk_0 x'\cos\phi'} + -T_0 \sum_{\substack{n=1 \\ n\,even}}^{N+1} \left( \prod_{p=1}^{n-1} R_p \right) T_n e^{jk_0 x' \sin q\theta_n^t} \cos\theta_n^t \Big] \hat{z} \qquad \text{(A.8)}$$

$$\left(\underline{J}_{ms}^{ext}\right)_0^L = \left(-\hat{n}_0^{ext}\right) \times \left(\underline{E}^+\right)^L\Big|_{S_0} = \left(-\hat{y}\right) \times \left( \underline{E}^i + \underline{E}^{r_0} + \sum_{\substack{n=1 \\ n\,even}}^{N+1} \underline{E}^{t_n} \right)\Big|_{S_0} =$$

$$= -E_0\left[\left(1+R_0\right)e^{jk_0x'\cos\phi'} + T_0\sum_{\substack{n=1\\ n\,even}}^{N+1}\left(\prod_{p=1}^{n-1}R_p\right)T_n e^{jk_0x'\sin q\theta_n^t}\right]\hat{x} \tag{A.9}$$

Moreover, by using eqns. (A.7) and (3.23), the currents on $S_n$ are given by:

$$\left(\underline{J}_s^{ext}\right)_n^L = \hat{n}_n^{ext}\times\left(\underline{H}^+\right)^L\big|_{S_n} = \left(-\hat{x}\sin\alpha - \hat{y}\cos\alpha\right)\times\left(\sum_{\substack{n=1\\ n\,odd}}^{N+1}\underline{H}^{t_n}\right)\Bigg|_{S_n} \Rightarrow$$

$$\Rightarrow \zeta_0\left(\underline{J}_s^{ext}\right)_n^L = -T_0E_0\left[\sum_{\substack{n=1\\ n\,odd}}^{N+1}\left(\prod_{p=1}^{n-1}R_p\right)T_n e^{jk_0\rho'\sin p\theta_n^t}\cos p\theta_n^t\right]\hat{z} \tag{A.10}$$

$$\left(\underline{J}_{m_s}^{ext}\right)_n^L = \left(-\hat{n}_n^{ext}\right)\times\left(\underline{E}^+\right)^L\big|_{S_n} = \left(\hat{x}\sin\alpha + \hat{y}\cos\alpha\right)\times\left(\sum_{\substack{n=1\\ n\,odd}}^{N+1}\underline{E}^{t_n}\right)\Bigg|_{S_n} =$$

$$= T_0E_0\left[\sum_{\substack{n=1\\ n\,odd}}^{N+1}\left(\prod_{p=1}^{n-1}R_p\right)T_n e^{jk_0\rho'\sin p\theta_n^t}\right]\left(\hat{x}\cos\alpha - \hat{y}\sin\alpha\right) \tag{A.11}$$

## Internal problem

By using eqns. (A.3), (A.4) and (3.22) it results on $S_0$:

$$\left(\underline{J}_s^{in}\right)_0^L = \hat{n}_0^{in} \times \left(\underline{H}^+\right)^L\Big|_{S_0} = \left(-\hat{y}\right) \times \left( \underline{H}^{t0} + \sum_{\substack{n=1 \\ n\,even}}^{N} \underline{H}^{r_n} \right)\Bigg|_{S_0} \Rightarrow$$

$$\Rightarrow \zeta_d \left(\underline{J}_s^{in}\right)_0^L = T_0 E_0 \left\{ -\cos\theta_{0L}^t e^{jk_d x' \sin\theta_{0L}^t} + \right.$$

$$\left. + \sum_{\substack{n=1 \\ n\,even}}^{N} \left( \prod_{p=1}^{n-1} R_p \right) e^{jk_d x' \sin\theta_n^i} \cos\theta_n^i \left(1 - R_n\right) \right\} \hat{z} \qquad \text{(A.12)}$$

$$\left(\underline{J}_{ms}^{in}\right)_0^L = \left(-\hat{n}_0^{in}\right) \times \left(\underline{E}^+\right)^L\Big|_{S_0} = \hat{y} \times \left( \underline{E}^{t0} + \sum_{\substack{n=1 \\ n\,even}}^{N} \underline{E}^{r_n} \right)\Bigg|_{S_0} =$$

$$= T_0 E_0 \left\{ e^{jk_d x' \sin\theta_{0L}^t} + \sum_{\substack{n=1 \\ n\,even}}^{N} \left( \prod_{p=1}^{n-1} R_p \right) e^{jk_d x' \sin\theta_n^i} \left(1 + R_n\right) \right\} \hat{x} \qquad \text{(A.13)}$$

The currents on $S_n$ can be determined by means of eqns. (A.5) and (3.22):

$$\left(\underline{J}_s^{in}\right)_n^L = \hat{n}_n^{in} \times \left(\underline{H}^+\right)^L\Big|_{S_n} = \left(\hat{x}\sin\alpha + \hat{y}\cos\alpha\right) \times \left( \sum_{\substack{n=1 \\ n\,odd}}^{N} \underline{H}^{r_n} \right)\Bigg|_{S_n} \Rightarrow$$

$$\Rightarrow \zeta_d \left(\underline{J}_s^{in}\right)_n^L = T_0 E_0 \left\{ \sum_{\substack{n=1 \\ n\,odd}}^{N} \left( \prod_{p=1}^{n-1} R_p \right) e^{jk_d \rho' \sin\theta_n^i} \cos\theta_n^i \left(1 - R_n\right) \right\} \hat{z} \qquad \text{(A.14)}$$

$$\left(\underline{J}_{ms}^{in}\right)_n^L = \left(-\hat{n}_n^{in}\right)\times\left(\underline{E}^+\right)^L\Big|_{S_n} = \left(-\hat{x}\sin\alpha - \hat{y}\cos\alpha\right)\times\left(\sum_{\substack{n=1\\ n\,odd}}^{N}\underline{E}^{r_n}\right)\Bigg|_{S_n} =$$

$$= T_0E_0\left[\sum_{\substack{n=1\\ n\,odd}}^{N}\left(\prod_{p=1}^{n-1}R_p\right)e^{jk_d\rho'\sin\theta_n^i}\left(1+R_n\right)\right]\left(-\hat{x}\cos\alpha+\hat{y}\sin\alpha\right) \tag{A.15}$$

## Post-inversion GO magnetic fields

The magnetic fields for the second series of rays propagating far from the apex can be simply obtained by applying the property of plane wave:

$$\underline{H}^{t_{0R}} = \frac{1}{\zeta_d}\hat{s}^{t_{0R}}\times\underline{E}^{t_{0R}} =$$

$$= \frac{1}{\zeta_d}E_0T_0\Gamma(N)e^{jk_d\sin(\phi-\theta_{0R}^t)}\left(-\cos\theta_{0R}^t\hat{x}-\sin\theta_{0R}^t\hat{y}\right) \tag{A.16}$$

$$\underset{m\,even}{\underline{H}^{r_m}} = \frac{1}{\zeta_d}\hat{s}_R^{r_m}\times\underline{E}^{r_m} =$$

$$= \frac{E_0T_0\Gamma(N)}{\zeta_d}\left(\prod_{p=1}^{m}R_p\right)e^{jk_d\rho\sin\left(\phi-\theta_m^i\right)}\left(-\cos\theta_m^i\hat{x}-\sin\theta_m^i\hat{y}\right) \tag{A.17}$$

$$\underset{m\,odd}{\underline{H}^{r_m}} = \frac{1}{\zeta_d}\hat{s}_R^{r_m} \times \underline{E}^{r_m} = \frac{E_0 T_0 \Gamma(N)}{\zeta_d} \cdot$$

$$\cdot \left( \prod_{p=1}^{m} R_p \right) e^{-jk_d \rho \sin\left(\phi+\alpha+\theta_m^i\right)} \left[ \cos\left(\theta_m^i + \alpha\right)\hat{x} - \sin\left(\theta_m^i + \alpha\right)\hat{y} \right] \tag{A.18}$$

$$\underset{m\,even}{\underline{H}^{t_m}} = \frac{1}{\zeta_0}\hat{s}_R^{t_m} \times \underline{E}^{t_m} =$$

$$= \frac{T_0 E_0 \Gamma(N)}{\zeta_0} \left( \prod_{p=1}^{m-1} R_p \right) T_m e^{-jk_0 \rho \sin\left(\phi+\theta_m^t\right)} \left( \cos\theta_m^t \hat{x} - \sin\theta_m^t \hat{y} \right) \tag{A.19}$$

$$\underset{m\,odd}{\underline{H}^{t_m}} = \frac{1}{\zeta_0}\hat{s}_R^{t_m} \times \underline{E}^{t_m} = \frac{T_0 E_0 \Gamma(N)}{\zeta_0} \cdot$$

$$\cdot \left( \prod_{p=1}^{m-1} R_p \right) T_m e^{jk_0 \rho \sin\left(\phi+\alpha-\theta_m^t\right)} \left[ -\cos(\theta_m^t - \alpha)\hat{x} - \sin(\theta_m^t - \alpha)\hat{y} \right] \tag{A.20}$$

wherein $\zeta_d$ is the wedge impedance, $\hat{s}_R^{t0} = \left(\sin\theta_{0R,}^t - \cos\theta_{0R,}^t\ 0\right)$ is the unit vector along the first ray reflected from the internal face of $S_0$ after the inversion, $\hat{s}_R^{r_m} = \left(\sin\theta_m^i, -\cos\theta_m^i, 0\right)$ for $m$ even is the unit vector along the rays reflected from the internal face of $S_0$, $\hat{s}_R^{r_m} = \left(\sin\theta_{m+1}^i, \cos\theta_{m+1}^i, 0\right)$ for $m$ odd is the unit vector along the rays reflected from the internal face of $S_n$, $\hat{s}_R^{t_m} = \left(\sin\theta_{m,}^t \cos\theta_{m,}^t\ 0\right)$ for $m$ even is the unit vector along the ray transmitted through $S_0$, and

$\hat{s}_R^{t_m} = \left[\sin(\theta_n^t - \alpha), -\cos(\theta_m^t - \alpha), 0\right]$ for $m$ odd is the unit vector along the ray transmitted through $S_n$.

Now, the equivalent currents in the radiation integrals (3.43), (3.44) are determined by means of a PO approximation.

## External problem

By using (A.19) and (3.33) it results on $S_0$:

$$\left(\underline{J}_s^{ext}\right)_0^R = \hat{n}_0^{ext} \times \left(\underline{H}^+\right)^R\Big|_{S_0} = \hat{y} \times \left(\sum_{\substack{m=1 \\ m\,even}}^{M} \underline{H}^{t_m}\right)\Big|_{S_0} \Rightarrow$$

$$\Rightarrow \zeta_0 \left(\underline{J}_s^{ext}\right)_0^R = -\left[E_0 T_0 \Gamma(N) \sum_{\substack{m=1 \\ m\,even}}^{M} \left(\prod_{p=1}^{m-1} R_p\right) T_m e^{-jk_0 x' \sin\theta_m^t} \cos\theta_m^t\right] \hat{z} \tag{A.21}$$

$$\left(\underline{J}_{ms}^{ext}\right)_0^R = \left(-\hat{n}_0^{ext}\right) \times \left(\underline{E}^+\right)^R\Big|_{S_0} = (-\hat{y}) \times \left(\sum_{\substack{m=1 \\ m\,even}}^{M} \underline{E}_m^t\right)\Big|_{S_0} =$$

$$= -E_0 T_0 \Gamma(N) \left[\sum_{\substack{m=1 \\ m\,even}}^{M} \left(\prod_{p=1}^{m-1} R_p\right) T_m e^{jk_0 x' \sin\theta_m^t}\right] \hat{x} \tag{A.22}$$

Moreover, by using eqns. (A.20) and (3.33), the currents on $S_n$ are given by:

$$\left(\underline{J}_s^{ext}\right)_n^R = \hat{n}_n^{ext} \times \left(\underline{H}^+\right)^R\Big|_{S_n} = \left(-\hat{x}\sin\alpha - \hat{y}\cos\alpha\right) \times \left( \sum_{\substack{m=1 \\ m\,odd}}^{M} \underline{H}^{t_m} \right)\Big|_{S_n} \Rightarrow$$

$$\Rightarrow \zeta_0 \left(\underline{J}_s^{ext}\right)_n^R = -T_0 E_0 \Gamma(N) \left[ \sum_{\substack{m=1 \\ m\,odd}}^{M} \left( \prod_{p=1}^{m-1} R_p \right) T_m e^{-jk_0 \rho' \sin\theta_m^t} \cos\theta_m^t \right] \hat{z} \tag{A.23}$$

$$\left(\underline{J}_{ms}^{ext}\right)_n^R = \left(-\hat{n}_n^{ext}\right) \times \left(\underline{E}^+\right)^R\Big|_{S_n} = \left(\hat{x}\sin\alpha + \hat{y}\cos\alpha\right) \times \left( \sum_{\substack{m=1 \\ m\,odd}}^{M} \underline{E}^{t_m} \right)\Big|_{S_n} =$$

$$= T_0 E_0 \Gamma(N) \left[ \sum_{\substack{m=1 \\ m\,odd}}^{M} \left( \prod_{p=1}^{m-1} R_p \right) T_m e^{-jk_0 \rho' \sin\theta_m^t} \right] \left(\hat{x}\cos\alpha - \hat{y}\sin\alpha\right) \tag{A.24}$$

## Internal problem

By using eqns. (A.16), (A.17) and (3.32) it results on $S_0$:

$$\left(\underline{J}_s^{in}\right)_0^R = \hat{n}_0^{in} \times \left(\underline{H}^+\right)^R\Big|_{S_0} = \left(-\hat{y}\right) \times \left( \underline{H}^{t_{0R}} + \sum_{\substack{m=1 \\ m\,even}}^{M} \underline{H}^{r_m} \right)\Big|_{S_0} \Rightarrow$$

$$\Rightarrow \zeta_d \left(\underline{J}_s^{in}\right)_0^R = T_0 E_0 \Gamma(N) \Bigg\{ -\cos\theta_{0R}^t e^{-jk_d \rho' \sin\theta_{0R}^t} +$$

$$+\sum_{\substack{m=1\\ m\,even}}^{M}\left(\prod_{p=1}^{m-1}R_p\right)e^{-jk_d x'\sin\theta_m^i}\cos\theta_m^i\left(1-R_m\right)\Bigg\}\hat{z} \qquad \text{(A.25)}$$

$$\left(\underline{J}_{ms}^{in}\right)_0^R=\left(-\hat{n}_0^{in}\right)\times\left(\underline{E}^{+}\right)^R\big|_{S_0}=\hat{y}\times\left(\underline{E}^{t_{0R}}+\sum_{\substack{m=1\\ m\,even}}^{M}\underline{E}^{r_m}\right)\Bigg|_{S_0}=$$

$$=T_0E_0\Gamma(N)\Bigg\{e^{-jk_d x'\sin\theta_{0R}^t}+\sum_{\substack{m=1\\ m\,even}}^{M}\left(\prod_{p=1}^{m-1}R_p\right)e^{-jk_d x'\sin\theta_m^i}\left(1+R_m\right)\Bigg\}\hat{x} \qquad \text{(A.26)}$$

The currents on $S_n$ can be determined by means of eqns. (A.18) and (3.32):

$$\left(\underline{J}_s^{in}\right)_n^R=\hat{n}_n^{in}\times\left(\underline{H}^{+}\right)^R\big|_{S_n}=\left(\hat{x}\sin\alpha+\hat{y}\cos\alpha\right)\times\left(\sum_{\substack{m=1\\ m\,odd}}^{M}\underline{H}^{r_m}\right)\Bigg|_{S_n}\Rightarrow$$

$$\Rightarrow\zeta_d\left(\underline{J}_s^{in}\right)_n^R=T_0E_0\Gamma(N)\cdot$$

$$\cdot\Bigg\{\sum_{\substack{m=1\\ m\,odd}}^{M}\left(\prod_{p=1}^{m-1}R_p\right)e^{-jk_d\rho'\sin\theta_m^i}\cos\theta_m^i\left(1-R_m\right)\Bigg\}\hat{z} \qquad \text{(A.27)}$$

$$\left(\underline{J}_{ms}^{in}\right)_n^R=\left(-\hat{n}_n^{in}\right)\times\left(\underline{E}^{+}\right)^R\big|_{S_n}=\left(-\hat{x}\sin\alpha-\hat{y}\cos\alpha\right)\times\left(\sum_{\substack{m=1\\ m\,odd}}^{M}\underline{E}^{r_m}\right)\Bigg|_{S_n}=$$

$$= T_0 E_0 \Gamma(N) \left[ \sum_{\substack{m=1 \\ m\,odd}}^{M} \left( \prod_{p=1}^{m-1} R_p \right) e^{-jk_d \rho' \sin\theta_m^i} \left(1 + R_m\right) \right] \left(-\hat{x}\cos\alpha + \hat{y}\sin\alpha\right) \tag{A.28}$$

## *H*-polarization

Starting from the expressions for GO electric fields shown in Subsec. 3.2.6, the equivalent currents in the radiation integrals (3.43), (3.44) are determined by means of a PO approximation.

### External problem

By using (3.112) it results on $S_0$:

$$\left(\underline{J}_s^{ext}\right)_0 = \hat{n}_0^{ext} \times \left(\underline{H}^+\right)\Big|_{S_0} = \hat{y} \times \left( \underline{H}^i + \underline{H}^{r_0} + \sum_{\substack{m=1 \\ m\,even}}^{M} \underline{H}^{t_m} \right)\Bigg|_{S_0} =$$

$$= H_0 \left[ \left(1 + R_0\right) e^{jk_0 x' \cos\phi'} + T_0 \sum_{\substack{m=1 \\ m\,even}}^{M} \left( \prod_{p=1}^{m-1} R_p \right) T_m e^{-jk_0 x' \sin\theta_m^t} \cos\theta_m^t \right] \hat{x} \tag{A.29}$$

$$\left(\underline{J}_{ms}^{ext}\right)_0 = \left(-\hat{n}_0^{ext}\right) \times \left(\underline{E}^+\right)\Big|_{S_0} = \left(-\hat{y}\right) \times \left( \underline{E}^i + \underline{E}^{r_0} + \sum_{\substack{m=1 \\ m\,even}}^{M} \underline{E}_m^t \right)\Bigg|_{S_0} =$$

$$= \zeta_0 H_0 \Big[ \left(1 - R_0\right) e^{jk_0 x' \cos\phi'} \cos\theta_0^i +$$

$$-T_0 \sum_{\substack{m=1 \\ m\,even}}^{M} \left( \prod_{p=1}^{m-1} R_p \right) T_m \cos\theta_m^t e^{-jk_0 x' \sin\theta_m^t} \Bigg] \hat{z} \qquad \text{(A.30)}$$

Moreover, the currents on $S_n$ are given by:

$$\left( \underline{J}_s^{ext} \right)_n = \hat{n}_n^{ext} \times \left( \underline{H}^+ \right)\Big|_{S_n} = \left( -\hat{x}\sin\alpha - \hat{y}\cos\alpha \right) \times \left( \sum_{\substack{m=1 \\ m\,odd}}^{M} \underline{H}^{t_m} \right)\Big|_{S_n} =$$

$$= T_0 H_0 \left[ \sum_{\substack{m=1 \\ m\,odd}}^{M} \left( \prod_{p=1}^{m-1} R_p \right) T_m e^{-jk_0 \rho' \sin\theta_m^t} \right] \left( -\cos\alpha\,\hat{x} + \sin\alpha\,\hat{y} \right) \qquad \text{(A.31)}$$

$$\left( \underline{J}_{ms}^{ext} \right)_n = \left( -\hat{n}_n^{ext} \right) \times \left( \underline{E}^+ \right)\Big|_{S_n} = \left( \hat{x}\sin\alpha + \hat{y}\cos\alpha \right) \times \left( \sum_{\substack{m=1 \\ m\,odd}}^{M} \underline{E}^{t_m} \right)\Big|_{S_n} =$$

$$= -T_0 H_0 \zeta_0 \left[ \sum_{\substack{m=1 \\ m\,odd}}^{M} \left( \prod_{p=1}^{m-1} R_p \right) T_m e^{-jk_0 \rho' \sin\theta_m^t} \cos\theta_m^t \right] \hat{z} \qquad \text{(A.32)}$$

## Internal problem

By using eq. (3.113) it results on $S_0$ :

$$\left(\underline{J}_s^{in}\right)_0 = \hat{n}_0^{in} \times \left(\underline{H}^+\right)\Big|_{S_0} = \left(-\hat{y}\right) \times \left( \underline{H}^{t_{0R}} + \sum_{\substack{m=1 \\ m\,even}}^{M} \underline{H}^{r_m} \right)\Big|_{S_0} =$$

$$= -T_0 H_0 \left\{ e^{-jk_d \rho' \sin\theta_{0R}^t} + \right.$$

$$\left. + \sum_{\substack{m=1 \\ m\,even}}^{M} \left( \prod_{p=1}^{m-1} R_p \right) e^{-jk_d x' \sin\theta_m^i} \left(1 + R_m\right) \right\} \hat{x} \qquad \text{(A.33)}$$

$$\left(\underline{J}_{ms}^{in}\right)_0 = \left(-\hat{n}_0^{in}\right) \times \left(\underline{E}^+\right)\Big|_{S_0} = \hat{y} \times \left( \underline{E}^{t_{0R}} + \sum_{\substack{m=1 \\ m\,even}}^{M} \underline{E}^{r_m} \right)\Big|_{S_0} =$$

$$= -\zeta_d T_0 H_0 \left\{ e^{-jk_d x' \sin\theta_{0R}^t} \cos\theta_{0R}^t + \right.$$

$$\left. + \sum_{\substack{m=1 \\ m\,even}}^{M} \left( \prod_{p=1}^{m-1} R_p \right) e^{-jk_d x' \sin\theta_m^i} \cos\theta_m^i \left(R_m - 1\right) \right\} \hat{z} \qquad \text{(A.34)}$$

The currents on $S_n$ are

$$\left(\underline{J}_s^{in}\right)_n = \hat{n}_n^{in} \times \left(\underline{H}^+\right)\Big|_{S_n} = \left(\hat{x}\sin\alpha + \hat{y}\cos\alpha\right) \times \left( \sum_{\substack{m=1 \\ m\,odd}}^{M} \underline{H}^{r_m} \right)\Big|_{S_n} =$$

$$=T_0 H_0 \left\{ \sum_{\substack{m=1 \\ m\,odd}}^{M} \left( \prod_{p=1}^{m-1} R_p \right) e^{-jk_d \rho' \sin\theta_m^i} \left(1+R_m\right) \right\} \left(\hat{x}\cos\alpha - \hat{y}\sin\alpha\right) \tag{A.35}$$

$$\left(\underline{J}_{ms}^{in}\right)_n = \left(-\hat{n}_n^{in}\right) \times \left(\underline{E}^{+}\right)\Big|_{S_n} = \left(-\hat{x}\sin\alpha - \hat{y}\cos\alpha\right) \times \left( \sum_{\substack{m=1 \\ m\,odd}}^{M} \underline{E}^{r_m} \right)\Big|_{S_n} =$$

$$= \zeta_d T_0 H_0 \left[ \sum_{\substack{m=1 \\ m\,odd}}^{M} \left( \prod_{p=1}^{m-1} R_p \right) e^{-jk_d \rho' \sin\theta_m^i} \cos\theta_m^i \left(1-R_m\right) \right] \hat{z} \tag{A.36}$$

# Bibliography


[1] J. B. Keller, "Geometrical theory of diffraction", *Journal Optical Soc. Amer.*, vol. 52, pp. 116-130, 1962.

[2] R. G. Kouyoumjian and P. H. Pathak, "A uniform geometrical theory of diffraction for an edge in a perfectly conducting surface", *Proc. IEEE*, vol. 62, pp. 1448-1461, 1974.

[3] R. G. Kouyoumjian, "The geometrical theory of diffraction and its applications", *Numerical and Asymptotic Techniques in Electromagnetism,* R. Mitra, Ed. Berlin: Springer, pp. 165-215, 1975.

[4] "Tecniche asintotiche in elettromagnetismo, Applicazioni all'analisi, delle antenne a riflettore e alla valutazione di sezioni radar", *Istituto di Teoria e Tecnica delle Onde Elettromagnetiche,* I.U.N.*,* Napoli, pp. 29-30, 1990.

[5] W. D. Burnside, M. C. Gilreath, R. J. Marefka, and C. L. Yu, "A study of KC-135 aircraft antenna patterns", *IEEE Trans. Antennas Propag.*, vol. 23, 1975.

[6] G. D. Maliuzhinets, "Excitation, reflection and emission of surface waves from a wedge with given face impedances", *Sov. Phys. Dokl*., vol. 3, pp. 752-755, 1958.

[7] W. D. Burnside and K. W. Burgener, "High frequency scattering by a thin lossless dielectric slab", *IEEE Trans. Antennas Propag.*, vol. 31, pp. 104-110, 1983.

[8] R. J. Luebbers, "Finite conductivity uniform GTD versus knife edge diffraction in prediction of propagation path-loss", *IEEE Trans. Antennas Propag.,* vol. 32, pp. 70-76, 1984.

[9] R. J. Luebbers, "A heuristic UTD slope diffraction coefficient for rough lossy wedges", *IEEE Trans. Antennas Propag.,* vol. 37, pp. 206-211, 1989.

[10] K. A. Remley, A. Weisshaar, and H. R. Anderson, "Improved diffraction coefficients for lossy dielectric wedges", *Electronics Letters*, vol. 35, pp. 1826-1827, 1999.

[11] P. D. Holm, "A new heuristic UTD diffraction coefficient for non perfectly conducting wedges*", IEEE Trans. Antennas Propag.,* vol. 48, pp. 1211-1219, 2000.

[12] H. M. El-Sallabi, I. T. Rekanos and P. Vainikainen, "A new heuristic diffraction coefficient for lossy dielectric wedges at normal incidence", *Antennas Wireless Propag., Lett.*, vol. 1, pp. 165-168, 2002.

[13] R. F. Harrington, *Time-Harmonic Electromagnetic heuristic fields*. New York: McGraw-Hill, 1961, pp. 127-128.

[14] C. Gennarelli, G. Pelosi, and G. Riccio, "Approximate diffraction coefficients for an anisotropic impedance wedge," *Electromagnetics*, n. 2, vol. 21, pp. 165-180, 2001.

[15] C. Gennarelli et al., "Uniform asymptotic PO diffraction coefficients for an anisotropic impedance half-plane ", *Journal of Electromagnetic Waves and Applications*, vol. 13, pp. 963-980, 1999.

[16] C. Gennarelli et al., "Electromagnetic scattering by non-planar junctions of resistive sheets", *IEEE Trans. Antennas Propag*., vol. 48, pp. 565-574, 2000.

[17] C. Gennarelli et al., "Diffraction by an anisotropic dielectric half-plane: a uniform asymptotic PO solution", *IEEE Trans. Antennas Propag.*, vol. 49, pp. 1624-1627, 2001.

[18] G. Riccio, Cap. 2 in "*Wave Propagation in Material for Modern Applications*", INTECH pp. 33-54, 2010.

[19] T. B. A Senior and J. L. Volakis, "Approximate boundary conditions in electromagnetics," *IEE Electromagnetic Waves Series*, 1995.

[20] R. Tiberio, G. Pelosi and G. Manara, "A uniform GTD formulation for diffraction by a wedge with impedance faces," *IEEE Trans. Antennas Propag.*, vol. 33, pp. 867-873, 1985.

[21] R. G. Rojas, "Electromagnetic diffraction of an obliquely incident plane wave field by a wedge with impedance faces," *IEEE Trans. Antennas Propag.,* vol. 36, pp. 956–970, 1988.

[22] A. D. Rawlins, "Diffraction by, or diffusion into, a penetrable wedge," *Proc. R. Soc. Lond. A*, vol. 455, pp. 2655-2686, 1999.

[23] A. D. Rawlins, "Diffraction by a dielectric wedge," *J. Inst. Math. Appl.*, vol. 19, pp. 231-279, 1977.

[24] S. Bernsten, "Diffraction of an electric polarized wave by a dielectric wedge", *SIAM J. Appl. Math*., vol. 43, pp. 186-211, 1983.

[25] C. S. Joo, J. W. Ra, and S. Y. Shin, "Scattering by a right angle dielectric wedge," *IEEE Trans. Antennas Propag.*, vol. 32, pp. 61-69, 1984.

[26] S. Y. Kim, J. W. Ra, and S. Y. Shin, "Diffraction by an arbitrary-angled dielectric wedge: Part I - physical optics approximation," *IEEE Trans. Antennas Propag.*, vol. 39, pp. 1272-1281, 1991.

[27] S. Y. Kim, J. W. Ra, and S. Y. Shin, "Diffraction by an arbitrary-angled dielectric wedge: Part II - Correction to physical optics solution," *IEEE Trans. Antennas Propag.*, vol. 39, pp. 1282-1292, 1991.

[28] R. E. Burge *et al.*, "Microwave scattering from dielectric wedges with planar surfaces: A diffraction coefficient based on

a physical optics version of GTD," *IEEE Trans. Antennas Propag.*, vol. 47, pp. 1515-1527, 1999.

[29] J. F. Rouviere, N. Douchin and P. F. Combes, "Diffraction by lossy dielectric wedges using both heuristic UTD formulations and FDTD," *IEEE Trans. Antennas Propag.*, vol. 47, pp. 1702-1708, 1999.

[30] P. Bernardi, R. Cicchetti and O. Testa, "A three-dimensional UTD heuristic diffraction coefficient for complex penetrable wedges," *IEEE Trans. Antennas Propag.,* vol. 50, pp. 217-224, 2002.

[31] G. Stratis, V. Anantha, and A. Taflove, "Numerical calculation of diffraction coefficients of generic conducting and dielectric wedges using FDTD," *IEEE Trans. Antennas Propag.*, vol. 45, no. 10, pp. 1525-1529, 1997.

[32] J. H. Chang and A. Taflove, "Three-dimensional diffraction by infinite conducting and dielectric wedges using a generalized total-field/scattered-field FDTD formulation," *IEEE Trans. Antennas Propag.*, vol. 53, pp. 1444-1454, 2005.

[33] J. Radlow, "Diffraction by a right-angled dielectric wedge", *Intern. J. Enging. Sci*., vol. 2, pp. 275-290, 1964.

[34] R. H. T. Bates, "Wavefunctions for prism", *Int. J. Electronics*., vol. 34, pp. 81-95, 1973.

[35] C. H. Seo and J. W. Ra, "Plane wave scattering by a lossy dielectric wedge", *Microwave Opt. Technol. Lett.,* vol. 25, pp. 360-363, 2000.

[36] M. A. Salem, A. H. Kamel and A. V. Osipov, "Electromagnetic fields in presence of an infinite dielectric wedge," *Proc. R. Soc. Lond*. *A*, vol. 462, pp. 2503-2522, 2006.

[37] V. Daniele and G. Lombardi, "The Wiener-Hopf solution of the isotropic penetrable wedge problem: diffraction and total field," *IEEE Trans. Antennas Propag.*, vol. 59, pp. 3797-3818, 2011.

[38] E. N. Vasilev and V.V. Solodukhov, "Diffraction of electromagnetic waves by a dielectric wedge," *Radiophysics and Quantum Electronics*, vol. 17, pp. 1161-1169, 1976.

[39] E. N. Vasilév, V.V. Solodukhov and A.I. Fedorenko, "The Integral Equation Method in the Problem of Electromagnetic Waves Diffraction by Complex Bodies," *Electromagnetics*, vol. 11, pp. 161-182, 1991.

[40] B. Budaev, "Diffraction by Wedges," London, *Longman Scient*., 1995.

[41] Gennarelli, G. and G. Riccio, "A uniform asymptotic solution for diffraction by a right-angled dielectric wedge," *IEEE Trans. Antennas Propag.*, vol. 59, pp. 898-903, 2011.

[42] Gennarelli, G. and G. Riccio, "Plane-wave diffraction by an obtuse-angled dielectric wedge," *J. Opt. Soc. Am. A,* vol. 28, pp. 627-632, 2011.

[43] G. Gennarelli, M. Frongillo, G. Riccio, "High-frequency evaluation of the field inside and outside an acute-angled dielectric wedge," *IEEE Trans. Antennas Propag.*, vol. 63, pp. 374-378, 2015.

[44] M. Frongillo, G. Gennarelli and G. Riccio, "Diffraction by arbitrary-angled dielectric wedges: closed form high-frequency solutions," *PIERS 2015 Proceedings,* pp. 964-967, July 6-9, Prague, 2015.

[45] A. Taflove and S. Hagness, "Computational Electrodynamics: The Finite Difference Time Domain Method," Norwood: Artech House, 2000.

[46] S. D. Gedney, "An anisotropic perfectly matched layer absorbing medium for the truncation of FDTD lattices," *IEEE Trans. Antennas Propag.*, vol. 44, pp. 1630-1639, 1996.

[47] G. Gennarelli and G. Riccio, "Diffraction by a planar metamaterial junction with PEC backing," *IEEE Trans. Antennas Propag.*, vol. 58, pp. 2903-2908, 2010.

[48] T.W. Veruttipong, "Time domain version of the uniform GTD," *IEEE Trans. Antennas Propag.*, vol. 38, no. 11, pp. 1757-1764, 1990.

[49] P. R. Rousseau and P. H. Pathak, "Time domain uniform geometrical theory of diffraction for a curved wedge," *IEEE Trans. Antennas Propag.*, vol. 43, no. 12, pp. 1375-1382, 1995.

[50] P. M. Johansen, "Time-domain version of the physical theory of diffraction," *IEEE Trans. Antennas Propag.*, vol. 47, no. 2, pp. 261-270, 1999.

[51] Y. E. Sun and W. V. T. Rusch, "Time-domain physical optics," *IEEE Trans. Antennas Propag.*, vol. 42, no. 1, pp. 9-15, 1994.

[52] P. R. Rousseau, P. H. Pathak, and H. T. Chou, "A time domain formulation of the uniform geometrical theory of diffraction for scattering from a smooth convex surface," *IEEE Trans. Antennas Propag.*, vol. 55, no. 6, pp. 1522-1534, 2007.

[53] H. T. Chou, P. H. Pathak, and P. R. Rousseau, "TD-UTD solutions for the transient radiation and surface fields of pulsed antennas placed on PEC smooth convex surfaces," *IEEE Trans. Antennas Propag.*, vol. 59, no. 5, pp. 1626-1637, 2011.

[54] A. Karousos and C. Tzaras, "Multiple time-domain diffraction for UWB signals," *IEEE Trans. Antennas Propag.*, vol. 56, no. 5, pp. 1420-1427, 2008.

[55] G. Pelosi, G. Manara, A. Freni, and J. M. L. Bernard, "Current evaluation on the faces of an impedance wedge illuminated by an electromagnetic pulse," *IEEE Trans. Antennas Propag.*, vol. 42, no. 12, pp. 1663-1667, 1994.

[56] C. Gennarelli, G. Pelosi, and G. Riccio, "Time domain version of the UAPO solution for the field diffracted by an anisotropic half-plane," *J. Electromagn. Waves Applicat.*, vol. 18, no. 7, pp. 969-981, 2004.

[57] F. Ferrara, C. Gennarelli, G. Pelosi, and G. Riccio, "TD-UAPO solution for the field diffracted by a junction of two highly conducting dielectric slabs, " *Electromagnetics*, vol. 27, no. 1, pp. 1-7, 2007.

[58] G. Gennarelli and G. Riccio, "Time domain diffraction by a right-angled penetrable wedge," *IEEE Trans. Antennas Propag.*, vol. 60, pp. 2829-2833, 2012.

[59] G. Gennarelli and G. Riccio, "Obtuse-angled penetrable wedges: a time domain solution for the diffraction coefficients," *J. Electromagn. Waves. Appl.*, vol. 27, pp. 2020-2028, 2013.

"*Mi appassionano i campi elettromagnetici perché sono il mezzo per raggiungere l'infinito*."

Prof. Giorgio Franceschetti.

Napoli, 27 Settembre 2004.